HEINRICH HEINE
UNIVERSITÄT DÜSSELDORF

Josephson current and Andreev level dynamics in nanoscale superconducting weak links

Inaugural Dissertation

zur Erlangung des Doktorgrades der
Mathematisch-Naturwissenschaftlichen Fakultät
der Heinrich-Heine-Universität Düsseldorf

vorgelegt von

Aldo Brunetti

aus Mönchengladbach

Düsseldorf, November 2014

Aus dem Institut für Theoretische Physik IV

der Heinrich-Heine Universität Düsseldorf

Gedruckt mit der Genehmigung der

Mathematisch-Naturwissenschaftlichen Fakultät

der Heinrich-Heine Universität Düsseldorf

Referent: Prof. Dr. Reinhold Egger

Koreferent: Prof. Dr. Dagmar Bruß

Tag der mündlichen Prüfung: . .2014

This thesis is based on the following original articles:

- Chapter 2

  Anomalous Josephson current, incipient time-reversal symmetry breaking, and Majorana bound states in interacting multilevel dots,
  Aldo Brunetti, Alex Zazunov, Arijit Kundu and Reinhold Egger,
  Phys. Rev. B **88**, 144515 (2013)

- Chapter 3

  Quasiparticle trapping, Andreev level population dynamics, and charge imbalance in superconducting weak links,
  Alex Zazunov, Aldo Brunetti, Alfredo Levy Yeyati and Reinhold Egger,
  Phys. Rev. B **90**, 104508 (2014)

Contents

A mio Padre. Al suo ricordo che vive.

To my Father. To his living memory.

Abstract

In this thesis we will focus on the interplay between proximity induced superconducting correlations and Coulomb interactions in a Josephson junction: i.e., in a system where two superconductors modeled as two s-wave superconductors at a phase difference φ are contacted by means of a weak link, in our case a quantum dot located in the contact. In the first part we will study the Josephson current-phase relation for a multi-level quantum dot tunnel-contacted by two conventional s-waves superconductors. We will determine in detail the conditions for observing a finite anomalous Josephson current, i.e. a supercurrent flowing at zero phase difference in a two-level dot with spin-orbit interactions, a weak magnetic (Zeeman) field, and in the presence of Coulomb interactions. This will lead to an onset behavior $I_a \propto \mathrm{sgn}(B)$, interpreted as the sign of an incipient spontaneous breakdown of time-reversal symmetry. Moreover, we will provide conditions for realizing spatially separated - but topologically unprotected - Majorana bound states, whose signature in the system will be detectable via the current-phase relation. In the second part of the thesis, we address the Andreev bound state population dynamics in superconducting weak links (a superconducting 'atomic contact'), in which a poisoning mechanism due to the trapping of single quasiparticles can occur. Our motivation is that quantum coherent superconducting circuits are the most promising candidates for future large-scale quantum information processing devices. Moreover, quasiparticle poisoning has recently been observed in devices which contain a short superconducting weak link with few transport channels. We will discuss a novel charge imbalance effect in the continuum quasiparticle population, which is due to phase fluctuations of the environment weakly coupled to the superconducting contact. This coupling enters the system as a transition rate connecting continuum quasiparticles and the Andreev bound state system. The charge imbalance is then due to the breaking of left-right symmetry in the rates. Moreover, it will be discussed how the system can generate a phase-dependent quasiparticle current and an asymmetric charge profile around the weak link.

Zusammenfassung

In dieser Dissertation betrachten wir das Wechselspiel zwischen Annäherung-induzierten supraleitenden- und Coulomb Wechselwirkungen in einem Josephson-Kontakt: d.h., in einem System, bei dem zwei s-Wellen-Supraleiter mit einer Phasendifferenz φ durch einen Quantenpunkt in Kontakt gesetzt werden. Im ersten Teil der Dissertation erforschen wir die Josephson Strom-Phasen-Beziehung in einem mit vielen Energieniveaus ausgestatteten Quantenpunkt, der in Kontakt mit zwei konventionellen s-Wellen-Supraleitern steht. Wir bestimmen die Bedingungen, um einen endlichen anomalen Josephson Strom zu messen: ein Suprastrom, der in einem Doppelquantenpunkt mit Spin-Bahn Kopplung, schwachem magnetischen Feld (Zeeman), und in Anwesenheit der Coulomb-Wechselwirkungen fließt. Das führt uns zu einem Verhalten des Stromes $I_a \propto \mathrm{sgn}(\alpha B)$, das als Anfang der spontanen Symmetriebrechung der Zeitumkehrinvarianz angesehen werden kann. Außerdem identifizieren wir die notwendigen Voraussetzungen, um räumlich getrennte - aber topologisch ungeschützte - gebundene Majorana-Zustände zu realisieren, deren Präsenz im System durch die Strom-Phasen-Beziehung detektiert werden kann. Im zweiten Teil der Dissertation betrachten wir die Dynamik der Population gebundener Andreev-Zustände in supraleitenden atomaren Punktkontakten mit wenigen Transportkanälen, wobei die Prozesse durch eingefangene Quasiteilchen im Kontakt gestört werden. Kohärente supraleitende quantenmechanische Bauelemente entsprechen den erfolgversprechendsten Kandidaten für zukünftig umfassende Verarbeitungsgeräte in der Theorie der Quanteninformation. Wir diskutieren einen neuartigen Ladungsasymmetrie, der in der Population der Quasiteilchen im Kontinuum stattfindet, infolge von Phasenfluktuationen der Umgebung, die an den supraleitenden Atomkontakt gekoppelt ist. Diese Kopplung wurde als eine Übergangsrate zwischen Quasiteilchen im Kontinuum und gebundenen Andreev-Zuständen angesehen. Dieser Ladungsasymmetrie zeigt sich infolge einer Links-Rechts Symmetriebrechung der Übergangsraten. Außerdem diskutieren wir, wie in unserem System ein phasenabhängiger Quasiteilchen-Strom und ein asymmetrisches Ladungsprofil um den supraleitenden atomaren Punktkontakt erzeugt werden kann.

Chapter 1

Introduction

The Josephson effect is the phenomenon of a supercurrent flow occurring in devices known as Josephson junctions. A supercurrent is defined as a current that flows indefinitely without any voltage difference applied to the system; and Josephson junctions are devices consisting of two superconducting banks, or leads throughout this thesis, coupled by a weak link. The weak link can be a thin insulating barrier, forming so a system that is a superconductor-insulator-superconductor (SIS) junction, that is also the initial theoretic work considered by B. D. Josephson in 1962, Ref. [1]. But the coupling between the two superconducting leads can occur also via nanoscale conductors ('quantum dots') tunnel coupled to the system, quantum point contacts or normal conducting layers. In this thesis we will deal with weak links in the specific case considered of quantum dots and superconducting atomic contacts (constrictions) in order to study specific properties and phenomena occurring in Josephson junctions and to investigate Andreev bound state population dynamics and quasiparticle trapping in devices containing a short superconducting weak link with few transport channels.

It is well known that, in devices made of an insulating thin barrier between two normal electrodes, a NIN system, electrons can tunnel through the insulating layer and that this tunneling occurs with an associated current density that decays exponentially as the thickness of the barrier increases. Along the guidelines of Ref. [2], let us consider then a SIS system at $T = 0$. Then we do not have anymore normal electrons at the Fermi level. Hence, we would expect no tunneling to be possible as long as the voltage difference applied $eV < 2\Delta$, with Δ energy-gap voltage. When $eV > 2\Delta$, Cooper pairs can break up into two normal electrons and hence tunnel through the barrier. The question whether a Cooper pair can actually tunnel through the barrier remains. The general idea in 1962 was that this event would not happen often enough to be measurable, apparently explained by the fact that, since the probability of a single electron to tunnel is of the order of $p_t \lesssim 10^{-4}$, then for a Cooper pair one would expect $p_t^2 \lesssim 10^{-8}$. But, in 1962, Josephson changed this idea by discovering that Cooper pairs tunnel through the barrier as a whole. The motivation is that Cooper pairs tunnel coherently: their tunneling is not depicted as two incoherent electron waves approaching the barrier, but rather it is a macroscopic wave function of the superconducting system that tunnels through the weak link. One year later, P.W. Anderson and J.M. Rowell, see Ref. [3], confirmed experimentally the prediction made by him. For this prediction, the Nobel Committee awarded Josephson the Nobel Price in 1973, together with L. Esaki and I. Giaever.

The tunnel properties of the Cooper pairs follows as consequence of the macroscopic nature of the superconducting state. Usually, if we consider the behavior of a macroscopic object consisting of a large number of atoms, quantization effects are not observable, even though every single atom obeys the law of quantum mechanics. The motivation for this is that the thermal effects have the property to overshadow quantum effects. Though it is believed that quantization occurs at microscopic scales only, for some phenomena, such as superconductivity, macroscopic quantization is found to be possible. In this sense, quantization of parameters is still observable at orders of magnitude larger than the microscopic scales, typical for objects like atoms. This occurs because, due to quantum coherence effects, electrons in a superconductor form a highly correlated system: then all superconducting electrons behave as a single mechanical object. There exists a macroscopic quantum wave function

$$\psi\left(\vec{r},t\right) = \psi_0\left(\vec{r},t\right) e^{i\,\Theta(\vec{r},t)} \tag{1.1}$$

that describes the behavior of the whole ensemble of the electrons in the superconductor. This hypothesis can be justified by the microscopic theory of superconductivity, the BCS-theory, [4], named after the physicists J. Bardeen, L.N. Cooper and J.R. Schrieffer, proposed in 1957 and Nobel Price awarded in 1972. The general idea of the theory is that in superconducting systems, electrons near the Fermi level exhibit an attractive force between them. Below a critical temperature, T_c, this binding of electrons gives rise to a quantum state different from the Fermi sea of normal metals. On a general level, a small portion of electrons near the Fermi level form Cooper pairs. If one considers a simple model of two electron added to the Fermi sea at $T = 0$, with the request that the added electrons interact with each other, but not with the rest of the sea, except via exclusion principle, one may require to build a two-particle wave-function. Following general arguments, based on the Bloch theorem, one may expect the lowest-energy level to have a total zero angular momentum (a s-wave superconductor). Consequently, Pauli's principle would force the electrons to show an antisymmetric spin state: the two spins must be in a singlet state. Differently from the binding of atoms in molecules, the orbitals state of the Cooper pair has a larger radius, orientative speaking between 10 nm and 1 μm. The spatial overlap then results to be strong.

Studies of the current-phase relation in a Josephson junction have been widely analyzed in pioneering works like Refs. [5, 6, 7]. The interest in such nanoscale hybrid devices has sharply increased recently since they allow to fabricate and manipulate well-characterized setups and raise the hope for new applications, as well as by the prospect of realizing Majorana fermions. Moreover, Josephson transport throughout quantum dots also tends to find application in the control of localized spin states by a Josephson current, and so the possibility to create entangled electron pairs via non-local Andreev processes. To mention just a few key experiments, gate-tunable supercurrents through the two-dimensional electron gas in semiconductors have been demonstrated, see for instance Refs. [9]-[13], the CPR of superconducting atomic point contacts has been measured using a loop geometry, as in Ref. [14], and the direct spectroscopy of Andreev bound states in carbon nanotube devices was reported, as one may find in deeper details in Ref. [15]. The phenomena studied below will be particularly pronounced for strong spin-orbit coupling (SOC) in the nanoscale conductor. Note that strong SOC is naturally present in InAs or InSb, widely reported in Refs. [16]-[25], and in self-assembled SiGe quantum dots, see Ref. [26]. SOC is often responsible for nontrivial topological properties and the emergence of Majorana fermions, see Refs. [27, 28], in very similar settings, as in the wide collection of Refs. [29]-[34]. Majoranas have attracted wide attention after recent experiments reported first transport signatures such as those expected for Majorana fermions, as in Refs. [36]-[39].
The anomalous Josephson effect is characterized by a finite supercurrent flowing at zero phase difference, $I_a \equiv I(\varphi = 0) \neq 0$. Comparing to the conventional Josephson relation in junctions where SOC is typically a crucial ingredient, we have $I(\varphi) = I_c \sin\varphi$ with critical current I_c. This is equivalent to a φ_0 phase shift, i.e., $I_a = I_c \sin\varphi_0$. Junctions with $I_a \neq 0$ are thus commonly referred to as 'φ_0-junctions'. The Josephson CPR for quantum dots with SOC has been studied in many theoretical works, see Refs. [40]-[53], and the conditions for φ_0-junction behavior have been clarified in the noninteracting case, in Refs. [41, 42, 48, 49, 50] for instance. Moreover, the φ_0-junction can act as a phase battery, as in Ref. [54] or as superconducting rectifier, see Refs. [48, 52]. While it is well-established, see Ref. [54], and also experimentally observed, see Ref. [55], that spin-active interfaces, e.g., for a ferromagnetic 'dot' region, allow one to realize a φ_0-junction, we here focus on semiconducting or molecular systems with spin-conserving and spin-independent interfaces, where φ_0-junction behavior is quite nontrivial. φ_0-junctions were also predicted but never observe in unconventional

superconductors, as in the collection of Refs. [56]-[60].
Besides analyzing the anomalous supercurrent, we also address the possibility of Majorana bound state formation in an interacting double dot with SOC and Zeeman field. The double dot is contained as special case in our general multi-level Hamiltonian, and our theory is directly applicable to such a two-orbital case with well separated orbitals. Majorana fermions are emergent quasi-particles that equal their own antiparticle and they are of much interest in the context of topological quantum computation, as in the collection of Refs. [29, 30, 31, 32, 33]. When our 'dot' region corresponds to a semiconductor nanowire, one effectively can realize Kitaev's chain model that, in the right parameter regime, allows for a pair of topologically protected Majorana bound states localized near the nanowire ends, see Refs. [35, 34]. As discussed by Lejinse and Flensberg, as in Ref. [67] and also Ref. [68], a simpler variant, with topologically unprotected Majorana fermions, can be realized for two Coulomb-blockaded single-level dots coupled to a superconductor. Similarly, in our setting a pair of spatially separated Majorana bound states can also be realized. Signatures of Majorana fermions could be detected through the highly unusual features in the 2π-periodic current-phase relation.

Moreover, in this thesis we focus on other phenomena occurring when weak links are considered. Namely, we study the Andreev bound state population dynamics in a single-channel superconducting atomic contact. This is linked to the fact that quantum coherent superconducting circuits have acquired importance among the scientific community for their potential in building large-scale quantum information processing devices, see Refs. [53] and [72]. Their functioning is often limited by the presence of residual nonequilibrium quasiparticles, whose uncontrolled tunneling provide a severe decoherence mechanism, see Refs. [73]-[76]. Remarkably, in some cases where the parity of the quantum state matters, the presence of a single extra quasiparticle can determine the macroscopic response of the device, see Refs. [77, 78]. In our theory we approach the phenomenon of trapping of single quasiparticles in superconducting islands, known as "poisoning" , as one might find in Ref. [79]. Although at temperatures well below the superconducting gap Δ, such states have an exponentially small chance to exist in thermal equilibrium, they can have very long lifetimes if generated in a nonequilibrium process. Quasiparticle poisoning has been also observed in recent experiments for devices containing a short superconducting weak link with only a few transport channels, as for instance in Refs. [80, 81, 82]. Those experiments reported the existence of long-lived nonequilibrium quasiparticles trapped in the Andreev bound states formed near the weak link. In our theoretical framework, we refer to such a superconducting constriction as a 'superconducting atomic contact' (SAC), see for instance also Ref. [83].

In our theory, we consider transitions between different Andreev bound state configurations and their interplay with continuum quasiparticles. Such transitions, triggered for instance by environmental phase fluctuations, also can change the fermion number parity in the Andreev levels. The system exhibits a ground state with even parity, although there are two spin-degenerate odd-parity Andreev bound state configurations with excitation energy

$$E_A(\varphi_0) = \Delta\sqrt{1 - \mathcal{T}\sin^2(\varphi_0/2)} \tag{1.2}$$

relative to the ground state, where φ_0 is the superconducting phase difference across the contact and $\mathcal{T}$ the normal-state transmission probability of the contact. The phase-dependent energy E_A also determines the transition frequencies between different Andreev configurations, which have recently been studied by microwave absorption and supercurrent spectroscopy [81, 82], where the odd-parity states can be excited together with a continuum quasiparticle. Events resulting in the occupation of one of these odd-parity states block the Josephson current causing the quasiparticle poisoning. The spin degree of freedom corresponding to the two odd-parity states has also been proposed as qubit platform, see Refs. [84, 85], because of its long lifetime. But the occupation of the odd-parity states has also strong limitations on the possibility of realizing the 'Andreev qubit', see Refs. [86, 87], which is built from the Andreev ground state configuration and the excited even-parity state of energy $2E_A$, see also Ref. [88]. Similar superconducting devices are also discussed in the context of Majorana fermion physics [89, 90], and questions pertaining to quasiparticle poisoning and the interplay between Andreev (or Majorana) and continuum quasiparticle distribution functions are important in that direction as well.

Chapter 2

Transport through Quantum Dots

2.1 Introduction

In this chapter, as pointed out in Ch. 1, we will present with more details the first part constituting this thesis. Here we study the combined effects of spin-orbit (SO) interaction, magnetic field, and Coulomb charging on the Josephson current-phase relation (CPR), $I(\varphi)$, for a multi-level quantum dot tunnel-contacted by two conventional s-wave superconductors with phase difference φ. A general model is formulated and analyzed in the cotunneling regime (weak tunnel coupling) and in the deep subgap limit, fully taking into account interaction effects. We determine the conditions for observing a finite anomalous supercurrent $I_a = I(\varphi = 0)$. For a two-level dot with spin-orbit coupling and arbitrarily weak Zeeman field B, we find the onset behavior $I_a \propto \mathrm{sgn}(B)$ in the presence of interactions, suggesting the incipient spontaneous breakdown of time-reversal symmetry (TRS). We also provide conditions for realizing spatially separated (but topologically unprotected) Majorana bound states (MBSs) in this system, which have a clear signature in the 2π-periodic current-phase relation.

Before going deeper into details, the structure of this chapter will be organized as follows.

In Sec. 2.2, we introduce the general model for the system: namely, we introduce and consider a S-Dot-S hybrid structure, i.e. a quantum dot sandwiched between two superconductors. We focus on an arbitrary single-particle Hamiltonian in the dot region, and take into account Coulomb charging effects. By means of a later-on described technique, we derive an effective partition function expressed in terms of dot variables only, which then allows to extract the Josephson current-phase relation by a phase derivative. In order to get concrete results, we reduce our analysis on a generic two-orbital dot with a Zeeman field and (Rashba or Dresselhaus) spin-orbit coupling (SOC) on it.

In Sec. 2.3, we present and discuss the two analytical approaches used in this work to calculate the Josephson current, pointing out the existence of an anomalous Josephson current in the system. First, we study the cotunneling regime by means of perturbation theory in the tunnel couplings. After having derived the general ground-state current-phase relation, as second approach, we study the 'atomic limit', i.e. the limit $\Delta \to \infty$, where Δ is the superconducting gap.
Then, Sec. 2.4 is devoted to the anomalous Josephson effect for the two-level dot, and in Sec. 2.5 we show how a suitably choice of parameters can let a pair of spatially separated Majorana bound states emerge.

2.2 Model and effective partition function

We consider here a general model describing the Josephson effect in an interacting nanostructure, where a central region, to which we refer as 'dot', is tunnel-coupled to two conventional s-wave superconducting leads. We take into account Coulomb interactions, SOC, and magnetic field effects only on the dot, but not in the bulk electrodes nor in the tunnel contact. The Hamiltonian of the system can be written as:

$$H = H_d + H_t + H_l. \tag{2.1}$$

The dot Hamiltonian

For M relevant and spin-degenerate electronic orbitals in the central dot region, the dot Hamiltonian is taken in the form

$$H_d = \sum_{n\sigma, n'\sigma'} d^\dagger_{n\sigma} h_{n\sigma,n'\sigma'} d_{n'\sigma'} + E_c(\hat{N} - n_g)^2, \tag{2.2}$$

where the operator $d^\dagger_{n\sigma}$ creates a dot electron in a single-particle state with orbital quantum number $n = 1, \dots, M$ and spin projection $\sigma =\uparrow, \downarrow$. The $2M \times 2M$ Hermitian matrix $h_{n\sigma,n'\sigma'}$ encapsulates the single-particle features, including SOC and magnetic field effects. For we still are in the preliminary stage, we don't make any assumptions about the nature of the SO couplings, in order to allow for the most general statements regarding the anomalous Josephson effect. Importantly, the h matrix can always be conveniently diagonalized by mean of a unitary transformation, $U^\dagger h U = \mathrm{diag}(E_\nu)$, with the single-particle energies E_ν ($\nu = 1, \dots, 2M$). So we get the associated fermionic operators, c_ν, with

$$d_{n\sigma} = \sum_{\nu=1}^{2M} U_{n\sigma,\nu}\, c_\nu, \tag{2.3}$$

which correspond to single-particle eigenstates of the isolated dot. The $d_{n\sigma}$ operators instead will be taken to represent dot fermion modes tunnel-coupled to the leads. Both representations are, of course, equivalent. After the unitary transformation, the Hamiltonian of the dot reads

$$H_d = \sum_{\nu} E_\nu c_\nu^\dagger c_\nu + E_c(\hat{N} - n_g)^2. \tag{2.4}$$

Moreover, the capacitive Coulomb charging energy term, that formally describes intra- and inter-orbital Coulomb interactions, is only sensitive to the total dot fermion number operator,

$$\hat{N} = \sum_{n\sigma} d_{n\sigma}^\dagger d_{n\sigma} \equiv \sum_{\nu} c_\nu^\dagger c_\nu, \tag{2.5}$$

according to the two equivalent representations. Here the charging energy, E_c, sets the energy cost for adding or removing electrons into or from the system. The real number n_g is tunable by a backgate voltage and regulates the average number of electrons on the dot. Usually, the above charging term generically describes the dominant interaction contribution.

The BCS Hamiltonian

The left and right ($j = L, R$) superconducting leads are described by standard bulk BCS Hamiltonian. Here, we assume that the leads have identical energy gap Δ and normal-state dispersion relation $\xi_{\mathbf{k}}$, with chemical potential $\mu_S = 0$. In this analysis, assuming different energy gap in the leads, $\Delta_L \neq \Delta_R$ does not lead to sensible changes in the physics of the system, but it resolves rather in an overall decrease of the supercurrent. Similarly, considering different $\xi_{\mathbf{k}}$ would only change the respective density of states.
Moreover, we use a gauge where the phase of the order parameter appears in the tunneling Hamiltonian H_t only, presented below, and $\Delta \geq 0$ is real-valued, see also Appendix A. It is then convenient to switch to the Nambu (particle-hole) space and introduce the Nambu spinor $\Psi_{j\mathbf{k}} = (c_{j,\mathbf{k},\uparrow}, c_{j,-\mathbf{k},\downarrow}^\dagger)^T$, where $c_{j,\mathbf{k},\sigma}^\dagger$ creates an electron in lead j with momentum $\mathbf{k}$ and spin projection σ. Finally, introducing a set of Pauli matrices $\varrho_{x,y,z}$, acting in the Nambu space, the lead Hamiltonian is given by

$$H_l = \sum_{j=L,R} \sum_{\mathbf{k}} \Psi_{j\mathbf{k}}^\dagger \left(\xi_{\mathbf{k}}\, \varrho_y + \Delta\, \varrho_x\right) \Psi_{j\mathbf{k}}. \tag{2.6}$$

The tunneling Hamiltonian

To conclude, we come to H_t, where a complex-valued tunneling matrix element $t_{j,\mathbf{k},\sigma;n,\sigma'}$ gives the probability amplitude for an electron to transfer from the dot state (n, σ') to the lead state $(j, \mathbf{k}, \sigma)$. To simplify the analysis, we neglect the $\mathbf{k}$-dependence of the tunneling matrix elements, adopting so the standard wide-band approximation for the leads. Moreover, the tunneling is assumed to be spin-conserving and spin-independent, $t_{j,\mathbf{k},\sigma;n\sigma'} = \delta_{\sigma\sigma'} t_{j,n}$, and H_t is fully determined by $2M$ complex-valued parameters $t_{j,n}$. Making use again of the Nambu spinor notation also for the dot fermions, $D_n = (d_{n,\uparrow}, d^\dagger_{n,\downarrow})^T$, we obtain

$$H_t = \sum_{j=L,R} \sum_{\mathbf{k}} \sum_{n=1}^{M} \Psi^\dagger_{j\mathbf{k}} T_{j,n} D_n + \text{H.c.}\,, \quad T_{j,n} = e^{i\varrho_z\,\phi_j/2}\,\varrho_z \begin{pmatrix} t_{j,n} & 0 \\ 0 & -t^*_{j,n} \end{pmatrix}, \tag{2.7}$$

where ϕ_j is the superconducting phase in lead j.

2.2.1 Current-phase relation

To push further on our analysis, since our aim is to obtain a formally exact expression for the CPR from the partition function, $Z = \text{Tr} e^{-\beta H}$, with inverse temperature[1] $\beta = 1/T$, we now study the equilibrium Josephson CPR in the zero-temperature limit, $T \to 0$.
By means of Wick's theorem, we can average over the leads in order to trace out the non-interacting lead fermions, since we want to derive an effective partition function written in terms of dot variables only. In the interaction picture, let $H_0 = H_d + H_l$ govern the imaginary-time (τ) evolution. For arbitrary operator $\mathcal{O}$, we use the notation

$$\mathcal{O}(\tau) = e^{H_0\tau}\mathcal{O}e^{-H_0\tau}, \quad \bar{\mathcal{O}}(\tau) = e^{H_0\tau}\mathcal{O}^\dagger e^{-H_0\tau}. \tag{2.8}$$

The partition function then reads

$$Z = \text{Tr}_d\,\text{Tr}_l \left(e^{-\beta H_0} \mathcal{T} e^{-\int_0^\beta d\tau H_t(\tau)} \right) = Z_l\,\text{Tr}_d \left(e^{-\beta H_d} \mathcal{T} e^{-S_t} \right), \tag{2.9}$$

where $\mathcal{T}$ denotes the time ordering. The traces $\text{Tr}_{d,l}$ are performed over the dot- and lead-Hilbert spaces respectively, with $Z_l = \text{Tr}_l\, e^{-\beta H_l}$. In Eq. (2.9), we have averaged over the leads, and using $\langle H_t(\tau)\rangle_l = Z_l^{-1}\text{Tr}_l[e^{-\beta H_l} H_t(\tau)] = 0$, Wick's theorem implies that S_t in Eq. (2.9) is completely determined by the Gaussian correlator

$$S_t = -\frac{1}{2}\int_0^\beta d\tau d\tau' \,\langle \mathcal{T} H_t(\tau) H_t(\tau')\rangle_l\,. \tag{2.10}$$

Inserting H_t of Eq. (2.7) into Eq. (2.10) , we obtain

$$S_t = \frac{1}{2}\int_0^\beta d\tau d\tau' \sum_{nn'} \bar{D}_n(\tau)\Lambda_{nn'}(\tau - \tau') D_{n'}(\tau'), \tag{2.11}$$

[1]Throughout this thesis we often use $\hbar = k_B = 1$

where

$$\Lambda_{nn'}(\tau-\tau') = 2\sum_j T^\dagger_{j,n} G_l(\tau-\tau') T_{j,n'} \tag{2.12}$$

is expressed in terms of the Matsubara-Green's function, that is a matrix in the Nambu space, for each uncoupled lead ($j = L/R$):

$$G_l(\tau-\tau') = -\sum_{\mathbf{k}} \left\langle \mathcal{T}\Psi_{j\mathbf{k}}(\tau)\bar{\Psi}_{j\mathbf{k}}(\tau')\right\rangle_l = -\pi\nu_0 T\sum_m \frac{e^{-i\omega_m(\tau-\tau')}}{\sqrt{\omega_m^2+\Delta^2}} \begin{pmatrix} i\omega_m & \Delta \\ \Delta & i\omega_m \end{pmatrix}, \tag{2.13}$$

which is identical for both leads. Here we have employed the wide-band approximation, with the (normal-conducting) lead density of states $\nu_0 = \sum_{\mathbf{k}} \delta(\xi_{\mathbf{k}})$, and fermionic Matsubara frequencies $\omega_m = \pi T(2m+1)$, with integer m. The kernel $\Lambda_{nn'}(\tau-\tau')$ in Eq. (2.12), describing the effects of the traced-out leads on the dot fermions, thus reads

$$\Lambda_{nn'}(\tau) = \sum_{j=L,R} \Gamma^{(j)}_{nn'} \left(\partial_\tau + \Delta e^{-i\varrho_z\phi_j}\varrho_x\right) f(\tau) \tag{2.14}$$

where we again make use of the set of Pauli matrices in the Nambu space, $\{\varrho_{x,y,z}\}$, and where the tunnel contacts are described by Hermitian $M\times M$ hybridization matrices,

$$\Gamma^{(j)}_{nn'} = 2\pi\nu_0 t^*_{j,n} t_{j,n'}, \tag{2.15}$$

where - it is worth to stress it further - we assume spin-conserving bare tunneling, i.e. there is no spin flip in absence of SO and Zeeman fields, and hence, taking into account TR symmetry, $t_{j,\sigma;n\sigma'} = \delta_{\sigma\sigma'} t_{j,n}$. Moreover we use the auxiliary function

$$f(\tau) = T\sum_m \frac{e^{-i\omega_m\tau}}{\sqrt{\omega_m^2+\Delta^2}}. \tag{2.16}$$

Notice that $\Lambda_{nn'}(\tau-\tau')$ factorizes in spin/orbital (n,σ) and Nambu $(\varrho_{x,y,z})$ subspaces.
The Josephson current flowing through the contact j to the dot follows from the ground-state average

$$I_j = \frac{2e}{\hbar}\partial_{\phi_j} F, \tag{2.17}$$

where $F = -T\ln Z$ is the free energy. Current conservation imposes $I_{L,R} = \pm I(\varphi)$, where $\varphi = \phi_L - \phi_R$ is the gauge-invariant phase difference. As concluding remark to this section, we point out that the expression derived for Z is formally exact, within the standard assumption of $\mathbf{k}$-independent tunneling matrix elements. This implies that the Josephson current found to be flowing in the system is the most general expression possible.
Next, we will leave the general case to consider a toy-model from which concrete results can be derived.

2.2.2 Two orbital levels: building the toy-model

For concrete results, we will consider a generic model with $M = 2$ dot orbital levels, which provides a minimal setting for studying SOC effects, the anomalous supercurrent, and Majorana fermions. The 4×4 matrix h describing the single-particle spectrum of the dot Hamiltonian H_d, see Eq. (2.2), is taken in the generic form

$$h = (\mu\tau_0 + \epsilon\tau_z)\sigma_0 + B\tau_0\sigma_z + \alpha\tau_y \left[\cos(\chi)\sigma_z + \sin(\chi)\sigma_y\right], \tag{2.18}$$

where $\tau_{x,y,z}$ ($\sigma_{x,y,z}$) are Pauli matrices in orbital (spin) space and the respective unity matrices are τ_0 (σ_0). The physics is here determined by the interplay of a Rashba-type SOC, whose strength is parameterized by the energy scale α, and the magnetic Zeeman field, with energy scale B.

Spin-orbit effects in quantum dots have attracted interest because of their versatile applications in spintronics and in quantum informations theory, as in Ref. [45].

Rashba spin-orbit, i.e. a particular SO coupling considered throughout this thesis, is linked to the asymmetry of the confining potential of the electrons in a 2DEG, i.e. an electron gas with a strong confinement along one direction. The essence of such a coupling is the action of an external electric field on a moving spin, see Ref. [46].

In Eq. (2.18), $0 \le \chi \le \pi$ denotes the angle between the effective spin-orbit field and the Zeeman field. The bare dot levels are $\mu \pm \epsilon$ for $\alpha = B = 0$.

The single-particle Hamiltonian in Eq. (2.18) plays the role of a toy-model but actually represents a realistic Hamiltonian, reported in detail in Appendix A.

Now we conveniently express the 2×2 hybridization matrices (in orbital space) written in Eq. (2.15) in the form

$$\Gamma^{(j=L,R)} = \gamma_j \begin{pmatrix} e^{\lambda_j} & e^{i\delta_j} \\ e^{-i\delta_j} & e^{-\lambda_j} \end{pmatrix}, \tag{2.19}$$

where $\gamma_j \ge 0$ gives the overall hybridization strength of the respective contact and λ_j parametrizes the orbital asymmetry. This means that, for $\lambda_j = 0$, both orbitals couple symmetrically to the jth lead, and δ_j is an inter-orbital phase shift. It is worth to point out that, since $\delta_{L,R}$ is independent of spin, these phase shifts are independent of SO coupling of any nature. For instance, they could be caused by orbital magnetic fields and they might pop up in the system by virtue of a gauge transformation transferring the orbital field dependence to the tunneling Hamiltonian. It is also worth emphasizing that, for $\alpha \neq 0$ and $\Delta \neq 0$, one cannot gauge away the resulting phases $\delta_{L,R}$.

For further convenience in the upcoming calculations, we define the relative inter-orbital phase shift

$$\delta = \delta_L - \delta_R. \tag{2.20}$$

Note that our assumption of **k**-independent tunneling matrix elements, that we made in Sec. 2.2.1, implies that the phase shifts δ_j are also momentum-independent. If this assumption is violated, the δ_j are best treated as statistical variables. While the resulting average may suppress the anomalous Josephson current I_a, it will leave the critical currents basically unaffected. Since such generalizations are straightforward to implement, we proceed here by assuming **k**-independent phase shifts $\delta_{L,R}$ too.

2.3 The Josephson current

As discussed briefly in Sec. 2.1, in this thesis we consider a multi-level quantum dot tunnel-contacted by two conventional s-waves BCS superconductor to investigate the equilibrium Josephson current using two complementary vantage points. The first approach is presented in an extensive way and corresponds to the perturbation theory in the cotunneling regime, while the second one will employ an effective Hamiltonian valid in the 'deep subgap' regime, or atomic limit, for $\Delta \to \infty$.

2.3.1 First approach: the cotunneling regime

We will start presenting the analytical progress that can be done by means of the first approach discussed above. The cotunneling regime is realized when all eigenvalues of the hybridization matrices $\Gamma^{(j)}$, $j = L/R$, are small against Δ, in other words, the condition

$$\Gamma^{(j)} \ll \Delta \tag{2.21}$$

will define the energy regime in which we will be working.
Let us start from Eqs. (2.11) and (2.14): since the Gaussian correlator defined in Sec. 2.2.1, $S_t \propto \Gamma^{(j)}$, the free energy F can be directly expanded in powers of S_t:

$$F = -\beta^{-1} \ln \left[1 - \langle S_t \rangle + \frac{1}{2!} \langle S_t^2 \rangle - \ldots \right]. \tag{2.22}$$

Since $\partial_{\phi_j} \langle S_t \rangle = 0$, the lowest-order contribution to the Josephson current (2.17) is proportional to the product of the hybridization matrices $\Gamma^L \Gamma^R$ and reads

$$I_j = -2\beta^{-1} \left\langle S_t \partial_{\phi_j} S_t \right\rangle_{GS}. \tag{2.23}$$

The current for each lead here is taken as the ground-state expectation value for the closed dot Hamiltonian H_d. Expressing the effective action S_t in function of the kernel $\Lambda_{nn'}(\tau-\tau')$, see Eq. (2.12), in accordance with current conservation, we find $I_j(\varphi)=\pm I(\varphi)$, where

$$I(\varphi)=I_0\sin\varphi+I_a\cos\varphi\,. \tag{2.24}$$

In the last equation we have divided the Josephson current into its conventional part, proportional to $\sin\varphi$, and its anomalous part, proportional to $\cos\varphi$. Both currents appear in the total Josephson current with a pertinent intensity, I_0 and I_a. Their forms are

$$\begin{aligned}\begin{pmatrix} I_0 \\ iI_a \end{pmatrix} &= \sum_{nm,n'm'} \begin{pmatrix} \Gamma^{(L)}_{nm}\Gamma^{(R)}_{n'm'}+\Gamma^{(R)}_{nm}\Gamma^{(L)}_{n'm'} \\ \Gamma^{(L)}_{nm}\Gamma^{(R)}_{n'm'}-\Gamma^{(R)}_{nm}\Gamma^{(L)}_{n'm'} \end{pmatrix} \\ &\times\ \frac{1}{2}\Delta^2\beta^{-1}\int_0^\beta d\tau_1 d\tau_2 d\tau_1' d\tau_2' \\ &\times\ f(\tau_1-\tau_2)f(\tau_1'-\tau_2')\left\langle \mathcal{T} d_{n\downarrow}(\tau_1)d_{m\uparrow}(\tau_2)\bar{d}_{n'\uparrow}(\tau_1')\bar{d}_{m'\downarrow}(\tau_2')\right\rangle .\end{aligned} \tag{2.25}$$

Before extending our analysis, we may comment on some of the previous points. Eq. (2.24) gives the basic idea of the anomalous Josephson effect. The anomalous contribution to the total Josephson current is characterized by a finite supercurrent flowing even at zero phase difference, $\varphi=0$.

Comparing to the conventional Josephson effect , where the supercurrent reads $I(\varphi)=I_c\sin\varphi$, with critical current I_c, this is equivalent to a phase-shift in the system. In fact:

$$I(\varphi)\to I(\varphi+\varphi_0)=[I_c\cos\varphi_0]\sin\varphi+[I_c\sin\varphi_0]\cos\varphi\,, \tag{2.26}$$

i.e., $I_0=I_c\cos\varphi_0$ and $I_a=I_c\sin\varphi_0$. Therefore, Junctions in which $I_a\neq 0$ are commonly referred to as 'φ_0-junctions'. The critical current for the system is $I_c=\sqrt{I_0^2+I_a^2}$.

It is now crucial to use the unitary transformation U in Eq. (2.3) to switch from the $d_{n\sigma}$ to the c_ν fermion representation, where the latter represent the eigenstates of the isolated interacting dot. Using the symmetry property $f(\tau)=f(-\tau)$, we observe that only the antisymmetric part of the transformed hybridization matrices enters the expressions for I_0 and I_a. In formula:

$$\tilde{\Gamma}^{(j=L,R)}_{\nu\mu}=\sum_{nm}\Gamma^{(j)}_{nm}\left(U_{n\downarrow,\nu}U_{m\uparrow,\mu}-U_{n\downarrow,\mu}U_{m\uparrow,\nu}\right), \tag{2.27}$$

By employing Eq. (2.25), we find for the following simple form for the anomalous Josephson current as product of two matrices

$$I_a=\frac{e\Delta^2}{\hbar}\sum_{\nu>\mu}J_{\nu\mu}\,Q_{\nu\mu}. \tag{2.28}$$

The first ones are the symmetric $2M \times 2M$ matrices

$$J_{\nu\mu} = \mathrm{Im}\left(\tilde{\Gamma}^{(L)}_{\nu\mu}[\tilde{\Gamma}^{(R)}]^*_{\nu\mu}\right), \tag{2.29}$$

written in terms of the antisymmetric matrices in Eq. (2.27), whose dimension is $2M \times 2M$. Note that $J_{\nu\mu}$ matrices depend only on single-particle quantities, such as tunneling matrix elements, SOC, and Zeeman fields. It is worth stressing that Josephson currents through nanoscale multilevel quantum dots are strongly affected by SOC, even without an external magnetic field, see Ref. [44].

In this analysis, the role of interactions is encoded in the Q matrix and can be crucial in breaking the balance between time-reversed processes, which may then induce the anomalous Josephson effect:

$$Q_{\nu\mu} = -\beta^{-1}\int_0^\beta d\tau_1 d\tau_2 d\tau_1' d\tau_2' \; f\left(\tau_1-\tau_2\right) f\left(\tau_1'-\tau_2'\right) \left\langle \mathcal{T} c_\nu(\tau_1) c_\mu(\tau_2) \bar{c}_\nu(\tau_1') \bar{c}_\mu(\tau_2')\right\rangle . \tag{2.30}$$

The time-ordered product generates $4! = 24$ terms with different time ordering:

$$Q_{\nu\mu} = \sum_{p=1}^{24} Q^{(p)}_{\nu\mu}. \tag{2.31}$$

To complete the derivation, the current I_0 follows in a similar form,

$$I_0 = \frac{e\Delta^2}{\hbar}\sum_{\nu>\mu}\mathrm{Re}\left(\tilde{\Gamma}^{(L)}_{\nu\mu}\;[\tilde{\Gamma}^{(R)}_{\nu\mu}]^*\right)\; Q_{\nu\mu}. \tag{2.32}$$

We can now use Eq. (2.28) to derive some general conditions for the anomalous Josephson effect to exist within the cotunneling regime. As necessary condition for $I_a \neq 0$, we observe that $J_{\nu\mu} \neq 0$ must be satisfied for at least one index pair $\nu > \mu$.

It is also worth noting that this condition is very general and holds for arbitrary matrices h determining the single-particle spectrum.

In Sec. 2.2.2, we inferred that $M = 2$ orbitals represent the minimal model to consider to carry out significant results. The reason is that for a single-level dot, $M = 1$, the hybridization matrices $\Gamma^{(L)}$ and $\Gamma^{(R)}$ are just real numbers. The antisymmetric $\tilde{\Gamma}^{(L,R)}$ matrices in Eq. (2.27) are then fully determined by

$$\tilde{\Gamma}^{(j)}_{21} = \Gamma^{(j)}(U_{\downarrow,2}U_{\uparrow,1} - U_{\downarrow,1}U_{\uparrow,2}) = 0, \tag{2.33}$$

which immediately yields $J = 0$ in Eq. (2.29).

Hence no anomalous Josephson current is possible in a single-orbital dot, even in presence of interactions.

In order to infer general considerations that are independent of the analytical method considered, i.e. beyond the cotunneling regime, one can use symmetry arguments. We show this by analyzing the supercurrent through an inversion-symmetric two-dimensional dot with in-plane (purely Zeeman) magnetic field B and SOC strength α.
To perform a spatial inversion operation, $(x, y) \to (-x, -y)$, the following operations apply:

- exchanging the lead indices, $L \leftrightarrow R$;
- inverting the phase difference, $\varphi \to -\varphi$;
- changing the sign of the SOC, $\alpha \to -\alpha$;
- changing the sign of the (in-plane) Zeeman field, $B \to -B$.

Since $I(\varphi) \to -I(-\varphi)$ under spatial inversion, Eq. (2.24) implies that the anomalous supercurrent must satisfy the symmetry relation

$$I_a\left(\Gamma^{(L)}, \Gamma^{(R)}, B, \alpha\right) = -I_a\left(\Gamma^{(R)}, \Gamma^{(L)}, -B, -\alpha\right). \tag{2.34}$$

Similarly, we deduce an additional condition from the supercurrent behavior under a time reversal operation,

$$I_a\left(\Gamma^{(L)}, \Gamma^{(R)}, B, \alpha\right) = -I_a\left(\Gamma^{(L)}, \Gamma^{(R)}, -B, \alpha\right), \tag{2.35}$$

which implies that I_a is always odd in B: $I_a(B) = -I_a(B)$.

Let us next address the Q matrix in Eq. (2.30), which only depends on properties of the closed dot. In the cotunneling regime, interactions can affect the CPR only through this matrix. In general, from Eq. (2.30), a total number $4! = 24$ terms involving all possible permutations of time-ordered fermion operators will be generated. However, if the closed dot has a non-degenerate interacting ground state $|GS\rangle$, Eq. (2.30) allows for simplifications in the $\beta \to \infty$ limit of interest here. Assuming a TRS-breaking magnetic field to be present, effectively, only three permutations in Eq. (2.30) are relevant and $Q_{\nu\mu}$ can be expressed in terms of the three real-valued functions

$$\mathcal{Q}_i(\epsilon_a, \epsilon_b, \epsilon_c) = \frac{1}{\beta}\int_0^{\beta} d\tau_a \int_0^{\tau_a} d\tau_b \int_0^{\tau_b} d\tau_c \int_0^{\tau_c} d\tau_d \tag{2.36}$$

$$\times \; e^{-\epsilon_a(\tau_a-\tau_b)-\epsilon_b(\tau_b-\tau_c)-\epsilon_c(\tau_c-\tau_d)} \begin{cases} f(\tau_a-\tau_b)f(\tau_c-\tau_d), & i=1, \\ f(\tau_a-\tau_d)f(\tau_b-\tau_c), & i=2, \\ f(\tau_a-\tau_c)f(\tau_b-\tau_d), & i=3, \end{cases}$$

where $\epsilon_{a,b,c} \geq 0$ are possible excitation energies. Switching to the frequency domain and using Eq. (2.16), we obtain[2]

$$\mathcal{Q}_i = \int \frac{d\omega_1 d\omega_2}{(2\pi)^2} \frac{1}{\sqrt{(\omega_1^2+\Delta^2)(\omega_2^2+\Delta^2)}} \tag{2.37}$$

$$\times \begin{cases} (1-\delta_{\epsilon_b,0})/[(i\omega_1+\epsilon_a)(i\omega_2+\epsilon_c)\epsilon_b], & i=1, \\ 1/[(i\omega_1+\epsilon_a)(i\omega_1+\epsilon_c)(i\omega_1+i\omega_2+\epsilon_b)], & i=2, \\ 1/[(i\omega_1+\epsilon_a)(i\omega_2+\epsilon_c)(i\omega_1+i\omega_2+\epsilon_b)], & i=3. \end{cases}$$

We also underline that the $\mathcal{Q}_i$ are invariant under the exchange $\epsilon_a \leftrightarrow \epsilon_c$. Let's consider now the ground state $|GS\rangle$ of the closed dot Hamiltonian H_d in Eq. (2.4), with N_0 electrons on the dot, $\hat{N}|GS\rangle = N_0|GS\rangle$. Assuming that $|GS\rangle$ is non-degenerate, the filling factor n_ν for each single-particle state $\nu = 1, \ldots, 2M$ is known. Arranging the E_ν as ordered sequence, $E_1 \leq E_2 \leq \cdots \leq E_{2M}$, the result is

$$n_\nu = \langle GS|c_\nu^\dagger c_\nu|GS\rangle = \begin{cases} 1, & \nu \leq N_0, \\ 0, & \nu > N_0. \end{cases} \tag{2.38}$$

For given index pair $\nu > \mu$, three possibilities arise, namely $(n_\nu, n_\mu) = (0,0)$, $(1,1)$, and $(0,1)$. For a matter of convenience, we also define the Coulomb energy differences W_k, with integer k,

$$W_k = E_c(N_0 + k - n_g)^2 - E_c(N_0 - n_g)^2, \tag{2.39}$$

[2]The double-frequency integrals in Eq. (2.37) can be carried out analytically by replacing $f(\tau) \to \tilde{f}(\tau)$ in Eq. (2.16), with $(\omega^2+\Delta^2)^{-1/2} \to (\tilde{\Delta}^2/\Delta)/(\omega^2+\tilde{\Delta}^2)$, where $\tilde{\Delta}$ is a fitting parameter of order Δ chosen such that $f(\tau)$ and $\tilde{f}(\tau)$ have the same low-energy behavior. Within 1% accuracy, analytical results (using $\tilde{f}$) were found to match numerics (using f) for all parameters studied. We have used $f \to \tilde{f}$ exclusively for generating the figures throughout the rest of this thesis.

where the integer N_0 denotes the ground-state electron number on the dot. To state the final result for Q, it is useful to introduce the positive energies

$$\begin{aligned} \tilde{E}_\nu &= (1-2n_\nu)E_\nu + W_{1-2n_\nu}, \\ \tilde{E}_{\nu\mu} &= (1-2n_\nu)E_\nu + (1-2n_\mu)E_\mu + W_{2-2n_\nu-2n_\mu}. \end{aligned} \tag{2.40}$$

For $E_c = 0$, we have $1-2n_\nu = \mathrm{sgn}(E_\nu)$ and hence $\tilde{E}_\nu = |E_\nu|$, recovering so the non-interacting case. We then obtain the symmetric Q matrix,

$$\begin{aligned} Q_{\nu\mu} &= (1-2n_\nu)(1-2n_\mu)\Big[2\mathcal{Q}_{i_1}(\tilde{E}_\nu, \tilde{E}_{\nu\mu}, \tilde{E}_\mu) \\ &+ \mathcal{Q}_{i_2}(\tilde{E}_\nu, \tilde{E}_{\nu\mu}, \tilde{E}_\nu)\mathcal{Q}_{i_2}(\tilde{E}_\mu, \tilde{E}_{\nu\mu}, \tilde{E}_\mu) + 2\mathcal{Q}_{i_3}(\tilde{E}_\nu, 0, \tilde{E}_\mu)\Big], \end{aligned} \tag{2.41}$$

where the indices are $i_1 = i_2 = 1$ and $i_3 = 3$ for $n_\nu = n_\mu$. For $n_\nu \neq n_\mu$, we instead have $i_1 = i_3 = 2$ and $i_2 = 3$.

Strong Coulomb blockade

For $E_c \to \infty$, the cotunneling supercurrent is generally strongly suppressed. Technically, this suppression can be seen from Eq. (2.37): all excitation energies scale as

$$\epsilon_{a,b,c} \propto E_c \to \infty, \tag{2.42}$$

which implies $Q_{\nu\mu} \to 0$ and thus $I_{0,a} \to 0$.
This argument only breaks down for half-integer values of n_g, where the strong charging term in H_d allows for two degenerate charge states with particle numbers $N_0 = N_{0,\pm} \equiv n_g \pm 1/2$. Let us therefore now focus on half-integer values of n_g, where $\{E_\nu\}$, the single-particle energy spectrum, determines the ground state and which particle number N_0 is realized: i.e., if it is either $N_{0,+}$ or $N_{0,-}$. Using this argument, and since the Coulomb energy difference $W_{\mp 1} = 0$, Eq. (2.41) simplifies to

$$\begin{aligned} Q_{\nu\mu}^{(N_{0,+})} &= 2n_\nu n_\mu \mathcal{Q}_3(-E_\nu, 0, -E_\mu) \\ &\quad - \left[(1-n_\nu)n_\mu \mathcal{Q}_3(-E_\mu, E_\nu - E_\mu, -E_\mu) + (\nu \leftrightarrow \mu)\right], \\ Q_{\nu\mu}^{(N_{0,-})} &= 2(1-n_\nu)(1-n_\mu)\mathcal{Q}_3(E_\nu, 0, E_\mu) \\ &\quad - \left[(1-n_\nu)n_\mu \mathcal{Q}_3(E_\nu, E_\nu - E_\mu, E_\nu) + (\nu \leftrightarrow \mu)\right]. \end{aligned} \tag{2.43}$$

It is interesting to discuss Eq. (2.43) for a spin-degenerate single-level dot, i.e., the $M = 1$ case, without SOC and without magnetic field.

In this case, the two single-particle states, defined by $\nu =\uparrow,\downarrow$, have identical energy, say $E_\nu = x\Delta$, where x plays the role of a dimensionless parameter, and Eq. (2.43) yields[3]

$$Q_{\uparrow\downarrow} = \mathcal{Q}_3(|x|\Delta, 0, |x|\Delta) \times \begin{cases} 2, & N_0 = 0, 2, \\ -1, & N_0 = 1, \end{cases} \tag{2.44}$$

where Eq. (2.37) gives ($x > 0$)

$$\mathcal{Q}_3(x\Delta, 0, x\Delta) = \frac{1}{\pi^2\Delta^3} \frac{(\pi/2)^2(1-x) - \mathrm{Arccos}^2 x}{x(1-x^2)}. \tag{2.45}$$

Since $I_a = 0$ for $M = 1$, the critical current I_c directly follows from Eq. (2.32): so, $I_c \equiv I_0$. As final remark, Eq. (2.44) predicts π-junction behavior, with $I(\varphi) = -I_c \sin\varphi$, for $N_0 = 1$; while for $N_0 = \{0, 2\}$ it predicts 0-junction, with $I(\varphi) = I_c \sin\varphi$. It is proper to point out that these are actually well-known results, [5, 7].
In general, in the strong Coulomb blockade limit $E_c \to \infty$, we find π-junction behavior for odd N_0 and half-integer n_g.

2.3.2 Second approach: the superconducting atomic limit

After having shown results of perturbation theory in the tunneling matrices, we now briefly focus on the second approach. It deals with the parameter regime where Δ represents the largest relevant energy scale of interest, and we can effectively put $\Delta \to \infty$: the atomic limit. This approach allows us to go beyond the perturbative cotunneling regime and to compute the free energy F exactly, without further approximations. Considering Eq. (2.14), one can set:

$$f(\tau) \to \Delta^{-1}\delta(\tau) \tag{2.46}$$

and the partition function reads $Z = \mathrm{Tr}_d e^{-\beta H_{\text{eff}}}$. The 'effective dot Hamiltonian' is

$$H_{\text{eff}} = H_d + \frac{1}{2}\sum_{j=L,R}\sum_{nm}\left(\Gamma^{(j)}_{nm} e^{i\phi_j} d_{n\downarrow} d_{m\uparrow} + \text{H.c.}\right), \tag{2.47}$$

with H_d in Eq. (2.2) and a proximity-induced s-wave pairing term due to the traced-out superconducting leads.
The CPR then follows again from Eq. (2.17). Our vantage point is that the Hilbert space of the dot can now be decomposed into two independent sectors with even and odd fermion parity, respectively.

[3]Note that for $N_0 = 1$, the ground-state is two-fold spin degenerate. Since both spin orientations lead to the same result, our derivation, based on the assumption of non-degenerate $|GS\rangle$, still holds.

The form of the effective dot Hamiltonian in Eq. (2.47) can be used to demonstrate that the two limits $E_c \to \infty$ and $\Delta \to \infty$ do not commute. For $\Delta \to \infty$, one needs to retain only those contributions in Eq. (2.30) where two fermions forming a Cooper pair are tunneling as a whole, with no retardation effect, with the correlator of the form

$$\langle \mathcal{T} c_\nu(\tau + 0^+) c_\mu(\tau) \bar{c}_\nu(\tau' + 0^+) \bar{c}_\mu(\tau') \rangle. \tag{2.48}$$

Using $\tilde{E}_{\nu\mu} \geq 0$ in Eq. (2.40), some algebra gives

$$Q_{\nu\mu} = \frac{\delta_{n_\nu, n_\mu}}{2\Delta^2} \, \frac{1 - \delta_{\tilde{E}_{\nu\mu}, 0}}{\tilde{E}_{\nu\mu}}. \tag{2.49}$$

Since now $Q_{\nu\mu} \geq 0$ for arbitrary N_0, π-junction behavior is never possible in the atomic limit, in contrast to what we found for $\Delta < E_c \to \infty$ in Sec. 2.3.1. This statement always applies within the atomic limit, or equivalently said, beyond the cotunneling regime. Moreover, in the atomic limit, $E_c < \Delta \to \infty$, current flows only in the vicinity of the $2e$-charge degenerate points, defined for $W_{\pm 2} = 0$. These points correspond to integer values of n_g. This again differs from the strong-blockade result in Eq. (2.43), where current flows only for half-integer n_g. We conclude that the limits $E_c \to \infty$ and $\Delta \to \infty$ do not commute.

2.4 The anomalous Josephson current

After the introductory part, in which we presented the model and gave details about the techniques used to derive preliminary results of the most general form, we now focus on the CPR solely and, in particular, we keep the further analysis on the anomalous supercurrent, $I_a = I(\varphi = 0)$, for the two-level dot in Sec. 2.2.2, with Rashba-like SOC and Zeeman magnetic field. The guidelines of this section have been imagined to recall the organization of Sec. 2.3: it will be devoted to achieve results following the two approaches presented above. Let us start with the results in the cotunneling regime.

2.4.1 The cotunneling regime

In the cotunneling regime, the currents I_a and I_0 determining the Josephson CPR follow from Eqs. (2.28) and (2.32), respectively.
The anomalous supercurrent is expressed in terms of the 4×4 matrices J and Q, see Eqs. (2.29) and (2.41), respectively, where a necessary condition for the anomalous Josephson effect is given by $J_{\nu\mu} \neq 0$ for at least one index pair $\nu > \mu$. To evaluate the J matrix, the unitary matrix U diagonalizing h is needed. Analytical results in several complementary limits, where

the algebra is simpler and allows for an intuitive picture, will be provided.

Let us first observe that when the spin-orbit field is perpendicular to the Zeeman field ($\chi = \pi/2$), h is a symmetric matrix. This implies that the diagonalizing matrix U can always be chosen to have only real-valued entries only, and for $\delta_j = 0$, ($j = L/R$), we obtain $J = 0$ from Eq. (2.29). One conclusion of this consideration is that we can check, in agreement with previous works, [50], that the anomalous current I_a is identically zero for $\chi = \pi/2$ and $\delta_j = 0$,

$$I(\varphi = 0) \equiv I_a = 0 \iff (\chi = \pi/2 \,, \delta_j = 0)\,. \tag{2.50}$$

2.4.1.1 Case of collinear spin-orbit and Zeeman fields

In this subsection, we consider the case of collinear spin-orbit and Zeeman fields, i.e. where spin-orbit and Zeeman fields point along the same direction, realized for $\chi = 0$. We thus consider h in Eq. (2.18) for $\chi = 0$. Its form then reads

$$h = (\mu\tau_0 + \epsilon\tau_z)\sigma_0 + B\tau_0\sigma_z + \alpha\tau_y\sigma_z. \tag{2.51}$$

The diagonalizating matrix is found to be

$$U = \begin{pmatrix} \cos(\theta/2) & 0 & i\,\sin(\theta/2) & 0 \\ 0 & \cos(\theta/2) & 0 & i\,\sin(\theta/2) \\ i\,\sin(\theta/2) & 0 & \cos(\theta/2) & 0 \\ 0 & i\,\sin(\theta/2) & 0 & \cos(\theta/2) \end{pmatrix} \tag{2.52}$$

or, using Pauli matrices in orbital and spin space, in a more compact form

$$U = e^{i\tau_x\sigma_z\theta/2}, \quad \sin\theta = \frac{\alpha}{E_d}, \quad E_d = \sqrt{\epsilon^2 + \alpha^2}, \tag{2.53}$$

The spectrum $(E_1, \ldots, E_4)$ is given by

$$\mu + (E_d + B, E_d - B, -E_d + B, -E_d - B). \tag{2.54}$$

Using Eq. (2.27), the antisymmetric hybridization matrices $\tilde{\Gamma}^{(L,R)}$ have the following nonvanishing entries

$$\begin{aligned} \tilde{\Gamma}^{(j)}_{23} &= -[\tilde{\Gamma}^{(j)}]^*_{14} = \gamma_j \left(\cos\delta_j + i\frac{\alpha\sinh\lambda_j + \epsilon\sin\delta_j}{E_d}\right), \\ \tilde{\Gamma}^{(j)}_{21} &= \gamma_j\left(\cosh\lambda_j + \frac{\epsilon\sinh\lambda_j - \alpha\sin\delta_j}{E_d}\right) = \tilde{\Gamma}^{(j)}_{43}\Big|_{\theta\to\theta+\pi}. \end{aligned}$$

Following the procedure sketched previously, the symmetric J matrix in Eq. (2.29) has the following non-zero elements

$$J_{32} = \frac{\gamma_L \gamma_R}{E_d} \left[\epsilon \sin \delta + \alpha (\cos \delta_R \sinh \lambda_L - \cos \delta_L \sinh \lambda_R) \right] \tag{2.55}$$

and $J_{41} = -J_{32}$. Note that, surprisingly, this result does not depend on the Zeeman field B. In the end, the anomalous supercurrent is

$$I_a = \Delta^2 J_{32} \left(Q_{32} - Q_{41} \right). \tag{2.56}$$

Several physical considerations can be drawn from the equations above.

First of all, we that $J_{32} = 0$ for $\Gamma^{(L)} = \Gamma^{(R)}$, where $\delta_L = \delta_R$ and $\lambda_L = \lambda_R$. This allows us to conclude that asymmetric tunnel contacts with matrices

$$\Gamma^{(L)} \neq \Gamma^{(R)} \iff \left[\Gamma^{(L)}, \Gamma^{(R)} \right] \neq 0 \tag{2.57}$$

are necessary for $I_a \neq 0$. This condition, present also in Ref. [50], is indicating that it is crucial to have off-diagonal entries in these tunneling matrices to observe a phase-shift. In other words: if the lead-to-dot tunneling has a conserved orbital degree of freedom (e.g., channel number, transverse momentum, angular momentum, as it might be in nanotube dots and/or in single-electron transistors), the off-diagonal entries vanish and therefore no φ_0-junction behavior is possible. Another point of view, from which one can equivalently formulate the argument, is that having anomalous current in the system requires to break the chirality symmetry.

Discussion of figures and results

Now we will illustrate the figures appearing in this section. We will start by analyzing the 'phase diagram' for the conventional and anomalous Josephson currents, I_0 and I_a respectively, in the α-B plane, as depicted in Fig. 2.1.
The upper row illustrates the anomalous supercurrent: it is most pronounced when $|\alpha| \approx |B|$. The standard Josephson effect, in the lower row, where one has either 0- or π-junction behavior with $|I_a/I_0| \ll 1$, is recovered when either α or B are small. Moreover, the lower panel (still on I_0) indicates that within the Zeeman-dominated regime $|B| > \sqrt{\alpha^2 + \epsilon^2}$, we have $I_0 < 0$, implying that π-junction behavior can be realized. Furthermore, we observe that, for the chosen parameter set described in the caption of Fig. 2.1, I_a is an odd function in the product αB.

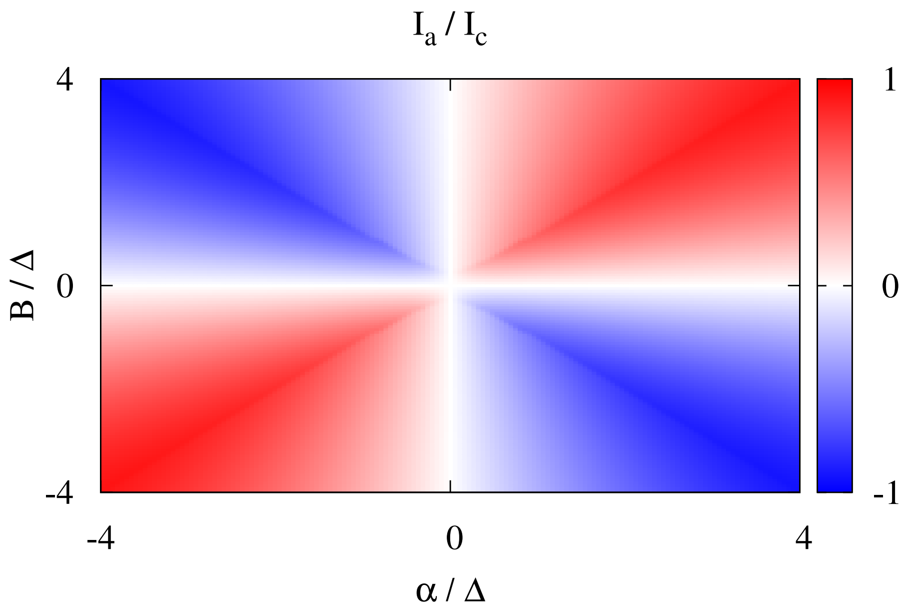

Figure 2.1: Anomalous supercurrent (I_a, top panel) and 'normal' supercurrent (I_0, bottom) determining the cotunneling CPR (2.24) in the B-α plane. The results are for the two-level dot with $\epsilon = 0.3\Delta$, $E_c = 2\Delta$, $n_g = 2$, and $\chi = \delta_{L,R} = \mu = \lambda_L = 0$. For the right contact, only the orbital level $n = 1$ is assumed to couple to the superconductor, i.e., $\lambda_R \to \infty$ with $\gamma_R e^{\lambda_R} \to \gamma_R$. Note that $I_{a,0}$ are normalized to the respective critical current $I_c = \sqrt{I_0^2 + I_a^2}$.

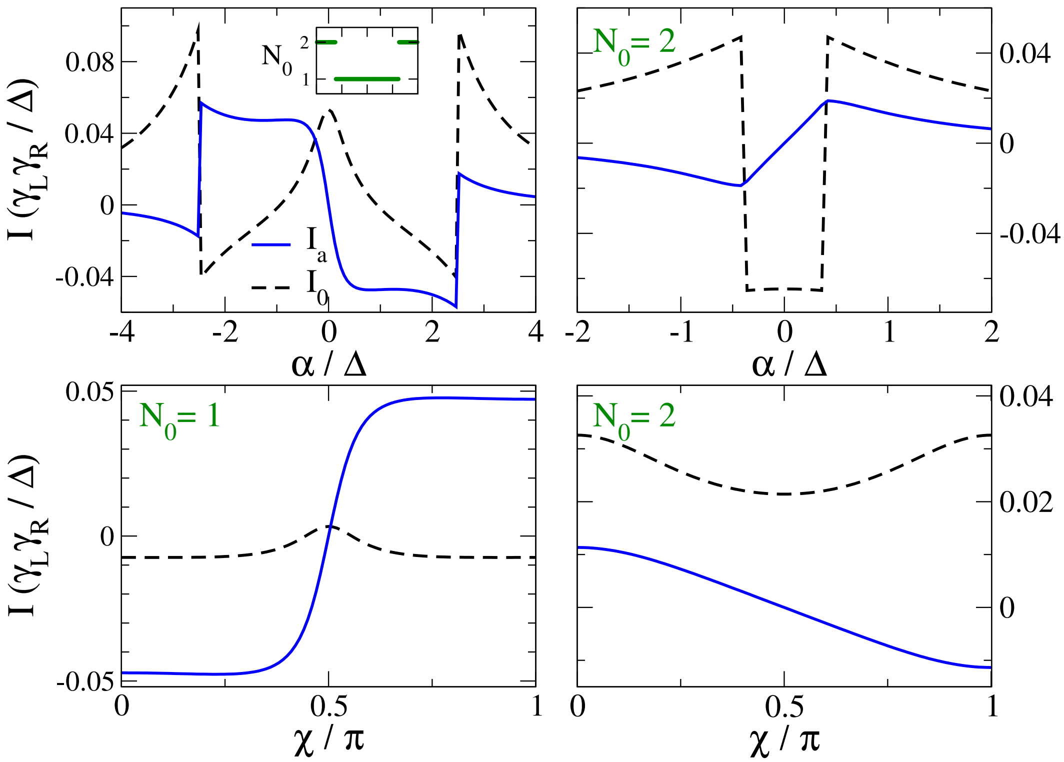

Figure 2.2: Parameter dependence of $I_{a,0}$ (main panels) and of the particle number N_0 (inset) for $B = 0.5\Delta$, with other parameters as in Fig. 2.1. Blue solid curves show I_a, and black dashed curves I_0, both in units of $e\gamma_L\gamma_R/\hbar\Delta$. Top row: SOC α is varied for fixed field angle $\chi = 0$, with $n_g = 1$ (left) and $n_g = 2$ (right). Bottom row: χ is varied for fixed $\alpha = 1.2\Delta$, with $n_g = 1$ (left) and $n_g = 2$ (right).

Fig. 2.2 presents results for the dependence of the Josephson currents on the SOC and χ, denoting the relative angle between the SOC and the Zeeman field in our system. The upper panel of Fig. 2.2 illustrates the behavior of $I_{0,a}$ and $I_{0,a}$ as function of α for fixed $B = 0.5\Delta$. The steps in $I_{0,a}$ vs α can be traced back to level degeneracies. In other words our analysis here is still a perturbative one, in which we retain the lowest-order contributions to the Josephson current as the main terms to study. In presence of level-degeneracies, higher-order perturbative terms become important and smear out the steps. For the chosen parameters and $n_g = 2$, we have $N_0 = 2$ for all shown SOCs, but for $n_g = 1$ (in the upper left panel), $N_0 = 1$ for certain α. As evidence from the plots, the anomalous supercurrent is generally enhanced for odd N_0, if compared to the even-N_0 case.

The lower-row panels in Fig. 2.2 show the χ-dependence of $I_{a,0}$ for SOC $\alpha = 1.2\Delta$, confirming that the anomalous supercurrent is maximized for $\chi = 0 \bmod \pi$ but vanishes for $\chi = \pi/2$.

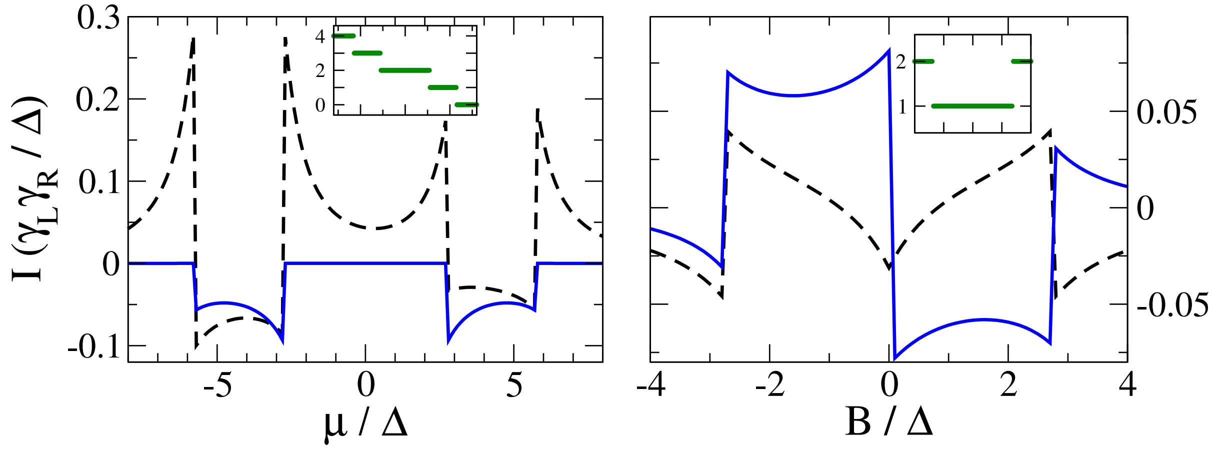

Figure 2.3: Same as Fig. 2.2 but showing $I_{a,0}$ vs μ for $B = 0.001\Delta$ (left), and $I_{a,0}$ vs B for $\mu = 3\Delta$ (right). Other parameters are as in Fig. 2.1 except for $E_c = 1.5\Delta$.

Further considerations to be made is that we observe that I_a is not drastically affected by interactions while I_0 becomes suppressed. This might suggest that the presence of interactions tends to enhance the relative importance of the anomalous supercurrent.

Next, we devote our analysis to the dependence of the Josephson current on the chemical potential μ and the Zeeman field. The left panel in Fig. 2.3, in fact, shows that even for $B = 0.001\Delta$, in the presence of interactions and with odd N_0, we can appreciate an anomalous supercurrent that is finite and sizeable.
Similarly, the right panel shows that for $B \to 0$, we obtain an unusual $I_a(B)$ dependence instead of the standard linear B-dependence reported in Ref. [50], where the non-interacting case has been studied and the following behavior for I_a has been found: $I_a \propto \alpha B$. In our analysis, as pointed out already, we expect higher-order perturbative corrections to smear out the cusps near $B = 0$ and eventually to lead to $I_a \propto \mathrm{sgn}(B)$. Next we observe that in general $Q_{32} \neq Q_{41}$, see Eq. (2.56). As long as $J_{32} \neq 0$, there are in principle no arguments that can let the anomalous supercurrent not flow. This could happen for arbitrary (including zero) SOC α. However, a finite Zeeman field is always needed to achieve this. In fact, when the $B = 0$ condition is realized, we find that $Q_{32} = Q_{41}$ due to level degeneracies ($E_1 = E_2$ and $E_3 = E_4$), see Eq. (2.54), and hence $I_a = 0$ for $B = 0$, as one might see in Fig. 2.1, upper plot. It is worth to point out that anomalous supercurrents can survive even for arbitrarily weak B, when interactions are present.

Let us now try to see analytically the case without SOC: setting $\alpha = 0$ in Eq. (2.55), we

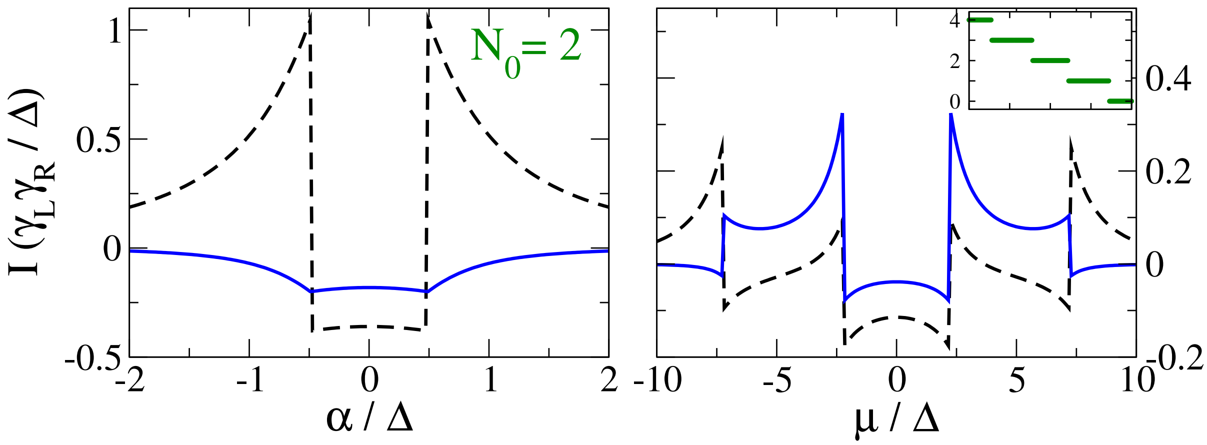

Figure 2.4: Same as Fig. 2.2 but showing $I_{a,0}$ vs α for $\mu = E_c = 0$ (left), and $I_{a,0}$ vs μ for $\alpha = 0$ and $E_c = 2\Delta$ (right). We use the parameters $\epsilon = 0.5\Delta$, $B = 0.7\Delta$, $n_g = 2$, $\chi = \lambda_{L,R} = \delta_R = 0$, and $\delta_L = \pi/2$.

observe that $I_a \neq 0$ is possible for relative inter-orbital phase shift $\delta \neq 0$, as one can read off from Eq. (2.20). So, we get the possibility of realizing an anomalous Josephson effect induced by the magnetic field alone, with no SOC, in a noninteracting multi-level dot.
This is evident in the left panel of Fig. 2.4, we present, for phase shifts $\delta_R = 0$ and $\delta_L = \pi/2$, a counter-intuitive increase in $|I_a|$ as the SOC is decreased and, moreover, the anomalous supercurrent is now an even function of the SOC parameter α. This is due to the fact that inter-orbital phase shifts $\delta = \pi/2$ are present. In this case $N_0 = 2$. As a matter of fact, here we find the largest possible anomalous supercurrent for $\alpha = 0$.
Finally, the right panel of Fig. 2.4 presents the μ-dependence of I_a, for $\alpha = 0$, where we see again that the anomalous supercurrent is enhanced whenever N_0 is odd.

2.4.1.2 Resonant level case

Another interesting and nontrivial situation emerges when the two bare levels are resonantly aligned. This case corresponds to $\epsilon = 0$ with arbitrary χ, in Eq. (2.18). The diagonalization matrix has the form:

$$U = \frac{1}{\sqrt{2}} \begin{pmatrix} \cos(\theta_+/2) & i\,\sin(\theta_+/2) & i\,\cos(\theta_-/2) & -\sin(\theta_-/2) \\ i\,\sin(\theta_+/2) & \cos(\theta_+/2) & -\sin(\theta_-/2) & i\,\cos(\theta_-/2) \\ i\,\cos(\theta_+/2) & -\sin(\theta_+/2) & \cos(\theta_-/2) & i\,\sin(\theta_-/2) \\ -\sin(\theta_+/2) & i\,\cos(\theta_+/2) & i\,\sin(\theta_-/2) & \cos(\theta_-/2) \end{pmatrix} \tag{2.58}$$

or, writing again by means of Pauli matrices in orbital and spin spaces:

$$U = e^{i\tau_x \pi/4} e^{i\hat{\theta}\sigma_x/2}. \tag{2.59}$$

In the last equation, $\hat{\theta} = \mathrm{diag}(\theta_+, \theta_-)$ is a diagonal matrix in orbital (τ) space. The angles $\theta_\pm$ follow from

$$\begin{aligned} \sin\hat{\theta} &= \begin{pmatrix} \sin\theta_+ & 0 \\ 0 & \sin\theta_- \end{pmatrix} = \frac{\alpha \sin\chi\, \tau_z}{\sqrt{\alpha^2 + B^2 + 2\alpha B \cos\chi\, \tau_z}}, \\ \cos\hat{\theta} &= \begin{pmatrix} \cos\theta_+ & 0 \\ 0 & \cos\theta_- \end{pmatrix} = \frac{B + \alpha \cos\chi\, \tau_z}{\sqrt{\alpha^2 + B^2 + 2\alpha B \cos\chi\, \tau_z}}. \end{aligned} \tag{2.60}$$

The angles can be put in a more compact form as follows:

$$e^{i\theta_\pm} = \frac{B \pm e^{i\chi}\alpha}{E_\pm}, \quad E_\pm = \sqrt{\alpha^2 + B^2 \pm 2\alpha B \cos\chi}. \tag{2.61}$$

$(E_1, \ldots, E_4) = \mu + (E_+, -E_+, E_-, -E_-)$ are the eigenstates of the matrix h as it appears in Eq. (2.18). The symmetric J matrix has the non-vanishing elements

$$J_{21} = \gamma_L \gamma_R \left(\cos\delta_L \sinh\lambda_R - \cos\delta_R \sinh\lambda_L\right) \tag{2.62}$$

and $J_{43} = -J_{21}$. Note that for $\epsilon \to 0$, Eq. (2.55) coincides with Eq. (2.62). For the anomalous Josephson current, we thus find

$$I_a = \Delta^2 J_{21} \left(Q_{21} - Q_{43}\right). \tag{2.63}$$

It is quite remarkably that J_{21} in Eq. (2.62) neither depends on the Zeeman field B nor on the SOC α. In principle, we may then expect $I_a \neq 0$ even for very small α and/or B. In addition, J_{21} does not depend on χ either. However, we also need to examine the contribution of the Q matrix. In fact, when $\alpha B \cos\chi = 0$, the level degeneracy $E_+ = E_-$ implies from Eq. (2.41) that $Q_{21} = Q_{43}$, which gives $I_a = 0$ for $\epsilon = 0$ and arbitrary E_c.

Discussion of figures and results

We now illustrate Fig. 2.5, for very small values of the magnetic field, for instance $B = 0.001\Delta$. The left panel indeed reveals a finite and sizeable anomalous supercurrent for $\alpha = B = 0.001\Delta$ if interactions are present, $E_c \neq 0$, and N_0 is odd. The right panel, instead, shows that $I_a \propto \mathrm{sgn}(\alpha B)$ for arbitrarily small but finite SOC α. We again encounter the possibility that $I_a \neq 0$ even for very small Zeeman field B and temperatures $T < |B|$, suggesting the

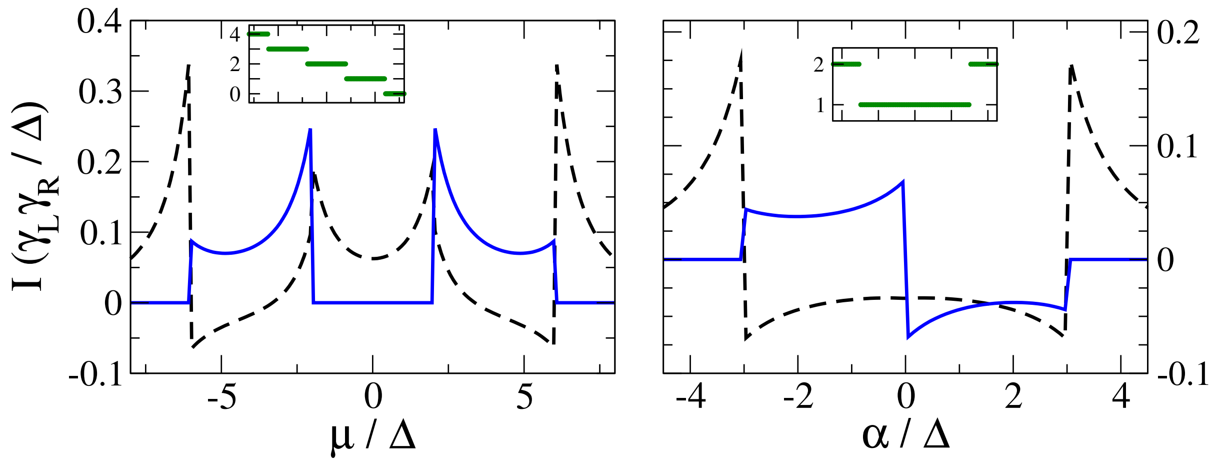

Figure 2.5: Same as Fig. 2.2 but for the resonant orbital ($\epsilon = 0$) case with tiny Zeeman field, $B = 0.001\Delta$. The left panel shows $I_{a,0}$ vs μ for $\alpha = 0.001\Delta$, while the right panel displays $I_{a,0}$ vs α for $\mu = 5\Delta$. The remaining parameters are as in Fig. 2.1.

incipient spontaneous breakdown of TRS. Here 'incipient' means that TRS is restored for $B = 0$. Remarkably, this onset behavior can be triggered by Coulomb interactions even for very small SOC α.

Next we aim at understanding the above $I_a \propto \mathrm{sgn}(\alpha B)$ onset behavior. We can simplify the algebra furthermore by putting $\chi = 0$. Thus we can consider the limiting case of very small but finite (B, α), where interactions play a crucial role. For $|\alpha| \gg |B|$, the arguments below show that the onset behavior $I_a \propto \mathrm{sgn}(B)$ is possible even when $E_c = 0$.

Equation (2.61) then gives $e^{i\theta_\pm} = \pm\mathrm{sgn}(\alpha)$ for $|\alpha| > |B|$, and thus the complex-valued unitary matrix in Eq. (2.59) has different limits for positive and negative SOC. In formula this reads: $\lim_{\alpha\to 0^+} U \neq \lim_{\alpha\to -0^+} U$.

To be more specific, we obtain

$$\lim_{\alpha\to 0^+} U = \frac{1}{\sqrt{2}} \begin{pmatrix} 1 & 0 & 0 & -1 \\ 0 & 1 & -1 & 0 \\ i & 0 & 0 & i \\ 0 & i & i & 0 \end{pmatrix}, \qquad \lim_{\alpha\to 0^-} U = \frac{1}{\sqrt{2}} \begin{pmatrix} 0 & i & i & 0 \\ i & 0 & 0 & i \\ 0 & -1 & 1 & 0 \\ -1 & 0 & 0 & 1 \end{pmatrix} \tag{2.64}$$

This corresponds to different residual 'magnetizations' of the $\tau \otimes \sigma$ isospin near the $SU(4)$ symmetric point in the parameter space defined by $B = \alpha = 0$. Next, the columns of U are eigenvectors of h and they four linearly independent isospin projections. The corresponding single-particle energy levels are

$$\mu + \{|\alpha| + \eta, -|\alpha| - \eta, |\alpha| - \eta, -|\alpha| + \eta\} \tag{2.65}$$

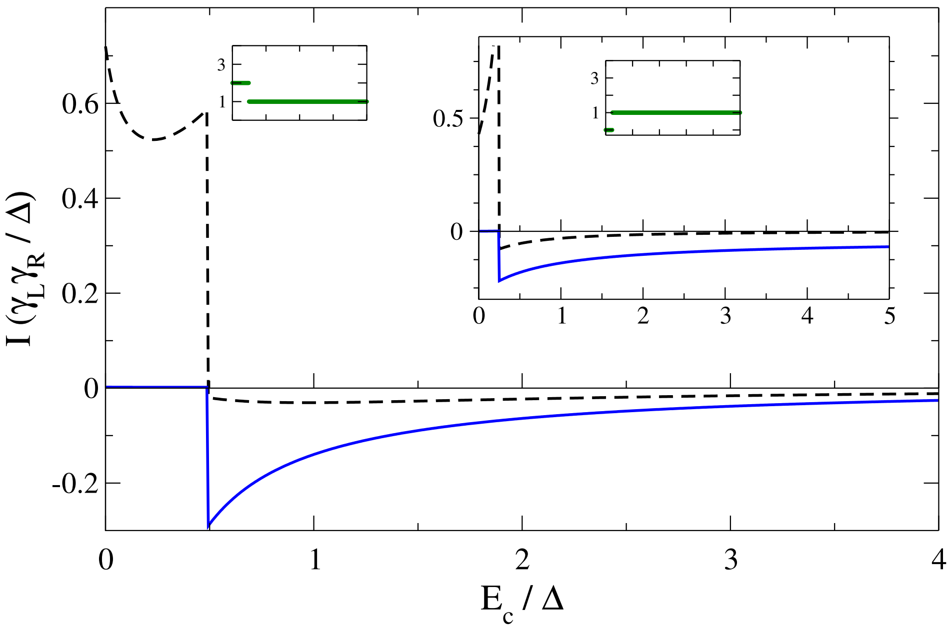

Figure 2.6: Same as Fig. 2.2 but showing $I_{a,0}$ vs E_c for $n_g = 2$ (main panel) and $n_g = 3/2$ (large right inset), with $\alpha = 0.5\Delta$, $B = 0.01\Delta$, and $\epsilon = 0.01\Delta$.

with $\eta = \text{sgn}(\alpha)B$. When μ is chosen such that $N_0 = 1$, assuming $B > 0$, one spin-down electron will occupy the single-particle level E_2 (E_4) for $\alpha > 0$ ($\alpha < 0$).
For $N_0 = 1$, we observe that

$$\text{sgn}(Q_{21}) = -\text{sgn}(Q_{43}) = -\text{sgn}(\alpha), \tag{2.66}$$

as one can see in Eq. (2.41), with $\mathcal{Q}_i > 0$. Therefore Eq. (2.63) suggests that we may have a finite anomalous supercurrent. However, for very small (B, α) and $E_c = 0$, the energy separation between states with different N_0 is also tiny. This could eventually lead to the mutual cancellation of all time-reversed contributions, having then $I_a = 0$ in the noninteracting case for very small B and α. Interactions play a crucial role because, for a finite charging energy, the energy gap between states with different N_0 scales with E_c, which effectively results in having a $N_0 = 1$ ground state more robust. Taking the small-(B, α) limit for finite E_c should then leave ground-state properties such as N_0 or the spin polarization unaffected, and $I_a \propto \text{sgn}(\alpha B)$ remains finite. However, the above arguments also show that I_a will be suppressed by thermal fluctuations once the temperature scale exceeds the Zeeman field scale, $T > |B|$. Therefore the $I_a \propto \text{sgn}(\alpha B)$ onset behavior just found for the ground state can 'only' be interpreted as incipient breakdown of TRS, i.e., TRS is restored by thermal fluctuations.

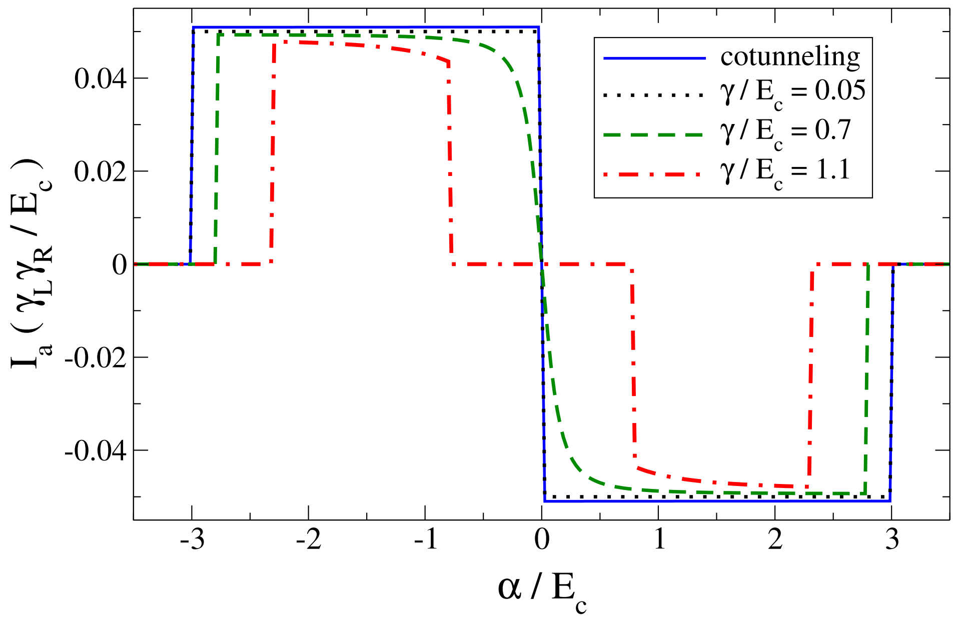

Figure 2.7: Anomalous supercurrent I_a for the two-orbital dot vs SOC α in the atomic limit ($\Delta \to \infty$) for several $\gamma = \gamma_L = \gamma_R$. The shown results follow from Eq. (2.68) and the effective dot Hamiltonian (2.47). The other parameters are as in the right panel of Fig. 2.5: $\epsilon = 0$, $B/E_c = 0.0005$, $\mu/E_c = 2.5$, $n_g = 2$, $\chi = \delta_{L,R} = \lambda_L = 0$, and $\lambda_R \to \infty$. The solid blue curve gives the respective cotunneling result [Eq. (2.63) with $\Delta \to \infty$] for $\gamma/E_c = 0.05$.

Finally, the interaction effects in this interesting parameter regime are displayed in Fig. 2.6, for values of SOC as $\alpha = 0.5\Delta$. While $I_a = 0$ for small E_c, we find $I_a \neq 0$ for $E_c \gtrsim |\alpha|$, with $|I_a|$ weakly decreasing in the limit of strong Coulomb blockade. For the resonant case of half-integer n_g, I_a saturates at a finite value for $E_c \to \infty$, cf. inset of Fig. 2.6.
Analytical results for the ground-state anomalous supercurrent are possible in the strong Coulomb blockade limit. For instance, at the charge degeneracy point $n_g = 3/2$ with $N_0 = 1$, Eq. (2.63) yields for small (B, α) the result

$$I_a = -3\,\mathrm{sgn}(\alpha B)\Delta^2 J_{21} \mathcal{Q}_3(\mu, 0, \mu) \quad \Longrightarrow \quad I_a \propto \mathrm{sgn}(\alpha B) \tag{2.67}$$

where J_{21} and $\mathcal{Q}_3(\mu, 0, \mu)$ are given in Eqs. (2.62) and (2.45), respectively. As conclusive remark, this confirms explicitly the onset behavior discussed above.

2.4.2 Superconducting atomic limit

In this section, we briefly discuss the anomalous Josephson effect in the superconducting atomic limit, already discussed in Sec. 2.3.2, where $\Delta \to \infty$, and the effective dot Hamiltonian

H_{eff}, in Eq. (2.47), allows us to go beyond the perturbative cotunneling regime. Evaluating the anomalous Josephson current, e.g., at the left contact, we obtain

$$I_a = -\frac{2e}{\hbar}\text{Im}\sum_{\nu<\mu}\tilde{\Gamma}^{(L)}_{\nu\mu}\langle c_\nu c_\mu\rangle\,, \tag{2.68}$$

where the brackets indicate a ground-state average using $H_{\text{eff}}(\varphi = 0)$. We consider the two-orbital dot in Sec. 2.2.2, where the 4×4 hybridization matrices $\tilde{\Gamma}^{(j)}$ follow from Eq. (2.19), after having performed the unitary transformation in favor of the c_ν fermion representation. As presented already in Sec. 2.3.2, the φ-dependent ground-state energies should be computed separately for the decoupled odd and even fermion parity subspaces. We then expect $I_a \neq 0$ only when the ground state, for $\varphi = 0$ has odd parity.

The dependence of I_a on the SOC α is illustrated in Fig. 2.7, where parameters are the same as in the right panel of Fig. 2.5. This allows us to study how the $I_a \propto \text{sgn}(\alpha B)$ onset behavior, the signature of incipient TRS breaking, emerges from the cusp features encountered in perturbation theory.

- We note from Fig. 2.7 that the cotunneling result (taking $\Delta \to \infty$ in the above expressions) matches the predictions of Eq. (2.68) for $\gamma_{L,R} \to 0$. This matching has also been confirmed analytically by perturbative expansion of the general $\Delta \to \infty$ cotunneling result, see Eqs. (2.28) and (2.49), to lowest nontrivial order in the hybridization matrices. Conclusion is that the limits $\gamma_{L,R} \to 0$ and $\Delta \to \infty$ do commute.

- Cusp-like features as seen in the right panel of Fig. 2.5 emerging under a perturbative theory will be smeared out by higher-order corrections, and indeed imply $I_a \propto \text{sgn}(\alpha B)$ onset behaviors associated with TRS breaking.

- Large hybridizations $\gamma_{L,R}$ could also possibly result in a change of the fermion parity of the resulting $\varphi = 0$ ground state. This is visible in Fig. 2.7, where we find $I_a = 0$ for small $|\alpha|$ and $\gamma/E_c = 1.1$ as a consequence of such a transition.

The message of this subsection is that the anomalous supercurrent tends to vanish either by raising $\gamma_{L,R}$ or by lowering E_c.

2.5 Majorana fermions physics

In this section, we will conclude the analysis of the ground-state Josephson CPR of the system by pointing out the second interesting phenomenon in such a setting, namely the possibility of realizing Majorana bound states (MBSs), in both non-interacting and interacting cases.

2.5.1 Introduction to Majorana fermions

A Majorana fermion is a particle that is its own antiparticle, whose notion can be tracked back to the early moments of the relativistic quantum mechanics. Their name is due to Ettore Majorana, [27], who showed, in 1937, that the complex Dirac equation can be decomposed into a pair of real wave-equations: each of them actually describes a real fermionic field, but with no possibility to distinguish between particle and antiparticle. This rewriting could look, at a first glance, as a mere formal step: it is possible to express a complex fermion as a superposition of two real Majorana fermions. Even though this seems a mathematical operation, the search for Majorana fermions in condensed matter physics has increased as well as the list of the proposals to realize them in various systems, see for instance Refs. [28, 31, 32]. We here focus on superconducting systems, in the specific case of a quantum dot between two s-waves superconducting leads, where the role of particles and antiparticles is played by electron and hole excitations, respectively. While electron excitations are filled states at energy $E > 0$, with $E = 0$ defining the Fermi level, holes are empty states with energy $-E$ below the Fermi level. At $E = 0$, from electron-hole symmetry it follows that the excitations are Majorana fermions. If we define the set $\{\xi^\dagger(E),\ \xi(E)\}$, of creation and annihilation operators for excitations at energy E, the relation between them will be

$$\xi(E) = \xi^\dagger(-E). \tag{2.69}$$

At the Fermi level they will coincide, implying $\xi = \xi^\dagger$. We can give some basic properties defining Majorana fermions. They anti-commute, for every pair of fermions considered

$$\xi_i\xi_j + \xi_j\xi_i = 2\delta_{ij}, \tag{2.70}$$

but the product $\xi_i^2 = 1$ doesn't vanish.
The first reasonably convincing experiment supporting the existence of Majorana fermions was reported in Ref. [36], where semiconductor nanowires coupled to superconductors have been considered. The presence of the s-wave superconductor induces a proximity superconducting gap ($\Delta \simeq 250\ \mu$V) on the nanowire. Moreover, such InSb nanowires are known to exhibit strong spin-orbit and a large g-factor. Here, the authors report spectroscopic measurements on the density of states in InSb nanowires contacted with one normal contact and one s-wave superconducting electrode held at temperature of the mK order. In the presence of magnetic fields, $B \sim 100$ mT, states at zero bias voltage, i.e. zero energy states, appear[4]. These bound

[4] A large g-factor is essential to dismiss the possible explanation of the zero-bias peak due to a Kondo resonance.

states remain fixed at zero bias even when magnetic fields and gate voltages vary considerably. They lead to a zero-energy peak (zero-bias peak), in the plot of the differential conductance (dI/dV) vs the applied voltage V, that is interpreted as a signature of Majorana fermions[5].

2.5.2 Realization of the Majorana bound states

We proceed by noting that all ingredients needed for the realization of Majorana fermions are in principle already present in our model, namely proximity-induced superconductivity, SOC, and a TRS-breaking magnetic field. The Majorana regime can be reached in the superconducting atomic limit of the two-level dot in Sec. 2.2.2, where the two orbitals correspond to two spatially separated single-level dots, i.e. a double quantum dot.

We use the atomic-limit effective Hamiltonian H_{eff} in Eq. (2.47) for the double dot. Using the basis

$$\{|1,\uparrow\rangle, |2,\downarrow\rangle, |1,\downarrow\rangle, |2,\uparrow\rangle\}, \tag{2.71}$$

the single-particle matrix h, as it appears in Eq. (2.18), has the representation

$$h = \begin{pmatrix} \mu + (\epsilon + B) & -\alpha \sin\chi & 0 & i\alpha\cos\chi \\ -\alpha\sin\chi & \mu - (\epsilon + B) & i\alpha\cos\chi & 0 \\ 0 & -i\alpha\cos\chi & \mu + (\epsilon - B) & \alpha\sin\chi \\ -i\alpha\cos\chi & 0 & \alpha\sin\chi & \mu - (\epsilon - B) \end{pmatrix}. \tag{2.72}$$

Without loss of generality, we consider the regime defined by $\alpha > 0$ and $B > 0$. The aim of this calculation is to map our system to a short Kitaev chain, see Refs. [30, 31, 32, 33], which is a 1D toy model with which one is able to theoretically observe the emergence of Majorana modes. Kitaev proposed a simple 1D tight-binding model of spinless electrons and a term encoding p-wave superconductivity. This chain can be rewritten through Majorana fermion operators and, according to the choice of parameters, the system can be driven to a (so-called non-trivial) phase so that every lattice site can host two Majorana fermion. Here, Majorana fermions sitting on different sites couple, leaving two unpaired Majorana fermions at both ends of the chain. The corresponding ground state is found to be two-fold degenerate.

To perform this mapping, we choose $\chi = \pi/2$, i.e., Zeeman and spin-orbit fields are perpendicular, consistent with Ref. [32]. Our single-particle matrix h is then block-diagonal with decoupled upper and lower two-state subspaces. The connection to the Kitaev chain becomes evident when ϵ is positive and chosen in the parameter regime

$$\Delta \gg \epsilon + B \gg \max\left(\alpha, |\epsilon - B|, \gamma_{L,R}, \mu, E_c\right). \tag{2.73}$$

[5]However, this interpretation is still debatable at this time.

The upper-block state $(2,\downarrow)$ will always be occupied, while the $(1,\uparrow)$ block is always empty. The upper left block in Eq. (2.72) can thus be projected away, and we are left to consider a truncated Hamiltonian, $H'_{\rm eff}$, which acts only within the lower right block described by the fermion operators, namely, $d_1 \equiv d_{1\downarrow}$ and $d_2 \equiv d_{2\uparrow}$, which can be regarded as spinless. The effective truncated Hamiltonian thus reads

$$\begin{aligned} H'_{\rm eff} &= (\mu+\epsilon-B)d_1^\dagger d_1 + [\mu-(\epsilon-B)]d_2^\dagger d_2 + E_c\left(d_1^\dagger d_1 + d_2^\dagger d_2 - n_g\right)^2 \\ &+ \left(\alpha d_1^\dagger d_2 + \tilde{\Delta}(\varphi)e^{i\vartheta(\varphi)}d_2^\dagger d_1^\dagger + \text{H.c.}\right), \end{aligned} \tag{2.74}$$

where the occupied $(2,\downarrow)$ state leads to a shift $n_g \to n_g+1$. With the hybridization matrix (2.19) for the double-dot, Eq. (2.47) yields the complex-valued effective pairing amplitude $\tilde{\Delta}e^{i\vartheta} = \frac{1}{2}\sum_j \gamma_j e^{-i(\phi_j+\delta_j)}$. Introducing $\gamma \equiv (\gamma_L+\gamma_R)/2$, and gauging away the overall phase $\sum_j(\phi_j+\delta_j)/2$, we obtain

$$\begin{aligned} \tilde{\Delta}(\varphi) &= \gamma\sqrt{1-T_0\sin^2[(\varphi+\delta)/2]}, \qquad T_0 = \frac{4\gamma_L\gamma_R}{(\gamma_L+\gamma_R)^2}, \\ \vartheta(\varphi) &= \tan^{-1}\left(\frac{\gamma_R-\gamma_L}{\gamma_R+\gamma_L}\tan[(\varphi+\delta)/2]\right), \end{aligned} \tag{2.75}$$

with the phase shift δ in Eq. (2.20). Note that $0 \le T_0 \le 1$ corresponds to the transmission probability of a single-channel quantum point contact (QPC), while $\tilde{\Delta}(\varphi)$ gives the Andreev level energy in the atomic limit, as in Ref. [69].

Non-interacting case

We proceed by first discussing the noninteracting case, $E_c = 0$, where two spatially resolved MBSs may appear when the necessary conditions

$$B = \epsilon, \quad \mu = 0 \tag{2.76}$$

are fulfilled. The effective Hamiltonian in Eq. (2.74) can be diagonalized in terms of fermionic Bogoliubov-de Gennes (BdG) quasiparticle operators,

$$\eta_\pm = \frac{1}{2}\left[d_1 + d_2 \pm e^{i\vartheta}\left(d_1^\dagger - d_2^\dagger\right)\right], \tag{2.77}$$

and re-formulated in the BdG Hamiltonian form

$$H'_{\rm eff} = \sum_\pm E_\pm(\varphi)\left(\eta_\pm^\dagger\eta_\pm - \frac{1}{2}\right), \quad E_\pm = \alpha \pm \tilde{\Delta}(\varphi). \tag{2.78}$$

The four possible single-particle eigenstates are constructed by applying the BdG operators $\eta_\pm^\dagger$ or $\eta_\pm$ to the vacuum state, with the respective energies $E_\pm/2$ and $-E_\pm/2$. The CPR follows as phase-derivative of Eq. (2.78),

$$I(\varphi) = 2\frac{\partial\tilde{\Delta}}{\partial\varphi}\,[\Theta(-E_+) - \Theta(-E_-)], \tag{2.79}$$

where Θ is the Heaviside function. Here

$$I(\varphi) = 0, \qquad \tilde{\Delta}(\varphi) < \alpha, \tag{2.80}$$

since both energies $E_\pm = \alpha \pm \tilde{\Delta}$ have the same sign. We therefore find

$$I(\varphi) = \Theta(\tilde{\Delta} - \alpha) I_0(\varphi), \qquad I_0(\varphi) = \frac{e\gamma}{2\hbar}\frac{T_0 \sin(\varphi + \delta)}{\sqrt{1 - T_0 \sin^2[(\varphi + \delta)/2]}}, \tag{2.81}$$

where $I_0(\varphi)$ coincides with the CPR of a single-channel quantum point contact with transparency T_0, as in Ref. [7], but here shifted by the inter-orbital phase difference δ.
The CPR (2.81) is 2π-periodic in φ and vanishes, or reappears, at the boundaries between ground states with opposite fermion parity. These boundaries are precisely the formation points of MBSs, as we show next.

Noting that both α and $\tilde{\Delta}$ are non-negative quantities, the zero-energy condition for MBS formation is satisfied for

$$E_-(\varphi) = 0 \iff \tilde{\Delta}(\varphi) = \alpha. \tag{2.82}$$

This corresponds to a pair of zero-energy MBSs, generated by the anticommuting Majorana fermion operators

$$\xi_1 = -i(\eta_- - \eta_-^\dagger), \qquad \xi_2 = \eta_- + \eta_-^\dagger, \tag{2.83}$$

that satisfy the condition in Eq. (2.69)

$$\xi_n = \xi_n^\dagger \tag{2.84}$$

and where $\xi_n^2 = 1$. Ensuring the MBSs to be spatially separated means avoiding recombination to a conventional fermion. This is achieved by imposing

$$\vartheta(\varphi) = 0 \bmod \pi, \tag{2.85}$$

where ξ_1 and ξ_2 have well-defined and different orbital quantum numbers. Therefore we claim that they correspond to different single-level dots in this double-dot configuration. Taking for instance $\vartheta = 0$, Eq. (2.77) yields $\xi_1 = -i(d_1 - d_1^\dagger)$ and $\xi_2 = d_2 + d_2^\dagger$, which indeed implies

that the MBS associated with $\xi_{n=1\ (2)}$ has the orbital wavefunction $n = 1$ (2).
We conclude that Eq. (2.85) ensures that both MBSs are 'separated' in orbital space. Through Eq. (2.75), there are two possibilities to satisfy this condition:

- We may choose equal hybridization strengths, $\gamma_L = \gamma_R = \gamma$. Therefore we get $T_0 = 1$, which implies $\tilde{\Delta} = \gamma|\cos[(\varphi + \delta)/2]| = \alpha$, with two solutions (for φ) when $\gamma > \alpha$. For these two phase values, MBSs will be present.

- Alternatively, for $\gamma_L \neq \gamma_R$, another possibility emerges by adjusting $\varphi = -\delta$ (mod 2π), where Eq. (2.82) allows for a MBS pair when $\gamma = \alpha$.

Interacting case

Now, it is interesting to study the result for the same system but in presence of weak electron-electron interactions, for which we continue using the global charging energy. This is justified by the fact that our double dot is in the regime of large-B field, see Eq. (2.73), and this means that both dots are occupied by one fermion at most. In this case the global charging energy equals a capacitative inter-dot interaction. For finite E_c, the system can be tuned to the MBS regime by replacing the condition $\mu = 0$ in Eq. (2.76) by $\mu = -2E_c(1 - n_g)$, i.e., by putting μ at the charge degeneracy point, always with $B = \epsilon$.
In terms of the $\eta_\pm$ operators in Eq. (2.77), the Hamiltonian (2.74) then reads

$$H = \sum_{\pm} E_\pm(\varphi)\left(\eta_\pm^\dagger \eta_\pm - \frac{1}{2}\right) + E_c\left(\eta_+^\dagger \eta_+ - \eta_-^\dagger \eta_-\right)^2, \tag{2.86}$$

with $E_\pm(\varphi)$ in Eq. (2.78). The MBS regime is realized when two ground states have opposite fermion parity. By examining the many-particle spectrum of Eq. (2.86),

$$\begin{aligned} E_{0,0} &= -\alpha, \quad E_{1,0} = \tilde{\Delta} + E_c, \\ E_{0,1} &= -\tilde{\Delta} + E_c, \quad E_{1,1} = \alpha, \end{aligned} \tag{2.87}$$

where E_{n_+,n_-} denotes the energy of a state with $n_\pm = \langle \eta_\pm^\dagger \eta_\pm \rangle$, the condition (2.82) for the appearance of MBSs is replaced by

$$\alpha = \tilde{\Delta}(\varphi) - E_c > 0. \tag{2.88}$$

In the MBS regime, one has a double-degenerate ground state, corresponding to negative energy eigenvalues $E_{0,1} = E_{0,0}$. Interactions thus only shift the conditions for Majorana formation, therefore below we focus on the non-interacting case.

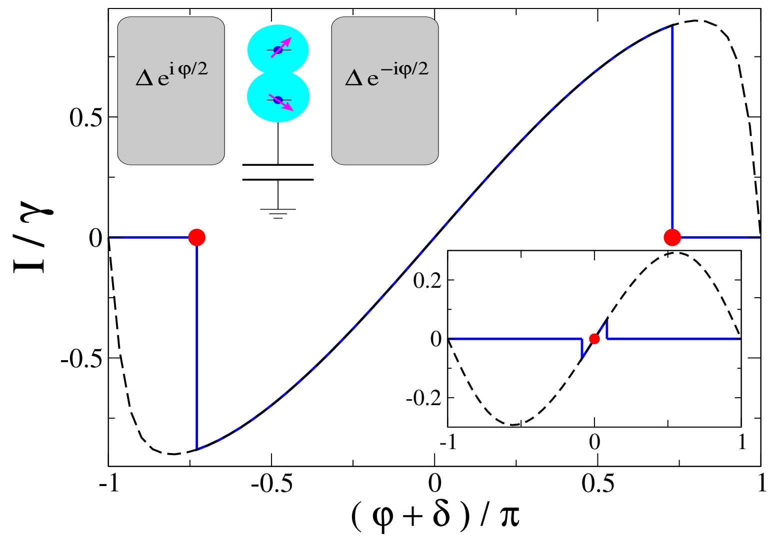

Figure 2.8: CPR in the atomic limit [see Eq. (2.73)] with $B = \epsilon$, $\mu = E_c = 0$, and $\chi = \pi/2$. Main panel: CPR (blue solid curve) for $\alpha = 0.4\gamma$, where $\gamma = (\gamma_L + \gamma_R)/2$ with slightly asymmetric $\gamma_{R,L}$ such that $T_0 = 0.99$. Red points on the CPR indicate that for the respective value of φ, a MBS pair is formed (see main text). The dashed black curve shows the CPR for $\alpha = 0$, where no MBSs occur. The top left inset shows the schematic setup. The bottom right inset gives the CPR for $\alpha = 0.99\gamma$ and significant hybridization asymmetry, $T_0 = 0.5$, as blue solid curve. The red point indicates MBS pair formation, and the dashed curve is for $\alpha = 0$ (without MBSs).

Discussion of the figure and results

In Fig. 2.8, we can notice that $I(\varphi) = 0$ within a part of the CPR: it represents the indirect signature for the MBSs. While jumps in the CPR can also have a different origin, the peculiar feature linked to the appearance of MBS pairs is the complete vanishing of the supercurrent in a finite phase interval. In the lower inset of Fig. 2.8, the asymmetric case is shown: it is illustrates the other two points on the CPR where the current vanishes correspond to spatially overlapping MBSs.

The Josephson current in Eq. (2.81) turns out to be nonzero (zero) for odd (even) N_0, where the CPR in general consists of two different regions: For $\tilde{\Delta}(\varphi) > \alpha$, we find $I = I_0(\varphi)$ as for a single-channel quantum point contact (but with a phase shift when $\delta \neq 0$), while $I = 0$ for $\tilde{\Delta} < \alpha$.

At the boundary between both regions, the parity $(-1)^{N_0}$ changes from odd to even, or eventually vice versa. It is precisely at these points that two degenerate 'half-fermion' BdG quasi-particle states appear. Under the described conditions, these can form a pair of spatially separated MBS.

Finally, as conclusion to this chapter, we point out that the MBSs discussed here do not mediate a Josephson current themselves, in contrast to the fractional Josephson effect for topologically protected Majoranas, as in Ref. [32].

Chapter 3

Andreev level population dynamics

3.1 Introduction

In this chapter, as briefly discussed already in Ch. 1, we present a comprehensive theoretical framework for the Andreev bound state population dynamics in another type of superconducting weak links. We investigate the Andreev bound state (ABS) population dynamics in a single-channel 'superconducting atomic contact' (SAC), i.e. a superconducting constriction or - equivalently - (short) weak link. Experiments, as in Ref. [7], have reported the existence of long-lived quasiparticles trapped in the ABS formed near these constrictions.

The structure of the remainder of this paper is as follows. In Sec. 3.2, we introduce a second-quantized formulation of the model. Here, the fermionic quasiparticles, i.e. the Andreev bound state and the continuum quasiparticles, are weakly coupled to the environmental phase fluctuations. In Sec. 3.3 we assume the electromagnetic environment to be in thermal equilibrium and we provide the master equation description of this model. We show that the density matrix for the quasiparticles can be factorized into an Andreev part, $\rho_A(t)$, and a diagonal density matrix describing the quasiparticles belonging to the continuum spectrum: important point is that diagonal and off-diagonal parts of $\rho_A(t)$ appear decoupled from each other. We also include relaxation of quasiparticles caused by phonons, and the resulting steady-state solution will be obtained solving two coupled nonlinear equations in a self-consistent way. In Sec. 3.4, as an application of our theory, we describe a charge imbalance effect, caused by an asymmetry in the transition rates between Andreev and continuum quasiparticles. Stressing that no external forces drive the system out of equilibrium in our model, the self-generated nonequilibrium distribution of continuum quasiparticles causes a phase-dependent quasiparticle current, and an asymmetric charge profile around the weak link. We also point

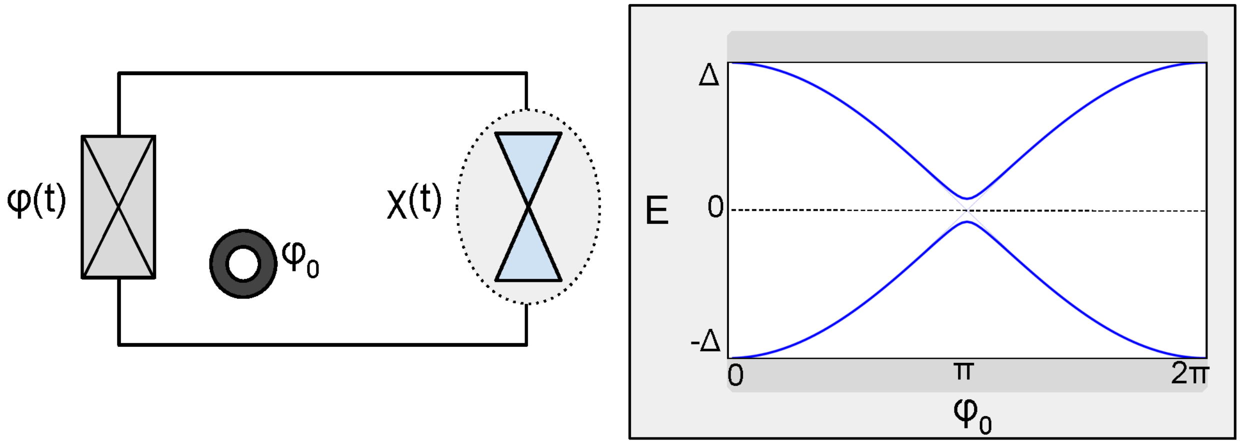

Figure 3.1: Left: schematic illustration of the SQUID geometry considered in this work, where the SAC is embedded into a ring containing a conventional Josephson junction that generates environmental phase fluctuations. The Andreev bound states are depicted in the right panel.

out that the predicted charge imbalance effect could be measured by superconducting-normal tunnel junction spectroscopy. To this one might refer to Refs. [94, 95, 96, 97]. Details about our calculations can be found in the Appendices.

3.2 Model

In the theory we will take into account transitions between different ABS configurations and also their interplay with quasiparticles constituting the continuum states. These transitions could be induced, e.g., by phonon-induced processes or by phase fluctuations caused by the environment: they also can change the fermion parity of the Andreev levels.
Even though the ground state has even parity, there are two spin-degenerate odd-parity Andreev bound state configurations with excitation energy

$$E_A(\varphi_0) = \Delta\sqrt{1 - \mathcal{T}\sin^2(\varphi_0/2)} \tag{3.1}$$

relative to the ground state, where φ_0 is the superconducting phase difference taken across the contact and $\mathcal{T}$ the normal-state transmission probability of the contact itself.
The occupation of such an odd-parity state causes quasiparticle poisoning, since the resulting Josephson current is blocked. This is a case in which the parity of the quantum state matters: here, the presence of a single quasiparticle can actually have effects on the macroscopic

response of the device.

In this section, we consider a single-channel SAC embedded in the asymmetric SQUID geometry sketched in Fig. 3.1, where the ring includes both the SAC and a conventional Josephson junction. In multi-channel quantum point contacts (QPC), one might observe long-living states of two trapped quasiparticles sitting in two different Andreev levels if they form a triplet state, keeping in mind that quasiparticle annihilation is forbidden in triplet states by spin conservation. Correspondingly, two transport modes result to be blocked ('spin blockade'). In the possible case of two-channels SAC, the SAC itself can be viewed as a quantum dot for $\Gamma \gg \Delta$ and it allows to study a two-orbital dot case with a mixture of spin-blockade and plasmon dynamics. But let us focus now on the single-channel SAC.
Denoting the superconducting phase differences across the SAC and the Josephson junction by φ and χ, respectively, both phases are linked by

$$\chi(t) - \varphi(t) + \varphi_0 = 0, \tag{3.2}$$

where the dimensionless parameter φ_0 is related to the magnetic flux threading the ring, in units of the flux quantum $h/2e$. Assuming $E_J \gg E_C$, i.e. the Josephson energy to be much bigger than the charging energy of the Josephson junction, $E_C = (2e)^2/2C$, with capacitance C, the SAC will see environmental electromagnetic modes that are well described by an effective LC circuit Hamiltonian,

$$H_{\mathrm{env}} = -E_C \frac{d^2}{d\chi^2} + \frac{E_J}{2}\chi^2, \tag{3.3}$$

corresponding to an undamped harmonic oscillator.
But, we will also include the effects of an additional shunt resistance R in the theory, as we will see in Sec. 3.3, and it will lead to a damping parameter $\eta_d = 1/(RC)$. We also stress that in the regime $E_J \gg E_C$ of interest here, fluctuations of χ are small, $\langle \chi^2 \rangle \ll 1$.
Turning to the single-channel SAC, the BCS Hamiltonian is written in terms of a two-component Nambu spinor

$$\psi(x) = (\psi_\uparrow(x), \psi_\downarrow^*(x))^T, \tag{3.4}$$

describing electrons in the left ($x < 0$) or right ($x > 0$) superconducting bank, with the SAC located at $x = 0$. Using the standard quasiclassical Andreev approximation, as in Ref. [69], we introduce the slowly varying envelope functions,

$$\psi(x) = e^{ik_F x}\psi_R(x) + e^{-ik_F x}\psi_L(x), \tag{3.5}$$

with Fermi momentum k_F. Combining the right- and left-moving envelopes into $\Psi(x) = (\psi_R, \psi_L)^T$, where each entry still carries the Nambu spinor structure, the time-dependent wave function satisfies the Bogoliubov-de Gennes (BdG) equation, whose details are to be found in Ref. [69], where we often set $\hbar = e = c = 1$

$$(i\partial_t - H_{\mathrm{BdG}})\,\Psi(x,t) = 0, \quad \text{with} \quad H_{\mathrm{BdG}} = v_F \tau_z \sigma_z(-i\partial_x) + \Delta \tau_0 \sigma_x, \tag{3.6}$$

with Fermi velocity v_F, the BCS gap Δ, and Pauli matrices $\sigma_{x,y,z}$ and $\tau_{x,y,z}$ in Nambu and right/left-mover space, respectively. In the remaining part of the chapter, the corresponding unit matrices σ_0 and τ_0 will not be written fully, but rather kept implicit.
Keeping as guideline for our calculations Ref. [87], the BdG solutions on both sides of the contact have to be matched at $x = 0$ by a transfer matrix,

$$\Psi(-0^+, t) = e^{i\sigma_z \varphi(t)/2} \begin{pmatrix} 1/d & r/d \\ r/d & 1/d \end{pmatrix} \Psi(0^+, t), \tag{3.7}$$

where $d = \sqrt{\mathcal{T}}$ and $r = \sqrt{\mathcal{R}}$ are the energy-independent transmission and reflection amplitudes, respectively, with $\mathcal{T} + \mathcal{R} = 1$. Eq. (3.10) can be rewritten in a more compact form in terms of the transmission probability only,

$$\Psi(-0^+, t) = \frac{e^{i\sigma_z \varphi(t)/2}}{\sqrt{\mathcal{T}}} \left(\tau_0 + \sqrt{1 - \mathcal{T}}\tau_x\right) \Psi(0^+, t), \tag{3.8}$$

which is 4π-periodic in φ.
For sake of simplicity, the transmission probability, $0 < \mathcal{T} \leq 1$, which characterizes the transparency of the constriction in the normal phase, is assumed to be energy-independent too. In our analysis, it is convenient to remove the time dependence from Eq. (3.8) by a gauge transformation,

$$\Psi(x,t) \to e^{-(i/4)\mathrm{sgn}(x)\chi(t)\tau_0\sigma_z}\Psi(x,t), \tag{3.9}$$

with $\chi(t)$ in Eq. (3.2). Since we assume low-inductance loop, i.e. small χ, and since the phase factor in Eq. (3.8) thereby becomes time-independent, with $\varphi(t) \to \varphi_0$, we obtain

$$H_{\mathrm{BdG}} \to H_{\mathrm{BdG}} + V, \tag{3.10}$$

where the interaction term is given by

$$V(x,t) = A(x)\dot{\chi}(t) + W(x)\chi(t) + \mathcal{O}\left(\chi^2\right), \tag{3.11}$$

with $\dot{\chi} = \partial_t \chi$, where

$$A(x) = -\frac{1}{4}\mathrm{sgn}(x)\tau_0\sigma_z, \quad W(x) = -\frac{\Delta}{2}\mathrm{sgn}(x)\tau_0\sigma_y. \tag{3.12}$$

Since $\langle \chi^2 \rangle \ll 1$, the linearized expression in Eq. (3.11) now couples the quasiparticle dynamics to the phase $\chi(t)$. Using the Josephson plasma frequency, $\Omega = \sqrt{2E_C E_J}$, where we assume $\Omega < \Delta$ throughout this thesis, the Lagrangian of the coupled system is

$$L(t) = \frac{1}{4E_C}\left(\dot{\chi}^2 - \Omega^2\chi^2\right) + \int dx\ \bar{\Psi}(i\partial_t - H_{\rm BdG} - V)\Psi. \tag{3.13}$$

with $\bar{\Psi} = (\Psi^*)^T$. Employing the momentum P_χ canonically conjugate to the phase χ, the corresponding Hamiltonian is

$$H = E_C\left(P_\chi + \int dx\ \bar{\Psi}A(x)\Psi\right)^2 + \frac{\Omega^2}{4E_C}\chi^2 + \int dx\ \bar{\Psi}[H_{\rm BdG} + W(x)\chi]\Psi. \tag{3.14}$$

3.2.1 Formulation in the second quantization language

We now switch to a second-quantized language by letting $\Psi(x) \to \hat{\Psi}(x)$, where the electron field operator, $\hat{\Psi}(x)$, is expanded in terms of the stationary solutions, $\Psi_\nu(x)$, with energy E_ν, of the BdG equation for time-independent matching condition (3.8), i.e., for $\varphi(t) = \varphi_0$. The wave functions $\Psi_\nu(x)$ thus represent the noninteracting SAC eigenstates.
We then reformulate the field operator $\hat{\Psi}(x)$ by introducing the corresponding quasiparticle creation (annihilation) operators $\gamma_\nu^\dagger$ (γ_ν), with the standard fermionic anticommutator algebra $\{\gamma_\nu, \gamma_{\nu'}^\dagger\} = \delta_{\nu\nu'}$, and we arrive at

$$\hat{\Psi}(x) = \sum_\nu \Psi_\nu(x)\gamma_\nu. \tag{3.15}$$

The noninteracting SAC Hamiltonian then reads

$$H_{\rm SAC} = \sum_\nu E_\nu \gamma_\nu^\dagger \gamma_\nu. \tag{3.16}$$

The quantum numbers ν include

- a pair of Andreev bound states, $\nu = \eta \equiv \pm$, where the energy $E_\eta = \eta E_A$, with $E_A(\varphi_0)$ in Eq. (3.1), is within the BCS gap, i.e. $E_A(\varphi_0) < |\Delta|$, and $\Psi_\eta(x)$ stays localized near the contact at $x = 0$;

- delocalized scattering states in the continuum, $\nu = p \equiv (E, s)$, where $|E| \geq \Delta$ and the index s (with $s = 1, 2, 3, 4$) refers to the four possible types of incoming states (from the left or right side, and of electron- or hole-like character).

The analytical form of the wave functions $\Psi_\nu(x)$ are provided in Appendix B, see also Ref. [93].

We discuss a second-quantization framework, stressing analogies and differences with Refs. [80, 93]. We here employ a semiconductor representation describing effectively spinless quasiparticles with either positive or negative energies, in contrast to Ref. [93], where the excitation picture, where one describes effectively spinless quasiparticles with only positive energies, is employed. In the semiconductor picture, in the ground state of H_{SAC}, all $E_\nu < 0$ states are occupied, including the ABS described by $\eta = -$. Using standard occupation number operators, $\hat{n}_\nu = \gamma_\nu^\dagger \gamma_\nu$, whose eigenvalues are $n_\nu = 0, 1$, the four possibilities for the occupation of the Andreev bound state sector are indexed by (n_+, n_-). The ground state, with energy $-E_A$, corresponds to the $(0,1)$ configuration, which we also denote by the Andreev state $|-\rangle_A$. This state carries the equilibrium Josephson supercurrent

$$I_A = -(2e/\hbar)\,\frac{\partial E_A}{\partial \varphi_0}. \tag{3.17}$$

The state $|-\rangle_A$ is an even-parity state, while the odd-parity sector corresponds to the spin-degenerate $(0,0)$ and $(1,1)$ states, with excitation energy E_A relative to the ground state. The odd-parity states, with $n_+ + n_- = 0$ and 2 respectively, are denoted by

$$|0\rangle_A = \gamma_- |-\rangle_A, \quad |2\rangle_A = \gamma_+^\dagger |-\rangle_A, \tag{3.18}$$

and imply a vanishing Andreev supercurrent, consistent with the 'quasiparticle poisoning' scenario. The lifetime of these states can reach the millisecond regime for high transparency, $\mathcal{T} \to 1$, and they decay as a function of E_A/Δ, exhibiting nearly universal scaling behavior. Finally, the $(1,0)$ even-parity state, denoted as

$$|+\rangle_A = \gamma_+^\dagger \gamma_- |-\rangle_A, \tag{3.19}$$

represents an excited 'Andreev Cooper pair' localized at the contact, with excitation energy $2E_A$ above the ground state. The $|+\rangle_A$ state carries the Josephson current $-I_A$, with opposite sign as compared to $|-\rangle_A$, but rather quickly relaxes to the ground state.

Turning back to our problem, the second-quantized form of the interacting Hamiltonian (3.14) is thus given by

$$H = E_C (P_\chi + \bar{A})^2 + \frac{\Omega^2}{4E_C}\chi^2 + H_{\mathrm{SAC}} + \chi \sum_{\nu,\nu'} W_{\nu\nu'} \gamma_\nu^\dagger \gamma_{\nu'}, \tag{3.20}$$

where $\bar{A} = \sum_{\nu,\nu'} A_{\nu\nu'} \gamma_\nu^\dagger \gamma_{\nu'}$ plays the role of a vector potential. The matrix elements

$$A_{\nu\nu'} = \int dx\ \Psi_\nu^\dagger A(x) \Psi_{\nu'}, \quad W_{\nu\nu'} = \int dx\ \Psi_\nu^\dagger W(x) \Psi_{\nu'}, \tag{3.21}$$

are discussed below. For convenience, we now shift

$$P_\chi \to P_\chi - \bar{A} \tag{3.22}$$

via a unitary transformation, $H \to UHU^\dagger$ with $U = e^{i\bar{A}\chi}$, and represent the unitarily transformed phase χ and its canonically conjugated momentum P_χ by a standard boson operator, b, with commutator $[b, b^\dagger] = 1$, such that

$$\chi = \sqrt{E_C/\Omega}\,(b + b^\dagger), \quad P_\chi = -i\,2\sqrt{\Omega/E_C}\,(b + b^\dagger). \tag{3.23}$$

We then arrive at the Hamiltonian in its final form, up to an irrelevant constant,

$$H = H_{\rm SAC} + \Omega b^\dagger b + \lambda\left(b + b^\dagger\right)\hat{I}_S, \tag{3.24}$$

describing fermionic (Andreev level and continuum) quasiparticles coupled to an oscillator mode with the plasma frequency Ω. For $E_J \gg E_C$, we are effectively in the weak-coupling regime, $\lambda \ll 1$, with the dimensionless coupling strength $\lambda = \sqrt{E_C/4\Omega}$.
Finally, the Josephson current operator in Eq. (3.24) is

$$\begin{aligned} \hat{I}_S &= \sum_{\nu,\nu'} \mathcal{I}_{\nu\nu'} \gamma_\nu^\dagger \gamma_{\nu'}, \\ \mathcal{I}_{\nu\nu'} &= 2W_{\nu\nu'} - 2i\left(E_\nu - E_{\nu'}\right) A_{\nu\nu'}. \end{aligned} \tag{3.25}$$

Let us discuss the matrix elements $\mathcal{I}_{\nu\nu'}$ in more detail. From Eq. (3.25), we first need to determine the corresponding matrix elements $A_{\eta,p}$ and $W_{\eta,p}$. Using the auxiliary quantities

$$\begin{aligned} u &= \frac{1}{\eta \sin\theta_\eta + i\eta_E \sinh\theta_E}, \\ z &= \frac{1}{2}\left(e^{(\theta_E + i\theta_\eta)/2} - \eta\eta_E e^{-(\theta_E + i\theta_\eta)/2}\right), \end{aligned} \tag{3.26}$$

as well as the definitions in App. B, we find

$$\begin{aligned} \begin{pmatrix} W_{\eta,p}/\Delta \\ 2A_{\eta,p} \end{pmatrix} &= \sqrt{\frac{\xi_0}{8L\cosh\theta_E}} \Bigg\{ u^*[(c - \eta_E a)\eta A_\eta + (b + \eta_E d)B_\eta] \begin{pmatrix} i\eta z \\ z^* \end{pmatrix} \\ &+ u\left[(\delta_{s,1} - \eta_E \delta_{s,4})A_\eta - (\eta_E \delta_{s,2} + \delta_{s,3})\eta B_\eta\right] \begin{pmatrix} i\eta z^* \\ z \end{pmatrix} \Bigg\}. \end{aligned} \tag{3.27}$$

Equation (3.25) then yields the current matrix elements $\mathcal{I}_{\eta,p}$.

3.2.2 Derivation of the current

This subsection is devoted to the study of the currents in the system: we will analyze the current generated from transitions between continuum states at the same (or different) energy, then we will write down the form of the current pertinent to the Andreev level sector only, and, finally, the contributions coming from the 'Andreev to Continuum' transitions.

We first note that due to the spatial homogeneity of the extended quasiparticle states, since they are plane waves, away from the contact, the matrix elements $A_{pp'}$ and $W_{pp'}$, and hence also $\mathcal{I}_{pp'}$, between continuum states can be finite only when their energies match, $E = E'$, i.e., phase fluctuations do not induce intraband transitions. Moreover, one finds that $W_{pp'} = 0$ even for $E = E'$, implying that $\mathcal{I}_{pp'} = 0$. The explanation is that in the limit $L \to \infty$, only states with $E = E'$ can have a finite matrix element. Taking into account that the Nambu spinors (B.5) satisfy the relations $\bar{\psi}_{e,h}\sigma_y\psi_{e,h} = 0$ and $\bar{\psi}_{e,h}\sigma_z\psi_{e,h} = \pm\tanh\theta_E$, one then finds $W_{pp'} = 0$. Although the matrix elements $A_{pp'}$ are nonzero, they do not contribute to $\mathcal{I}_{pp'}$ because they appear together with a factor $(E - E') = 0$.
In this theoretical framework, delocalized continuum states can contribute to the supercurrent $\hat{I}_S$ only via transitions mixing them with Andreev levels.

The Josephson current operator then contains a part $\hat{I}_A$, coming from the Andreev sector only, and a part $\hat{I}_{cA}$, describing the mixing of continuum and Andreev states,

$$\hat{I}_S = \hat{I}_A + \hat{I}_{cA}. \tag{3.28}$$

For the pure Andreev current, as in Refs. [86, 87], we find

$$\hat{I}_A = -\frac{\mathcal{T}\Delta^2\sin(\varphi_0/2)}{E_A}\ \gamma^\dagger\left[\cos(\varphi_0/2)\eta_z - \sqrt{1-\mathcal{T}}\sin(\varphi_0/2)\eta_y\right]\gamma, \tag{3.29}$$

where $\gamma = (\gamma_+, \gamma_-)^T$ combines the two Andreev level fermion operators, and the Pauli matrices set, $\{\eta_{x,y,z}\}$, acts in the corresponding space. Note that the Andreev current operator (3.29) is written in the energy representation, and that in this representation the Hamiltonian projected to the Andreev sector is diagonal,

$$H_A = E_A\gamma^\dagger\eta_z\gamma. \tag{3.30}$$

For non-ideal transparency of the contact, $\mathcal{T} < 1$,

$$[\hat{I}_A, H_A] \neq 0. \tag{3.31}$$

This renders the Andreev level eigenstates superpositions of current eigenstates implying that strong fluctuations of the supercurrent, resulting form the normal backscattering in the SAC, are generated for $\varphi_0 \approx \pi$, as in Ref. [87].

Similarly, the supercurrent contribution caused by the mixing of continuum and Andreev states is

$$\hat{I}_{cA} = \sum_{\eta=\pm} \sum_{p=(E,s)} \mathcal{I}_{\eta,p} \gamma_\eta^\dagger \gamma_p + \text{h.c.}, \tag{3.32}$$

where the matrix elements $\mathcal{I}_{\eta,p}$ are specified in Eq. (3.25). $\hat{I}_{cA}$ describes the mixing of the Andreev bound state at energy ηE_A, with $\eta = \pm$, and the continuum state with $p = (E, s)$, where $\eta_E = \text{sgn}(E)$ and $|E| \geq \Delta$.

Finally, the total current flowing through the contact also contains a conventional dissipative quasiparticle contribution due to continuum states, I_{qp}, on top of the supercurrent contribution $\langle \hat{I}_S \rangle$. This contribution follows from the Ψ_p in Eq. (B.4),

$$I_{\text{qp}} = e v_F \sum_{p=(E,s)} n_p \bar{\Psi}_p \tau_z \Psi_p, \tag{3.33}$$

where the Pauli matrix τ_z acts in left-right mover space, see Sec. 3.2. Using the s-dependent scattering amplitudes (a, b, c, d) in App. B, we find

$$\begin{aligned} I_{\text{qp}} &= \frac{e}{2\pi\hbar} \sum_{s=1}^{4} \int_{|E|\geq\Delta} \frac{|E| dE}{\sqrt{E^2 - \Delta^2}} \, n_{(E,s)} \\ &\times \left[(\delta_{s,1} + \delta_{s,2}) \left(|c_s|^2 - |d_s|^2 \right) + (\delta_{s,3} + \delta_{s,4}) \left(|a_s|^2 - |b_s|^2 \right) \right] \end{aligned} \tag{3.34}$$

3.3 The master equation approach

To study the physics described by the interacting Hamiltonian,

$$H = H_0 + V, \tag{3.35}$$

with the noninteracting piece and the interaction contribution

$$H_0 = H_{\text{SAC}} + \Omega b^\dagger b, \quad V = \lambda (b + b^\dagger) \hat{I}_S \tag{3.36}$$

we now turn to a master equation approach. To this aim, we assume that the plasma mode remains in thermal equilibrium with a heat bath of temperature T_{env} at all times, in order to neglect feedback effects on the phase dynamics.

Within the master equation framework, see Ref. [69], the Liouville-von Neumann equation for the density matrix of the complete system, ρ_{tot}, is expanded to second order in the small interaction parameter $\lambda \ll 1$. Writing time-dependent operators in the interaction picture as $\mathcal{O}(t) = e^{iH_0 t}\mathcal{O}e^{-iH_0 t}$, the density matrix then obeys the equation

$$\partial_t \rho_{\text{tot}}(t) = -\int_0^t d\tau \, [V(t), [V(t-\tau), \rho_{\text{tot}}(t-\tau)]] - i[V(t), \rho_{\text{tot}}(0)]. \tag{3.37}$$

Our assumption of thermal equilibrium for the plasma mode allows for a factorized form of the density matrix,

$$\rho_{\text{tot}}(t) = \rho_{\text{osc}} \otimes \rho(t), \tag{3.38}$$

where $\rho_{\text{osc}} \sim e^{-(\Omega/T_{\text{env}})b^\dagger b}$ is a thermal density matrix for the plasma mode and $\rho(t)$ describes the time evolution of fermionic quasiparticles. Taking the trace over the oscillator degree of freedom, Eq. (3.37) yields

$$\partial_t \rho(t) = -\int_0^\infty d\tau \Big[D(\tau)\hat{I}_S(t)\hat{I}_S(t-\tau)\rho(t) - D(-\tau)\hat{I}_S(t)\rho(t)\hat{I}_S(t-\tau) \Big] + \text{h.c.}\,, \tag{3.39}$$

where we have employed the Markov approximation[1], valid at long times t and not too low temperatures. In Eq. (3.39) the boson correlator function reads

$$D(\tau) = \int_0^\infty d\omega J(\omega) \left[(n_B(\omega) + 1)\, e^{-i\omega\tau} + n_B(\omega) e^{i\omega\tau} \right], \tag{3.40}$$

with the Bose function,

$$n_B(\omega) = \frac{1}{e^{\omega/T_{\text{env}}} - 1}, \tag{3.41}$$

and the environmental spectral density function, with the property $J(\omega) = -J(-\omega)$,

$$J(\omega) = \frac{\lambda^2 \eta_d}{2\pi} \left(\frac{1}{(\omega-\Omega)^2 + \eta_d^2/4} - \frac{1}{(\omega+\Omega)^2 + \eta_d^2/4} \right). \tag{3.42}$$

Moreover

$$J(\omega)\,(1 + n_B(\omega)) = J(-\omega) n_B(-\omega). \tag{3.43}$$

We use Eq. (3.42) below also for $\omega < 0$, and directly include the Ohmic damping parameter, η_d, to capture the effects of a shunt resistance. For $\eta_d \to 0$, the spectral density has the limit

$$J(\omega) = \lambda^2 \delta(|\omega| - \Omega)\text{sgn}(\omega). \tag{3.44}$$

[1]Specifically, the Markov approximation amounts to replacing $\rho(t-\tau) \to \rho(t)$ and neglecting the last term (describing correlations with the initial state) in Eq. (3.37). This step is valid for temperatures above λ^2/Δ.

For finite η_d, Eq. (3.42) exhibits sharp peaks for $|\omega| = \Omega$.

The equation of motion (3.39) is still quite difficult to deal with, and we shall here proceed by making two approximations.

- We neglect entanglement between the Andreev and continuum quasiparticles, which means that the reduced density matrix factorizes into an Andreev part and a continuum part,

$$\rho(t) = \rho_A(t) \otimes \rho_c(t). \tag{3.45}$$

  This approximation is justified in the weak-coupling regime $\lambda \ll 1$, since higher-order terms in λ are needed to coherently couple Andreev and continuum states[2]. The factorized density matrix (3.45) is expected to be highly accurate away from the zero-temperature limit, since the thermal energy uncertainty causes a blurring of continuum quasiparticle wavepackets that rapidly destroys entanglement between Andreev and continuum states.

- We also assume that the density matrix $\rho_c(t)$ describing continuum quasiparticles remains diagonal during the time evolution. This approximation is justified by noting that there are no direct matrix elements in H connecting different continuum states, and implies that $\rho_c(t)$ is fully determined by specifying the time-dependent occupation probabilities $n_p(t)$ of continuum states,

$$\rho_c(t) = \prod_p \Big[n_p(t) \, |1_p\rangle \, \langle 1_p| + [1 - n_p(t)] \, |0_p\rangle \, \langle 0_p| \Big], \tag{3.46}$$

  where $|1_p\rangle = \gamma_p^\dagger |0_p\rangle$ corresponds to a filled single-particle state $p = (E, s)$. Note that $\rho_c(t)$ in Eq. (3.46) is always normalized, $\mathrm{Tr}_c\,[\rho_c(t)] = 1$. On the other hand, the density matrix $\rho_A(t)$ describing the Andreev sector, with normalization condition $\mathrm{Tr}_A\,[\rho_A(t)] = 1$, may have off-diagonal entries reflecting quantum coherence.

Tracing over the Andreev part in Eq. (3.39) then yields an equation of motion for the continuum state occupation numbers $n_p(t)$. Similarly, tracing instead over the continuum states, one obtains an equation for the time evolution of the reduced Andreev density matrix

[2] Mathematically speaking, we here construct an asymptotic solution for the reduced density matrix of the form $\rho_0(\zeta t) + \zeta \rho_1(t)$, where ζ is a small expansion parameter $\propto \lambda^2 \ll 1$, which reflects the weakness of the coupling λ. The first term corresponds to Eq. (3.45) and is 'slow' on the timescale $1/\Delta$, while the second term contains off-diagonal terms oscillating with frequencies $\gtrsim (\Delta - E_A)$. This term is therefore 'fast' and remains small.

$\rho_A(t)$. In these equations, the transition rates between different levels follow from the Fermi golden rule,

$$\Gamma_{\nu\nu'} = \frac{2\pi}{\hbar} |\mathcal{I}_{\nu\nu'}|^2 \left[1 + n_B\left(E_\nu - E_{\nu'}\right)\right] J\left(E_\nu - E_{\nu'}\right), \tag{3.47}$$

with the Bose function $n_B(\omega)$ in Eq. (3.41) and the spectral density $J(\omega)$ in Eq. (3.42). By using Eq. (3.29), we observe that the direct rates connecting different Andreev states are given by

$$\Gamma_{\eta,-\eta} = \frac{2\pi}{\hbar}(1-\mathcal{T})\frac{(\Delta^2 - E_A^2)^2}{E_A^2}\left[\delta_{\eta,+} + n_B(2E_A)\right] J(2E_A). \tag{3.48}$$

These rates vanish for perfect transparency, $\mathcal{T} \to 1$.

Recalling now that $\mathcal{I}_{pp'} = 0$ for arbitrary $\mathcal{T}$, we see that transition rates between continuum states are always absent, $\Gamma_{pp'} = 0$. Finally, the supercurrent matrix elements between Andreev and continuum states, $\mathcal{I}_{\eta p}$, see Eq. (3.25), determine the corresponding transition rates, $\Gamma_{\eta,p}$, for exciting an Andreev quasiparticle into the continuum, plus the reverse process with rate $\Gamma_{p,\eta}$. Such transitions must involve the absorption or emission of an environmental photon. Since $|E| \geq \Delta$ and the spectral density is sharply peaked around the Josephson plasma frequency Ω, those rates are sizeable only when $\Omega > \Delta - E_A$, see Ref. [93].

Tracing now over the Andreev sector in Eq. (3.39), we find

$$\partial_t n_p = -\sum_{\eta=\pm}\left[\Gamma_{p,\eta}(1-n_\eta)n_p - \Gamma_{\eta,p}(1-n_p)n_\eta\right]. \tag{3.49}$$

The time-dependent continuum state distribution function, $\{n_p(t)\}$, thereby couples to the Andreev level occupation probabilities,

$$n_\eta(t) = \mathrm{Tr}_A\left[\hat{n}_\eta \rho_A(t)\right], \quad \hat{n}_\eta = \gamma_\eta^\dagger \gamma_\eta. \tag{3.50}$$

Tracing instead over the continuum states in Eq. (3.39), we find ($\{A, B\}$ denotes the anti-commutator)

$$\begin{aligned}
\partial_t \rho_A(t) &= -\frac{1}{2}\sum_\eta \Gamma_{\eta,-\eta}\left\{\hat{n}_\eta(1-\hat{n}_{-\eta}), \rho_A(t)\right\} + \sum_\eta \Gamma_{-\eta,\eta}\gamma_\eta^\dagger\gamma_{-\eta}\rho_A(t)\gamma_{-\eta}^\dagger\gamma_\eta \\
&- \sum_{p,\eta}\Gamma_{p,\eta}n_p(t)\left(\frac{1}{2}\left\{1-\hat{n}_\eta, \rho_A(t)\right\} - \gamma_\eta^\dagger\rho_A(t)\gamma_\eta\right) \\
&- \sum_{p,\eta}\Gamma_{\eta,p}[1-n_p(t)]\left(\frac{1}{2}\left\{\hat{n}_\eta, \rho_A(t)\right\} - \gamma_\eta\rho_A(t)\gamma_\eta^\dagger\right).
\end{aligned} \tag{3.51}$$

Moreover, the terms $\sim \gamma_\eta^\dagger \rho_A(t)\gamma_\eta$ and $\sim \gamma_\eta \rho_A(t)\gamma_\eta^\dagger$ in Eq. (3.51) describe 'parity jumps', in the language of Andreev quasiparticles, where the fermion number parity of Andreev quasiparticles can change. The basis we are going to use here and in Sec. 3.3.2 is the Andreev level basis: the generic matrix element is

$$\rho_{\nu\nu'}(t) = \langle \nu|\rho(t)|\nu'\rangle, \tag{3.52}$$

and the basis used is

$$|\nu\rangle \in \{|0\rangle,\ |\eta = \pm\rangle = \gamma_\eta^\dagger|0\rangle,\ |2\rangle = \gamma_+^\dagger\gamma_-^\dagger|0\rangle\} \tag{3.53}$$

Since there are four Andreev configurations (n_+, n_-), the Andreev density matrix is a 4×4 matrix. We here represent $\rho_A(t)$ in the basis spanned by the Andreev ground state $|-\rangle_A$, corresponding to the $(0,1)$ configuration, the spin-degenerate odd-parity states $|0\rangle_A$ and $|2\rangle_A$ in Eq. (3.18), and the excited even-parity state $|+\rangle_A$ in Eq. (3.19).

3.3.1 Diagonal Andreev density matrix elements

The diagonal elements of $\rho_A(t)$ yield the respective occupation probabilities, $P_0(t) = {}_A\langle 0|\rho_A(t)|0\rangle_A$, and likewise for $P_{\eta=\pm}(t)$ and $P_2(t)$. Thereby the normalization condition for $\rho_A(t)$ gives

$$P_0(t) + P_2(t) + \sum_\eta P_\eta(t) = 1, \tag{3.54}$$

and the $n_{\eta=\pm}(t)$ in Eq. (3.49) are expressed as

$$n_\eta(t) = P_\eta(t) + P_2(t). \tag{3.55}$$

We now observe that the off-diagonal components of $\rho_A(t)$ decouple from the equations for the diagonal part in Eq. (3.51): the latter determines the dynamics of the Andreev state occupation probabilities, where we find

$$\dot{P}_\eta = -\Gamma_{\eta,-\eta}P_\eta + \Gamma_{-\eta,\eta}P_{-\eta} \sum_p \Big[n_p\left(\Gamma_{p,-\eta}P_\eta - \Gamma_{p,\eta}P_0\right) + (1-n_p)\left(\Gamma_{\eta,p}P_\eta - \Gamma_{-\eta,p}P_2\right)\Big] \tag{3.56}$$

and

$$\begin{aligned} \dot{P}_0 &= -\sum_{p,\eta=\pm}\left[\Gamma_{p,\eta}n_pP_0 - \Gamma_{\eta,p}(1-n_p)P_\eta\right], \\ \dot{P}_2 &= -\sum_{p,\eta}\left[\Gamma_{\eta,p}(1-n_p)P_2 - \Gamma_{p,-\eta}n_pP_\eta\right]. \end{aligned} \tag{3.57}$$

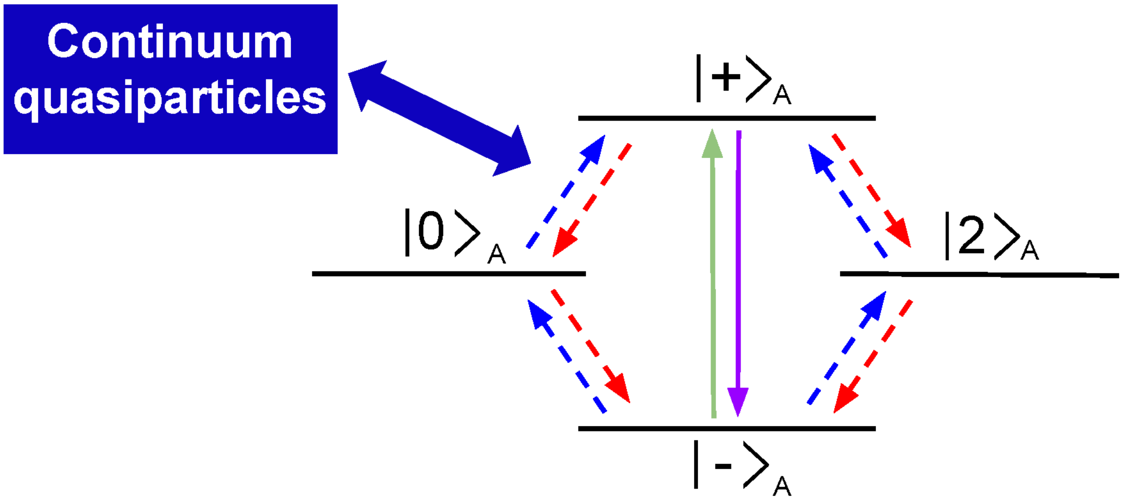

Figure 3.2: Schematic illustration of the rate equation dynamics (see text). Direct transitions (solid arrows) connect the Andreev level ground state, $|-\rangle_A$, to the excited state $|+\rangle_A$. Transitions to the two degenerate odd-parity states (dashed arrows), $|0\rangle_A$ and $|2\rangle_A$, are mediated through quasiparticle continuum states with energy $|E| \geq \Delta$, which we indicate by a blue box.

Together with Eq. (3.49), we thereby arrive at a set of coupled nonlinear equations determining the time-dependent continuum distribution function, $\{n_p(t)\}$, and the Andreev level probabilities, $P_{\pm,0,2}(t)$. Importantly, despite of the approximations involved in their derivation, these coupled equations automatically satisfy the normalization condition (3.54). The resulting Andreev bound state population dynamics is schematically illustrated in Fig. 3.2. The rates $\Gamma_{\eta,-\eta}$ in Eq. (3.48) connect the even-parity Andreev states $|\eta = \pm\rangle_A$, without involving continuum quasiparticles. However, processes that populate or depopulate odd-parity Andreev states sensitively depend on the continuum distribution function $\{n_p(t)\}$.

3.3.2 Off-diagonal Andreev density matrix elements

Within the master equation approach, we saw that diagonal and off-diagonal components of the Andreev density matrix $\rho_A(t)$ are actually decoupled from each other, with the off-diagonal sector obeying its own set of dynamical equations.

Taking into account Hermiticity of the Andreev density matrix $\rho_A(t)$, we can project the off-diagonal parts of the Andreev density matrix on the basis in Eq. (3.53), by using

$$\gamma_\eta = |0\rangle\langle\eta| + \eta|-\eta\rangle\langle 2|. \tag{3.58}$$

The dynamics of the even-parity matrix elements is determined by

$$\partial_t \rho_{+,-}(t) = -\frac{1}{2}\sum_{\eta}\Big[\Gamma_{\eta,-\eta} + \sum_{p}\Big\{n_p(t)\Gamma_{p,\eta} + [1-n_p(t)]\Gamma_{\eta,p}\Big\}\Big]\rho_{+,-}(t). \tag{3.59}$$

and for matrix elements connecting states with different parity we obtain

$$\begin{aligned}
\partial_t \rho_{\eta,0} &= -\frac{1}{2}\Big\{\Gamma_{\eta,-\eta} + \sum_p\Big[n_p\left(2\Gamma_{p,-\eta} + \Gamma_{p,\eta}\right)(1-n_p)\Gamma_{\eta,p}\Big]\Big\}\rho_{\eta,0} \\
&- \eta\sum_p (1-n_p)\Gamma_{-\eta,p}\rho_{2,-\eta}\,, \qquad (3.60) \\
\partial_t \rho_{2,-\eta} &= -\frac{1}{2}\Big\{\Gamma_{-\eta,\eta} + \sum_p\Big[(1-n_p)\left(2\Gamma_{-\eta,p} + \Gamma_{\eta,p}\right) \\
&+ n_p\Gamma_{p,\eta}\Big]\Big\}\rho_{2,-\eta} - \eta\sum_p n_p\Gamma_{p,-\eta}\rho_{\eta,0}\,. \qquad (3.61)
\end{aligned}$$

As conclusion, from now on we assume that the initial state (at $t = 0$) is diagonal. In that case, the decoupled off-diagonal density matrix elements remain zero during the entire time evolution.

3.3.3 Steady-state distribution of quasiparticles

Under the assumption that the initial Andreev density matrix, $\rho_A(0)$, is diagonal in the basis $\{|\pm\rangle_A, |0\rangle_A, |2\rangle_A\}$, see Eq. (3.53), in the long-time limit, the system will reach a time-independent steady-state distribution, which is fully characterized by the probabilities $P_{\pm,0,2}$ together with the continuum quasiparticle distribution function $\{n_p\}$. In order to determine these quantities, we first observe that $P_2 = P_0$ due to the spin degeneracy of the two odd-parity states (equiprobable spin-up and spin-down configurations in the excitation picture).
By using the normalization condition in Eq. (3.54), P_0 can be expressed in terms of $P_\pm$ alone,

$$P_0 = P_2 = \frac{1}{2}\left(1 - P_+ - P_-\right). \tag{3.62}$$

For the Andreev level occupations, we thus find

$$n_+ = 1 - n_- = \frac{1}{2}\left(1 + P_+ - P_-\right). \tag{3.63}$$

The steady-state reformulation of Eq. (3.49) yields

$$0 = -\sum_{\eta}\left[\Gamma_{p,\eta}(1-n_\eta)n_p - \Gamma_{\eta,p}(1-n_p)n_\eta\right] - \frac{n_p - n_p^{(0)}}{\tau_{\rm qp}}, \tag{3.64}$$

In the last equation we have added a phenomenological relaxation term for continuum quasiparticles describing, for instance, the effect of phonons, in analogy with Ref. [93], and, according to this reference, estimates for SACs made of aluminum in the phonon-dominated regime, given by $E_A < \Delta - \Omega$, we expect $\tau_{\rm qp}\Delta \approx 10^4$. For simplicity, we here assume an energy-independent relaxation time, $\tau_{\rm qp}$, and a Fermi distribution function for the noninteracting continuum quasiparticles,

$$n^{(0)}_{p=(E,s)} = \frac{1}{e^{E/T_{\rm qp}}+1}, \tag{3.65}$$

where the temperature $T_{\rm qp}$ may differ from the temperature $T_{\rm env}$ governing environmental phase fluctuations. In order to point out analogies and differences with Ref. [93], our case here corresponds there to the fast equilibration case with $\Gamma_{p,\eta}\tau_{\rm qp} \ll 1$.
Taking into account Eq. (3.62), the rate equation (3.56) then yields the steady-state relation

$$0 = -\Gamma_{\eta,-\eta}P_\eta + \Gamma_{-\eta,\eta}P_{-\eta} - \sum_p \Big[n_p\Big(\Gamma_{p,-\eta}P_\eta - \Gamma_{p,\eta}P_0\Big) + (1-n_p)\left(\Gamma_{\eta,p}P_\eta - \Gamma_{-\eta,p}P_0\right)\Big], \tag{3.66}$$

and Eq. (3.57) is automatically fulfilled.

Now we can proceed to solve Eq. (3.64) for the continuum quasiparticle distribution function,

$$n_p = \frac{\tilde{\Gamma}^{(-)}_p}{\tilde{\Gamma}^{(-)}_p + \tilde{\Gamma}^{(+)}_p}, \tag{3.67}$$

which is thereby expressed by the $P_\pm$-dependent effective rates

$$\begin{aligned} \tilde{\Gamma}^{(-)}_p &= \sum_\eta \Gamma_{\eta,p} n_\eta + \frac{n^{(0)}_p}{\tau_{\rm qp}}, \\ \tilde{\Gamma}^{(+)}_p &= \sum_\eta \Gamma_{p,\eta}(1-n_\eta) + \frac{1-n^{(0)}_p}{\tau_{\rm qp}}. \end{aligned} \tag{3.68}$$

To obtain the Andreev level probabilities $P_\pm$, we then plug the continuum quasiparticle distribution function in Eq. (3.67) into Eq. (3.66). We finally arrive at two coupled nonlinear equations,

$$\begin{pmatrix} \Gamma_{+,-} + 2G_- + G_+ & G_+ - \Gamma_{-,+} \\ G_- - \Gamma_{+,-} & \Gamma_{-,+} + 2G_+ + G_- \end{pmatrix} \begin{pmatrix} P_+ \\ P_- \end{pmatrix} = \begin{pmatrix} G_+ \\ G_- \end{pmatrix}, \tag{3.69}$$

with the auxiliary functions

$$G_{\eta=\pm}(P_+,P_-) = \nu_0 \sum_{s=1}^{4} \int_{|E|\geq\Delta} dE \frac{|E|}{2\sqrt{E^2-\Delta^2}} \left[\Gamma_{p,\eta}n_p + \Gamma_{\eta,p}(1-n_p)\right], \tag{3.70}$$

where $p = (E, s)$ encodes the continuum energy index and the scattering channel s, and $\nu_0 = L/(\pi\hbar v_F)$ is the normal density of states at the Fermi level.
The nonlinear system in Eq. (3.69) can be solved by numerical iteration, where a relative accuracy of 10^{-6} was ensured by using a Newton-Raphson algorithm. This is necessary because the continuum quasiparticle distribution $\{n_p\}$, Eq. (3.67), derived from the self-consistent solution for P_+ and P_-, strongly responds even to tiny changes in the $P_\pm$.

Furthermore, it will be useful to translate our analysis into a 'parity-language'. This means that we consider the rate Γ_{in} for transitions from the even-parity to the odd-parity sector: in this case, P_0 increases. We consider the escape rate as well, Γ_{out}, out of the odd-parity state, which will mean that P_0 decreases. In Ref. [93] the authors consider those rates by assuming an equilibrium quasiparticle distribution function $\{n_p\}$.
Here we employ the self-consistent continuum quasiparticle distribution function, and both rates can be read off from Eq. (3.57),

$$\Gamma_{\text{in}} = \sum_{p,\eta} \Gamma_{\eta,p}(1 - n_p), \quad \Gamma_{\text{out}} = \sum_{p,\eta} \Gamma_{p,\eta} n_p. \tag{3.71}$$

Since our interest is mostly captured by the current flowing in the system, we will discuss the quasiparticle current I_{qp}, which follows with our self-consistent solution for $\{n_p\}$ by using standard scattering theory expressions, see Eq. (3.34).

3.3.4 Perfect transparency case

Applications of our theoretical framework, presented further on in this thesis, are actually simplified when we consider a SAC with perfect transparency, $\mathcal{T} = 1$.
The quasiparticle wave functions for ideal contact transparency, $\mathcal{T} \to 1$, can be written down fully. In the Andreev bound state wave functions, $\Psi_{\eta=\pm}(x)$ in Eq. (B.1), the coefficients A_η and B_η now take the form

$$\begin{aligned} A_\eta &= \sqrt{\sin(\varphi_0/2)}\ \delta_{\eta,-\text{sgn}(\pi-\varphi_0)}, \\ B_\eta &= \sqrt{\sin(\varphi_0/2)}\ \delta_{\eta,\text{sgn}(\pi-\varphi_0)}. \end{aligned} \tag{3.72}$$

where $0 \le \varphi_0 < 2\pi$. Turning to the continuum state wave functions $\Psi_{p=(E,s)}(x)$ in Eq. (B.4), we need the scattering amplitudes (a_s, b_s, c_s, d_s) for an incoming state of type $s = \{1, 2, 3, 4\}$, which have been specified for arbitrary $\mathcal{T}$ in Eqs. (B.8) and (B.9). For $\mathcal{T} = 1$, these results can be simplified to yield

$$\begin{pmatrix} a_1 \\ b_1 \\ c_1 \\ d_1 \end{pmatrix} = \begin{pmatrix} c_4 \\ b_4 \\ a_4 \\ d_4 \end{pmatrix} = \frac{1}{\sinh(\theta_E + i\varphi_0/2)} \begin{pmatrix} -i\sin(\varphi_0/2) \\ 0 \\ \sinh\theta_E \\ 0 \end{pmatrix},$$

$$\begin{pmatrix} a_2 \\ b_2 \\ c_2 \\ d_2 \end{pmatrix} = \begin{pmatrix} a_3 \\ d_3 \\ c_3 \\ b_3 \end{pmatrix} = \frac{1}{\sinh(\theta_E - i\varphi_0/2)} \begin{pmatrix} 0 \\ i\sin(\varphi_0/2) \\ 0 \\ \sinh\theta_E \end{pmatrix}.$$

The Andreev bound state energies, ηE_A with $\eta = \pm$, then follow from $E_A(\varphi_0) = \Delta|\cos(\varphi_0/2)|$, see Eq. (3.1), and for $\varphi_0 \to \pi$, the Andreev levels tend to zero energy. Moreover, Eq. (3.48) shows that transition rates between different Andreev states vanish for $\mathcal{T} = 1$, i.e., $\Gamma_{\eta,-\eta} = 0$.

For a given energy E with $|E| \geq \Delta$, there are two decoupled types of scattering states $\Psi_{p=(E,s)}$, namely $s = \{1,4\}$ and $s = \{2,3\}$. Those channels correspond to a net charge transfer across the weak link in *opposite* directions.

Charge flows from the left to the right side for $s = \{1,4\}$, but from the right to the left when $s = \{2,3\}$, as it follows from the definition of the scattering states, see Eqs. (B.4) and (B.6). This also implies that the supercurrent matrix elements between Andreev and continuum states, $\mathcal{I}_{p,\eta}$, are nonzero only when

$$\begin{aligned} \eta &= -\operatorname{sgn}(\pi - \varphi_0), \quad s = \{1,4\} \\ \eta &= +\operatorname{sgn}(\pi - \varphi_0), \quad s = \{2,3\}. \end{aligned} \tag{3.73}$$

In what follows, we take the phase difference across the contact as $0 \leq \varphi_0 \leq \pi$. With $\eta_E = \operatorname{sgn}(E)$, we find the transition rates from Eq. (3.47), as in Refs. [93].

$$\begin{aligned} \Gamma_{p=(E,s),\eta} &= \frac{2\pi}{\hbar}\frac{1}{4\pi\nu_0}\frac{(E^2-\Delta^2)\sqrt{\Delta^2 - E_A^2}}{|E|\omega_{\eta\eta_E}} \\ &\times \left[\delta_{\eta,-}(\delta_{s,1}+\delta_{s,4}) + \delta_{\eta,+}(\delta_{s,2}+\delta_{s,3})\right]\,\left[\delta_{\eta_E,+} + n_B\left(\omega_{\eta\eta_E}\right)\right] J(\omega_{\eta\eta_E}), \end{aligned} \tag{3.74}$$

with the following transition energies

$$\omega_{\eta\eta_E=\pm} = |E| \mp E_A \geq 0, \tag{3.75}$$

but noting that, for each scattering channel s, $|\mathcal{I}_{\eta,p=(E,s)}|^2$ in Eq. (3.74) is invariant under a particle-hole transformation, $(E, \eta E_A) \to (-E, -\eta E_A)$.

3.4 The charge imbalance effect

In this final section of this chapter, we now address the charge imbalance effect, which is predicted to be observable in high-transparency SACs. We discuss this effect for a perfectly transmitting, i.e. transparent, SAC, where, as we saw already, $\mathcal{T} = 1$, and by assuming $\varphi_0 \in [0, \pi]$; for $\varphi_0 \in (\pi, 2\pi)$, the sign of the induced quasiparticle current discussed below is reversed.

In a transparent SAC, Eq. (3.74) only allows for transitions between Andreev and continuum current states propagating in the same direction. This results in generating a charge imbalance effect.
We note that, since the matrix elements in Eq. (3.74) are identical for $s = \{1, 4\}$, as well as for $s = \{2, 3\}$, the steady-state distribution function $n_{p=(E,s)}$ for continuum quasiparticles corresponds to a single distribution function for left-movers, $n_L(E)$, and one for right-movers, $n_R(E)$, respectively,

$$\begin{aligned} n_{(E,s=1)} &= n_{(E,s=4)} = n_R(E), \\ n_{(E,s=2)} &= n_{(E,s=3)} = n_L(E). \end{aligned} \tag{3.76}$$

For $n_R(E) \neq n_L(E)$, continuum quasiparticles are driven out of equilibrium. For given steady-state Andreev occupation probabilities $P_\pm$, the distribution functions in Eq. (3.76) follow from Eqs. (3.67) and (3.68).

Using Eqs. (3.74) and (3.34), the quasiparticle current flowing through the SAC, in terms of the Andreev level occupation, is given by

$$I_{\mathrm{qp}} = \frac{e}{\pi\hbar} \int_{|E|\geq\Delta} dE \; j_{\mathrm{qp}}(E) \left[n_R(E) - n_L(E) \right], \tag{3.77}$$

with the energy-resolved dimensionless quasiparticle current ($|E| \geq \Delta$),

$$j_{\mathrm{qp}}(E) = \frac{|E|\sqrt{E^2 - \Delta^2}}{E^2 - E_A^2}, \tag{3.78}$$

and the self-consistent distribution functions $n_{L,R}(E)$ in Eq. (3.76). Evidently, $n_L(E) \neq n_R(E)$, will cause a charge imbalance, and therefore a finite quasiparticle current $I_{\mathrm{qp}} \neq 0$ from Eq. (3.77).
We can also define the total accumulated quasiparticle charge

$$Q_{\mathrm{qp}} = e\nu_0 \int_{|E|\geq\Delta} dE \frac{|E|}{\sqrt{E^2 - \Delta^2}} \left[n_R(E) - n_L(E) \right]. \tag{3.79}$$

In a very narrow constriction, the density of states, that is

$$\nu_0 \propto L/\xi_0, \tag{3.80}$$

where L is the channel length and $\xi_0 = \hbar v_F/\Delta$ the BCS coherence length, tends to vanish. As consequence,

$$Q_{\rm qp} \to 0$$

for a very short channel, while the induced quasiparticle current remains finite in that limit.

Presentation of figures and discussion of the results

Let us first address the steady-state Andreev populations, $P_{\pm,0,2}$, where the two $P_\pm$ follow from the self-consistent solution of Eq. (3.69). The occupation probability of the degenerate odd-parity state, $P_0 = P_2$, is then given by Eq. (3.62).

Representative results for $P_{\pm,0}$ vs E_A/Δ are shown in Fig. 3.3, where the parameters chosen have experimental relevance. We essentially show the phase dependence of the Andreev state probabilities for $\varphi_0 \in [0, \pi]$. The charge imbalance turns out to be absent in the strong relaxation regime $\tau_{\rm qp}\Delta < 1$, where our theory reduces to the approach of Ref. [93] and thus the self-consistency plays no role at all. We therefore focus on the weak relaxation regime $\tau_{\rm qp}\Delta \gg 1$ in this section. The main panel in Fig. 3.3 is for $T_{\rm env} = T_{\rm qp}$, while the inset studies a case where $T_{\rm env} > T_{\rm qp}$. From Fig. 3.3, we can distinguish two qualitatively different regimes

$$\begin{aligned} E_A &> \Delta - \Omega, \quad \text{where} \quad P_0 \to 0 \\ E_A &< \Delta - \Omega, \quad \text{where} \quad P_0 \neq 0 \end{aligned} \tag{3.81}$$

For $E_A > \Delta - \Omega$, environmental photons can rapidly excite quasiparticles from an odd-parity state into the continuum. As net effect the system remains quite close to the ground state, $|-\rangle_A$. Instead, for $E_A < \Delta - \Omega$, the frequency Ω is too low to achieve such a transition.

The corresponding rates $\Gamma_{\rm in}$ and $\Gamma_{\rm out}$, see Eq. (3.71), for populating and depopulating the odd parity states, respectively, are shown in Fig. 3.4, again as a function of E_A/Δ. The existence of two regimes, as defined before, $E_A > \Delta - \Omega$ and $E_A < \Delta - \Omega$, becomes clearer now.
For $E_A \approx \Delta - \Omega$, the rates increase over several orders in magnitude with very small φ_0 variation, and one enters a regime where the odd-parity state quickly decays. This regime, $E_A > \Delta - \Omega$, has been termed 'fast relaxation regime' in Refs. [80, 93].

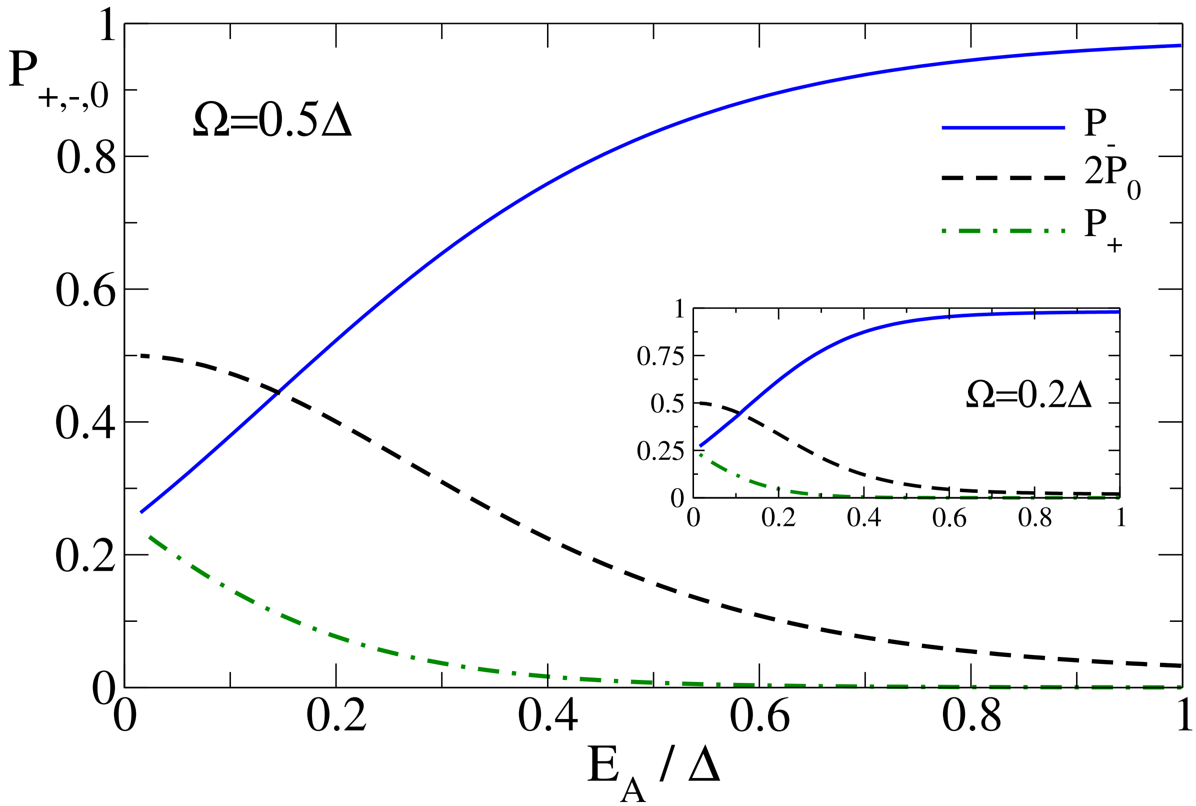

Figure 3.3: Self-consistent solution of Eq. (3.69) for the steady-state Andreev level occupation probabilities in a transparent SAC, $\mathcal{T} = 1$. Here, $P_\pm$ refers to the even-parity Andreev levels, with $|-\rangle_A$ being the ground state, and $P_0 = P_2$ to the degenerate pair of odd-parity states. These results have been obtained for plasma frequency $\Omega = 0.5\Delta$, quasiparticle-photon coupling $\lambda = \sqrt{E_C/4\Omega} = 0.1$, environmental temperature $T_{\rm env} = 0.2\Delta$, quasiparticle temperature $T_{\rm qp} = 0.2\Delta$, channel length $L = \xi_0$, Ohmic damping constant $\eta_d = 0.01\Delta$, and $\tau_{\rm qp}\Delta = 10^5$ (weak quasiparticle relaxation). The inset shows the case $\Omega = 0.2\Delta$, $T_{\rm env} = 0.5\Delta$, and $T_{\rm qp} = 0.01\Delta$, where all other parameters are as in the main panel.

Next, in Fig. 3.5 we show the induced quasiparticle current $I_{\rm qp}$ as function of E_A for $\Omega = 0.5\Delta$. This quantity clearly demonstrates that there is a significant charge imbalance effect throughout the regime $E_A > \Delta - \Omega$, but not for $E_A < \Delta - \Omega$. The induced current gets reduced as the quasiparticle relaxation rate $1/\tau_{\rm qp}$ increases, and is only significant for $\tau_{\rm qp}\Delta \gg 1$, which is the typical regime for aluminum-made SACs, as in Ref. [80].
More understanding of the generated charge imbalance is obtained by analyzing the distribution functions $n_{R,L}(E)$ for right- and left-moving quasiparticles, as they appear in Eq. (3.76). As illustrated by the insets in Fig. 3.5, the generated imbalance is maximal for $E_A \to \Delta$, and

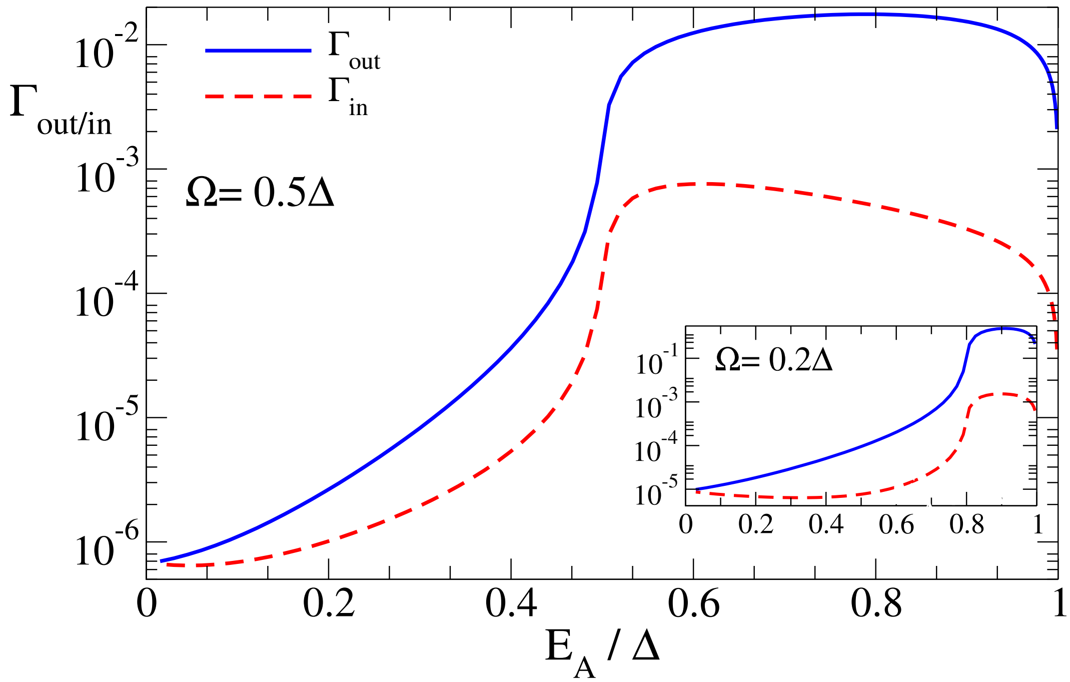

Figure 3.4: Transition rates $\Gamma_{\rm in}$ and $\Gamma_{\rm out}$ (in units of $\Delta/\hbar$) vs E_A/Δ on a semi-logarithmic scale. $\Gamma_{\rm in}$ describes the rate for entering the odd-parity sector, and $\Gamma_{\rm out}$ is the decay rate of odd-parity states. Parameters are as in Fig. 3.3. The inset shows the rates for parameters as in the inset of Fig. 3.3.

becomes smaller as E_A decreases. Moreover, it is worth stressing that $E_A \to \Delta$ corresponds to the case $\varphi_0 \to 0$, where the supercurrent $\langle \hat{I}_S \rangle$ can be vanishingly small.
In the insets of Fig. 3.5, we find that the smaller $n(E)$ curves (indicated by dotted curves), i.e., the n_R component for $E > 0$, and $1 - n_L$ for $E < 0$, coincide with the Fermi distribution at the corresponding temperature, for the present case $T_{\rm qp} = T_{\rm env}$.
Noting that the Josephson current for a fully transparent SAC is of order

$$\langle \hat{I}_S \rangle = \langle \hat{I}_A \rangle \approx e\Delta/\hbar, \tag{3.82}$$

the induced quasiparticle current is a few percent of this value for the parameters in Fig. 3.5. This imbalance discussed here is due to the breaking of the left-right symmetry in the rates connecting continuum quasiparticles and the Andreev bound states and induces a quasiparticle current on top of the Josephson current in the ring geometry, depicted in Fig. 3.1.
The quasiparticle current $I_{\rm qp}$ flows in opposite direction to the Josephson current $\langle \hat{I}_S \rangle$, even if $P_+ < P_-$ favors the same sign of $I_{\rm qp}$ and $\langle \hat{I}_S \rangle$. This can be seen as follows. The rate from $|+\rangle_A$ to the left-moving $s = 2$ continuum states with $E > 0$ carries negative current

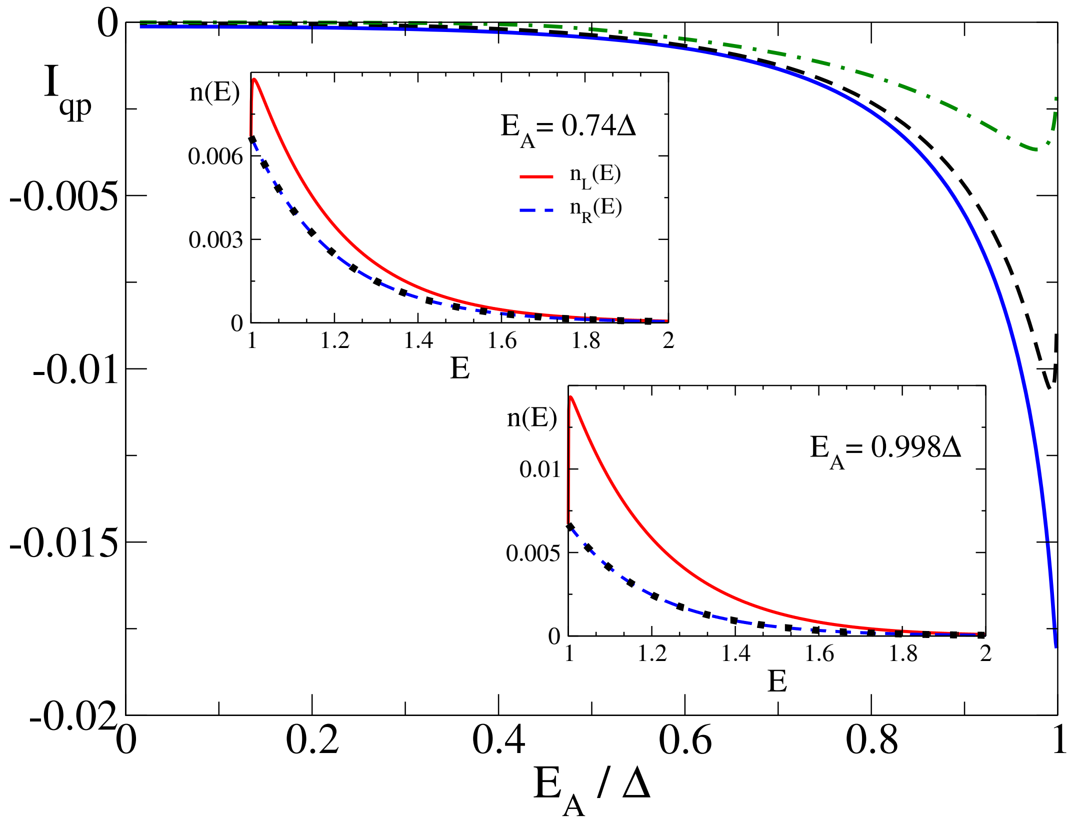

Figure 3.5: Main panel: Induced quasiparticle current I_{qp} (in units of $e\Delta/\hbar$) vs E_A/Δ for varying $\tau_{\text{qp}}\Delta = 10^5, 10^4$ and 10^3 from bottom to top; other parameters are as in the main panel of Fig. 3.3. Insets: Continuum quasiparticle distributions $n_{L,R}(E)$ vs E/Δ for two E_A/Δ values and $\tau_{\text{qp}}\Delta = 10^5$. For $E < 0$, the distribution functions follow by using the electron-hole symmetry relation $n_R(-E) = 1 - n_L(E)$. Dotted curves indicate the corresponding equilibrium Fermi distributions.

and results to be much bigger than the one from $|-\rangle_A$ to the $(E > 0, s = 1)$ states carrying positive current, because of the much shorter distance in energy.

As we show next, it is also interesting to consider an alternative classical regime, where the temperature of the environmental modes is high, $T_{\text{env}} \gg \Omega$. Experimental realization of this scenario is possible by replacing the electromagnetic environment by an external microwave radiation source at frequency Ω. We here consider the case $\Omega = 0.2\Delta$, with $T_{\text{env}} = 0.5\Delta \equiv 2.5\Omega$ and quasiparticle temperature $T_{\text{qp}} = 0.01\Delta$, significantly smaller than T_{env}. The Andreev state populations for this case are shown in the inset of Fig. 3.3, and the

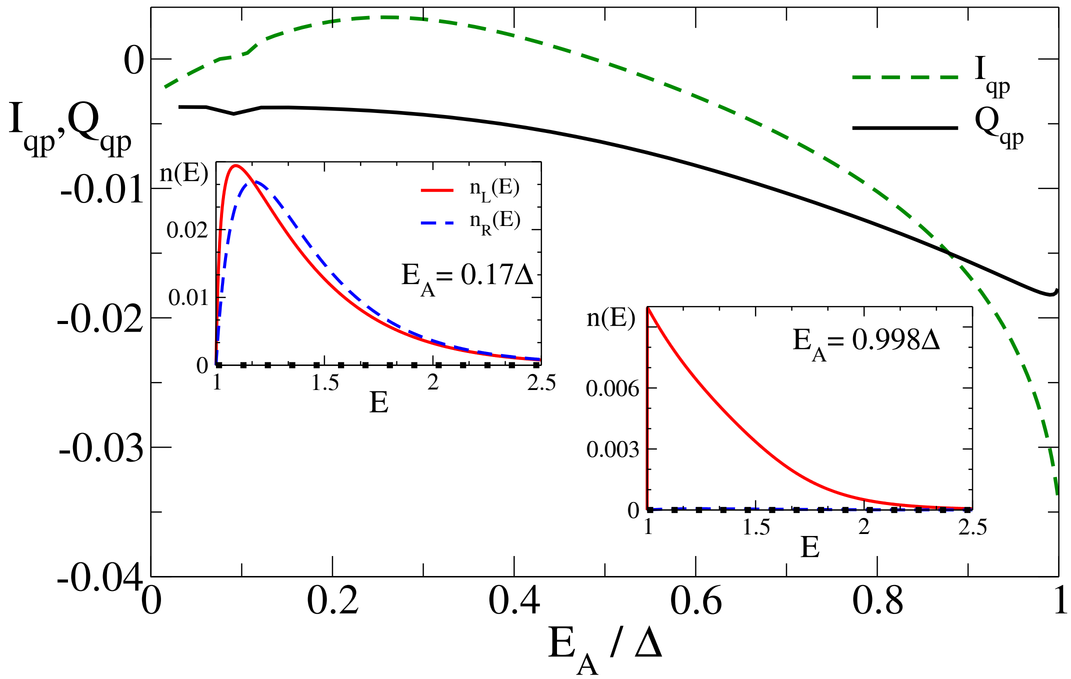

Figure 3.6: Main panel: Quasiparticle current I_{qp} (in $e\Delta/\hbar$) and accumulated charge Q_{qp} (in units of e) vs E_A/Δ for the parameters in the inset of Fig. 3.3, i.e., $\Omega = 0.2\Delta, T_{\text{env}} = 0.5\Delta$ and $T_{\text{qp}} = 0.01\Delta$. The insets show the continuum quasiparticle distributions, $n_{R,L}(E)$, for two different E_A values. In contrast to the case studied in Fig. 3.5, the induced quasiparticle current is now significant for the whole E_A range, and exhibits a sign change for $E_A \simeq \Omega$.

corresponding $\Gamma_{\text{in/out}}$ rates in the inset of Fig. 3.4.

By noting that the induced quasiparticle current exhibits a sign change for $E_A \simeq \Omega$, in the main panel of Fig. 3.6, a significant quasiparticle current is induced throughout the whole E_A range. Again fast and slow relaxation regimes can be identified, for $E_A > \Delta - \Omega$ and $E_A < \Delta - \Omega$, respectively. In this case, the generated quasiparticle populations differ more strongly from the Fermi distributions, as shown in the insets of Fig. 3.6.

Chapter 4

Conclusions

In this chapter we will collect the conclusive remarks derived from the results presented in the previous chapters. The results of Ch. 2 are published in Ref. [8], where we have analyzed two particularly interesting aspects of Josephson transport in hybrid superconductor-dot systems. First, a pair of conventional BCS superconductors is connected through a multi-level quantum dot, where spin-orbit coupling, Coulomb charging and magnetic field effects are taken into account. We have studied the conditions for deriving an anomalous Josephson current, i.e., a supercurrent flowing at zero phase difference. It is remarkable that Coulomb interactions can qualitatively affect this phenomenon to allow for ground-state anomalous supercurrents even when time-reversal breaking perturbations are very small compared to all other relevant scales. As a result, we have found that the system is close to a spontaneously broken time-reversal symmetry, with an anomalous supercurrent flowing for arbitrarily weak but finite Zeeman field. Second, in the deep subgap case, we have addressed the possibility of having topologically unprotected Majorana bound states in a double dot, where a spatial separation is naturally defined. This is related to a vigorous debate in the scientific community, see Refs. [67, 68] where similar - though different in details - issues are studied. In our setup a strong spin-orbit coupling is present as well and, together with a Zeeman field, is responsible for the emergence of Majorana fermions, see Refs. [29]-[34]. This results in an easier realization of Majorana physics. However, here a fine tuning of parameters is needed, but this seems a 'fair prize to pay' given the high degree of control that experimentalist physicists have over quantum dots. Signatures of Majorana fermions are then indirectly detected in the current-phase relation through the critical phases φ, where the current switches from a finite value to zero. Finally, while a large Zeeman field is required, Coulomb interactions play no role for the formation of Majorana bound states in our setup.

The results presented in Ch. 3, present in Ref. [71], have been carried out in a theoretical framework for the Andreev bound state population dynamics in single-channel superconducting weak links. Taking into account phase fluctuations by the electromagnetic environment, we have developed a master equation approach for the quasiparticle dynamics, to capture the interplay between the Andreev states and the continuum states. In particular, we have stressed the role of odd-parity Andreev states and the need for a self-consistent treatment of the generated nonequilibrium continuum quasiparticle distribution. As an application of our theory, we have shown that the coupling of the superconducting weak link to the environmental phase fluctuations causes an intriguing charge transfer across the weak link, i.e. a charge imbalance of the continuum population. This charge imbalance is due to the breaking of the left-right symmetry in the rates connecting continuum quasiparticles and the Andreev bound states, and manifests itself as a persistent (i.e., in absence of subgap voltage) quasiparticle current, circulating on top of the Josephson current in the system. Our theory could be also applied for the study of the quantum coherent dynamics of this system, including the effect of parity mixing processes. This is of relevance for the various proposals of using Andreev levels as qubits [84, 85, 87, 88]. Another extension of our formalism would be to study the Andreev- and Majorana bound state dynamics in topological superconductor weak links, or to study the interaction-induced effects (see also Ref. [99]) on Andreev bound state dynamics when the constriction contains a quantum dot with sizeable charging energy, or couples to local phonon modes.

We are confident that the results illustrated so far throughout this thesis contributed positively to this relatively new and flourishing field and we hope that these effects can soon be observed in experiments.

Appendix A

Orbital magnetic field effects in a realistic quantum dot

We consider the Hamiltonian of the quantum dot (QD)

$$H_{QD} = H_0 + H_Z + H_{SO} \equiv \int d^2r \; d^\dagger(\vec{r}) \left[\frac{(-i\vec{\nabla})^2}{2m} + V(\vec{r}) + h_Z + h_{SO} \right] d(\vec{r}) \,, \tag{A.1}$$

where $d = (d_\uparrow \,, d_\downarrow)^T$. We aim to understand what is the effect of the presence of an orbital magnetic field $\vec{b}$. For simplicity, one can consider the orbital magnetic field normal to the 2DEG plane. This allows a choice of a vector potential $\vec{a}(\vec{r})$

$$\vec{a}(\vec{r}) = (a_x(x,y), a_y(x,y), 0) \equiv \vec{a}(x,y) \implies \vec{b} = \vec{\nabla} \times \vec{a}(\vec{r}) \propto \hat{z} \tag{A.2}$$

The free dot

We start by analyzing the free dot case ($h_0 = -(\nabla^2/2m) + V(\vec{r})$), studying in detail the effects on the Zeeman field and the spin-orbit (SO) in different subsections. By mean of the minimal prescription

$$h_0 = -\frac{1}{2m}\vec{\nabla}^2 + V(\vec{r}) \longrightarrow h_0 = -\frac{1}{2m}\vec{\nabla}^2 + V(\vec{r}) - i\nabla_x a_x(x,y) - i\nabla_y a_y(x,y) - i a_x(x,y)\nabla_x - i a_y(x,y)\nabla_y$$

and for the free dot case the Hamiltonian in Eq. (A.1) becomes,

$$H_0 = \int d^2r \; d^\dagger(\vec{r}) \left[h_0 - i\nabla_x a_x(x,y) - i\nabla_y a_y(x,y) - i a_x(x,y)\nabla_x - i a_y(x,y)\nabla_y \right] d(\vec{r})$$

We gauge away the vector potential from the Hamiltonian through a transformation of the general form

$$d(\vec{r}) \to e^{-i\int_C d\vec{l}\cdot\vec{a}(\vec{r})} d(\vec{r}) \tag{A.3}$$

with C regular curve to be parametrized

$$C\,:\,t\in[t_1,t_2]\longmapsto\vec{C}(t)=(C_x(t),C_y(t))\implies\int_C d\vec{l}\cdot\vec{a}(\vec{r})=\int_{t_1}^{t_2}\vec{a}\left(\vec{C}(t)\right)\cdot\vec{C}'(t)\equiv\delta\in\mathbb{R}$$

The result of the line integration is, of course, C-independent and is a real number, that we identify as a phase. One may wonder to go as general as possible in the calculations, but the choice of a specific gauge for $\vec{a}(\vec{r})$ and the choice of how to model the dot (so, how to choose the confinement types) simplifies the calculations.
We choose the symmetric gauge [1]

$$\vec{a}(\vec{r})=\frac{b}{2}\,(-y,x,0)$$

and we assume that the QD is confined in a box of length L in the $\hat{x}$ direction and by a parabolic potential in the $\hat{y}$ direction. The set of the eigenfunctions of the dot, in absence of SO or Zeeman field, are given by

$$\left(-\frac{1}{2m}\vec{\nabla}^2+V(\vec{r})\right)\chi_n(\vec{r})=\epsilon_n\,\chi_n(\vec{r}) \tag{A.4}$$

with $d(\vec{r})=\sum_n\chi_n(\vec{r})d_n$ and $\chi_n(\vec{r})=\psi_{n_x}(x)\Phi_{n_y}(y)$ assumed to be real orbital functions.

As a concrete example we assume, without loss of generality, a coordinate system where the tunnel contacts are located at $(x,y)=(\mp L/2,0)$ and moreover we consider the dot states given by the first two oscillator eigenstates ($n_y=0,1$) in the longitudinal ground state ($n_x=1$).

Without Zeeman field and SO, one may conclude that the orbital magnetic field has no effects on H_0

$$H_0=\int_{-L/2}^{L/2}dx\int_{-\infty}^{\infty}dy\;\psi_{n_x}(x)\Phi_{n_y}(y)\left[h_0+i\frac{b}{2}y\nabla_x-i\frac{b}{2}x\nabla_y\right]\psi_{n'_x}(x)\Phi_{n'_y}(y) \tag{A.5}$$

and that the term proportional to $y\nabla_x-x\nabla_y$ will give zero integrals of the orbital wave functions, because of their symmetry properties. In fact, since we are in the longitudinal ground state ($n_x=1$)

$$\int_{-L/2}^{L/2}dx\;\psi_{n_x}(x)\nabla_x\psi_{n_x}(x)=\int_{-L/2}^{L/2}dx\;x\;[\psi_{n_x}(x)]^2=0\qquad(\forall\,n_x)$$

[1] Please note that, in this gauge, no matter what regular C curve is chosen, the line integral will always be proportional to the magnitude of $\vec{b}$, or, in other form, $\int_C d\vec{l}\cdot\vec{a}(\vec{r})\propto b$.

Then the result for the free dot case has to be what already we know from Eq. (A.4), so one may write

$$H_0 = \sum_n \epsilon_n d_n^\dagger d_n \tag{A.6}$$

Now we may investigate the Zeeman field and the SO terms.

The Zeeman Term

The general integral to study is

$$H_Z = \int d^2r \; d^\dagger(\vec{r})\, e^{i\int_C d\vec{l}\cdot\vec{a}(\vec{r})}(\vec{B}\cdot\vec{\sigma})\, e^{-i\int_C d\vec{l}\cdot\vec{a}(\vec{r})}\, d(\vec{r})$$

Assuming an in-plane magnetic field $\vec{B} = (B, 0, 0)$, whose entries do not depend on the coordinates, the Zeeman field term is found to be

$$H_Z = \sum_{nn'} d_n^\dagger \left(\vec{B}_{nn'}\cdot\vec{\sigma}\right) d_{n'} \tag{A.7}$$

where

$$\vec{B}_{nn'}\cdot\vec{\sigma} = \int_{-L/2}^{L/2} dx \int_{-\infty}^{\infty} dy \; \psi_{n_x}(x)\Phi_{n_y}(y)\,(\vec{B}\cdot\vec{\sigma})\,\psi_{n_x'}(x)\Phi_{n_y'}(y) = (\vec{B}\cdot\vec{\sigma})\,\delta_{n_x n_x'}\delta_{n_y n_y'} \equiv \vec{B}_{n_y n_y'}\cdot\vec{\sigma}$$

one may conclude that the the Zeeman field term is transparent to the gauge transformation in Eq. (A.3) and, moreover, the Hermitian matrix $\vec{B}$ is symmetric. It is worth stressing that the symmetric nature of the $\vec{B}$ matrix is consequence of having assumed real orbital wave functions.

The Spin Orbit Term

The general integral to study is

$$H_{SO} = \int d^2r \; d^\dagger(\vec{r})\, e^{i\int_C d\vec{l}\cdot\vec{a}(\vec{r})}(h_{SO})\, e^{-i\int_C d\vec{l}\cdot\vec{a}(\vec{r})}\, d(\vec{r})$$

where h_{SO} gets modifies because of the minimal substitution

$$h_{SO} = \sigma_x\left[\frac{\alpha_R}{m}\left(-i\,\nabla_y + \frac{b}{2}\,x\right) - \frac{\alpha_D}{m}\left(i\,\nabla_x + \frac{b}{2}\,y\right)\right] + \sigma_y\left[\frac{\alpha_R}{m}\left(i\,\nabla_y + \frac{b}{2}\,y\right) + \frac{\alpha_R}{m}\left(i\,\nabla_y - \frac{b}{2}\,x\right)\right]$$

The SO term has then the following form

$$H_{SO} = \sum_{nn'} d_n^\dagger \left(\vec{A}_{nn'}\cdot\vec{\sigma}\right) d_{n'} \tag{A.8}$$

With the choice of the confinement parameters made above

$$\begin{aligned}\vec{A}_{nn'}\cdot\vec{\sigma} &= \sigma_x\left[-i\,\frac{\alpha_R}{m}\int_{-\infty}^{\infty}dy\;\Phi_{n_y}(y)\nabla_y\Phi_{n'_y}(y)-i\,\frac{b}{2}\,\frac{\alpha_D}{m}\int_{-\infty}^{\infty}dy\;\Phi_{n_y}(y)\,y\,\Phi_{n'_y}(y)\right]+\\ &+\;\sigma_y\left[\frac{b}{2}\,\frac{\alpha_R}{m}\int_{-\infty}^{\infty}dy\;\Phi_{n_y}(y)\,y\,\Phi_{n'_y}(y)+i\,\frac{\alpha_D}{m}\int_{-\infty}^{\infty}dy\;\Phi_{n_y}(y)\nabla_y\Phi_{n'_y}(y)\right]\equiv\vec{A}_{n_yn'_y}\cdot\vec{\sigma}\end{aligned}$$

Particular focus on the previous integrals shows that, for $n_y=0$ and $n'_y=1$

$$\mathrm{I}\left(n_y,n'_y\right)=\int_{-\infty}^{\infty}dy\;\Phi_{n_y}(y)\nabla_y\Phi_{n'_y}(y)\quad\Longrightarrow\quad\mathrm{I}\,(0,1)=\int_{-\infty}^{\infty}dy\;\Phi_0(y)\nabla_y\Phi_1(y)=1$$

$$\mathcal{I}\left(n_y,n'_y\right)=\int_{-\infty}^{\infty}dy\;\Phi_{n_y}(y)\,y\,\Phi_{n'_y}(y)\quad\Longrightarrow\quad\mathcal{I}\,(0,1)=\int_{-\infty}^{\infty}dy\;\Phi_0(y)\,y\,\Phi_1(y)=\sqrt{\pi}$$

Note that the $\vec{A}$ Hermitian matrix is totally skew-symmetric. Again, this comes essentially by having assumed real orbital wave functions in shaping our QD.

Building the effective Hamiltonian

We have the ingredients for building the Hamiltonian matrix H_{QD}. Collecting informations from Eqs. (A.6)-(A.7)-(A.8), when expanded into the basis Eq. (A.4), H_{QD} is

$$H_{QD}=\sum_n\epsilon_n d_n^\dagger d_n+\sum_{nn'}d_n^\dagger\left(\vec{A}_{nn'}+\vec{B}_{nn'}\right)\cdot\vec{\sigma}\,d_{n'}\tag{A.9}$$

Defining the ladder operators $A^{\pm}_{nn'}=A_{x,nn'}\pm iA_{y,nn'}$ and $A^z=A_{z,nn'}$ (same holds for $\vec{B}_{nn'}$) and taking into account the symmetry arguments stated above, the H_{QD} matrix explicitly becomes

$$H_{QD}=\begin{pmatrix}\epsilon_1+\mu & B^-_{00} & 0 & A^-_{01}\\ B^+_{00} & \epsilon_1+\mu & A^+_{01} & 0\\ 0 & -A^-_{01} & \epsilon_2+\mu & B^-_{00}\\ -A^+_{01} & 0 & B^+_{00} & \epsilon_2+\mu\end{pmatrix}$$

Note that $B^{\pm}_{00}=B$ and

$$A^{\pm}_{01}=-i\,\tilde{\alpha}_R\mp\tilde{\alpha}_D$$

where

$$\tilde{\alpha}_R=\frac{1}{m}\left(1\mp\frac{\sqrt{\pi}}{2}\,b\right)\alpha_R\qquad\text{and}\qquad\tilde{\alpha}_D=\frac{1}{m}\left(1\pm\frac{\sqrt{\pi}}{2}\,b\right)\alpha_D$$

or, in other words, the orbital magnetic field effect reveals its presence only by mean of a renormalization of the Rashba and Dresselhaus SO couplings. It is then clear that, as soon as one tunes the orbital magnetic field to zero

$$\tilde{\alpha}_R=\alpha_R\qquad\text{and}\qquad\tilde{\alpha}_D=\alpha_D$$

Then, H_{QD} takes the form

$$H_{QD} = \begin{pmatrix} \epsilon_1 + \mu & B & 0 & -i\,\tilde{\alpha}_R + \tilde{\alpha}_D \\ B & \epsilon_1 + \mu & -i\,\tilde{\alpha}_R - \tilde{\alpha}_D & 0 \\ 0 & i\,\tilde{\alpha}_R + \tilde{\alpha}_D & \epsilon_2 + \mu & B \\ i\,\tilde{\alpha}_R - \tilde{\alpha}_D & 0 & B & \epsilon_2 + \mu \end{pmatrix}$$

Finally, if one neglects the orbital magnetic field and the Dresselhaus SO coupling and, for sake of simplicity one sets $\alpha_R = \alpha$:

$$H_{QD} = \begin{pmatrix} \epsilon_1 + \mu & B & 0 & -i\,\alpha \\ B & \epsilon_1 + \mu & -i\,\alpha & 0 \\ 0 & i\,\alpha & \epsilon_2 + \mu & B \\ i\,\alpha & 0 & B & \epsilon_2 + \mu \end{pmatrix} = (\mu\tau_0 + \epsilon\tau_z)\,\sigma_0 + B\tau_0\sigma_x + \alpha\tau_y\,\sigma_x$$

where the the bare energy levels are rewritten as $\epsilon_{1,2} = \mu \pm \epsilon$. Through a rotation $\sigma_x \to \sigma_z$ and parametrizing the SO coupling through a parameter χ, H_{QD} takes the final form that we use in our analysis throughout the Sec. 2.2.2.

Finally, the gauge transformation Eq. (A.3) yields a phase term entering the tunneling Hamiltonian

$$H_t = \sum_{j=L,R} \sum_{\vec{k}} \sum_{n=1}^{M} \Psi^{\dagger}_{j\vec{k}}\, T_{j,n}\, D_n + \text{H.c.}\ , \qquad D_n = \left(d_{n,\uparrow}, d^{\dagger}_{n,\downarrow}\right)^T$$

as it appears in Eq. (2.7).

As last remark, it is worth to stress that these phases get adsorbed in the tunneling Hamiltonian and actually appear in the hybridization matrices (in the level space), and they are not related to the SOC.

Appendix B

Quasi-particle wave functions

In this Appendix, we provide the wave functions, $\Psi_\nu(x)$, solving the stationary BdG equation, $H_0\Psi_\nu = E_\nu\Psi_\nu$, under the matching condition Eq. (3.8) for time-independent phase difference, $\varphi(t) = \varphi_0$, with $0 \le \varphi_0 < 2\pi$.

Andreev bound states, $\nu = \eta = \pm$, with energy $\eta E_A(\varphi_0)$, see Eq. (3.1), have the wave function

$$\Psi_\eta(x) = \xi_0^{-1/2} e^{-\sqrt{\mathcal{T}}\sin(\varphi_0/2)|x|/\xi_0} \left[\Theta(-x)\begin{pmatrix} A_\eta\tilde{\psi}_h \\ B_\eta\tilde{\psi}_e \end{pmatrix} + \Theta(x)\begin{pmatrix} -\eta A_\eta\tilde{\psi}_e \\ \eta B_\eta\tilde{\psi}_h \end{pmatrix}\right], \tag{B.1}$$

where $\Theta(x)$ the Heaviside step function. We use the Nambu spinors

$$\tilde{\psi}_{e,h} = \frac{e^{\pm i\theta_\eta\sigma_z/2}}{\sqrt{2}}\begin{pmatrix} 1 \\ \eta \end{pmatrix}, \tag{B.2}$$

where $\cos\theta_\eta = E_A/\Delta$ with $\eta\sin\theta_\eta \ge 0$. We also define the parameters

$$\begin{aligned} A_\eta &= \sqrt{\mathcal{N}_\eta}\sin(\varphi_0/2 - \theta_\eta), \\ B_\eta &= \sqrt{\mathcal{N}_\eta(1-\mathcal{T})}\sin(\varphi_0/2), \\ \mathcal{N}_\eta &= \frac{\sqrt{\mathcal{T}}}{2\cos(\theta_\eta)\sin(\varphi_0/2-\theta_\eta)}. \end{aligned} \tag{B.3}$$

The Andreev bound states (B.1) satisfy the normalization condition $\int dx\, \Psi_\eta^\dagger(x)\cdot\Psi_{\eta'}(x) = \delta_{\eta\eta'}$.

Next we summarize the stationary solutions of the BdG equation in the continuum, $\Psi_{p=(E,s)}(x)$ with $|E| \ge \Delta$. Using $\eta_E = \mathrm{sgn}(E) = \pm$ and $\cosh\theta_E = |E|/\Delta$ (with $\theta_E \ge 0$), and denoting the wavenumber by $k = \eta_E\sqrt{E^2-\Delta^2}/v_F$, we find

$$\Psi_p = \Psi_p^{(\mathrm{in})} + \Theta(-x)\frac{e^{-ikx}}{\sqrt{2L}}\begin{pmatrix} a\psi_h \\ b\psi_e \end{pmatrix} + \Theta(x)\frac{e^{ikx}}{\sqrt{2L}}\begin{pmatrix} c\psi_e \\ d\psi_h \end{pmatrix}, \tag{B.4}$$

where the electron- and hole-type Nambu spinors $\psi_{e,h}$ follow by analytic continuation of Eq. (B.2),

$$\psi_{e,h} = \frac{e^{\pm\theta_E\sigma_z/2}}{\sqrt{2\cosh\theta_E}} \begin{pmatrix} 1 \\ \eta_E \end{pmatrix}. \tag{B.5}$$

There are four different solutions ($s = 1, 2, 3, 4$), describing electron- or hole-type states incoming from the left or right side,

$$\Psi_p^{(\mathrm{in})} = \Theta(-x)\frac{e^{ikx}}{\sqrt{2L}} \begin{pmatrix} \psi_e\delta_{s,1} \\ \psi_h\delta_{s,2} \end{pmatrix} + \Theta(x)\frac{e^{-ikx}}{\sqrt{2L}} \begin{pmatrix} \psi_h\delta_{s,4} \\ \psi_e\delta_{s,3} \end{pmatrix}. \tag{B.6}$$

With $Q = \sinh^2\theta_E + \mathcal{T}\sin^2(\varphi_0/2)$, the scattering amplitudes (a, b, c, d) appearing in Eq. (B.4) can be expressed in terms of four functions,

$$\begin{aligned}
A(\theta,\varphi) &= -\frac{i\mathcal{T}}{Q}\sin(\varphi/2)\sinh(\theta - i\varphi/2), \\
B(\theta,\varphi) &= \frac{\sqrt{1-\mathcal{T}}}{Q}\sinh^2\theta, \\
C(\theta,\varphi) &= \frac{\sqrt{\mathcal{T}}}{Q}\sinh(\theta)\sinh\left(\theta - i\varphi/2\right), \\
D(\theta,\varphi) &= \frac{i\sqrt{(1-\mathcal{T})\mathcal{T}}}{Q}\sin(\varphi/2)\sinh\theta,
\end{aligned} \tag{B.7}$$

such that for $s = 1$,

$$\begin{pmatrix} a_1 \\ b_1 \\ c_1 \\ d_1 \end{pmatrix} = \begin{pmatrix} A(\theta_E,\varphi_0) \\ B(\theta_E,\varphi_0) \\ C(\theta_E,\varphi_0) \\ D(\theta_E,\varphi_0) \end{pmatrix} \tag{B.8}$$

For the other three possible values of s, we find

$$\begin{pmatrix} a_2 \\ b_2 \\ c_2 \\ d_2 \end{pmatrix} = \begin{pmatrix} B(-\theta_E, \varphi_0) \\ A(-\theta_E, \varphi_0) \\ D(-\theta_E, \varphi_0) \\ C(-\theta_E, \varphi_0) \end{pmatrix}, \tag{B.9}$$

$$\begin{pmatrix} a_3 \\ b_3 \\ c_3 \\ d_3 \end{pmatrix} = \begin{pmatrix} -D(\theta_E, -\varphi_0) \\ C(\theta_E, -\varphi_0) \\ -B(\theta_E, -\varphi_0) \\ A(\theta_E, -\varphi_0) \end{pmatrix},$$

$$\begin{pmatrix} a_4 \\ b_4 \\ c_4 \\ d_4 \end{pmatrix} = \begin{pmatrix} C(-\theta_E, -\varphi_0) \\ -D(-\theta_E, -\varphi_0) \\ A(-\theta_E, -\varphi_0) \\ -B(-\theta_E, -\varphi_0) \end{pmatrix}.$$

Notice that for all s, the relation $ab + cd = 0$ is fulfilled.

Bibliography

[1] B.D. Josephson, Phys. Lett **1**, 251-253 (1962).

[2] R. Gross and A. Marx, *Festkörper Physik*, (Oldenbourg Verlag, 2012).

[3] P.W. Anderson and J.M. Rowell, Phys. Rev. Lett. **10**, 230-232 (1963).

[4] J. Bardeen, L.N. Cooper and J.R. Schrieffer, Phys. Rev. **108**, 1175 (1957).

[5] A.A. Golubov, M.Yu. Kupriyanov, and E. Il'ichev, Rev. Mod. Phys. **76**, 411 (2004).

[6] S. Di Franceschi, L. Kouwenhoven, C. Schönenberger, and W. Wernsdorfer, Nature Nanotech. **5**, 703 (2010).

[7] A. Martín-Rodero and A. Levy Yeyati, Adv. Phys. **60**, 899 (2011).

[8] A. Brunetti, A. Zazunov, A. Kundu and R. Egger, Phys. Rev. B **88**, 144515 (2013)

[9] H. Takayanagi, T. Akazaki, and J. Nitta, Phys. Rev. Lett. **75**, 3533 (1995).

[10] Th. Schäpers, V.A. Guzenko, R.P. Müller, A.A. Golubov, A. Brinkman, G. Crecilius, A. Kaluza, and H. Lüth, Phys. Rev. B **67**, 014522 (2003).

[11] M. Ebel, C. Busch, U. Merkt, M. Grajcar, T. Plecenik, and E. Il'ichev, Phys. Rev. B **71**, 052506 (2005).

[12] J. Xiang, A. Vidan, M. Tinkham, R.M. Westervelt, and C.M. Lieber, Nature Nanotech. **1**, 208 (2006).

[13] S. Tirelli, A.M. Savin, C.P. Garcia, J.P. Pekola, F. Beltram, and F. Giazotto, Phys. Rev. Lett. **101**, 077004 (2008).

[14] M.L. Della Rocca, M. Chauvin, B. Huard, H. Pothier, D. Esteve, and C. Urbina, Phys. Rev. Lett. **99**, 127005 (2007).

[15] J.D. Pillet, C.H.L. Quay, P. Morfin, C. Bena, A. Levy Yeyati, and P. Joyez, Nature Phys. **6**, 965 (2010).

[16] R. Winkler, *Spin-Orbit Coupling Effects in Two-Dimensional Electron and Hole Systems* (Springer, New York, 2003).

[17] Y.J. Doh, J.A. van Dam, A.L. Roest, E.P.A.M. Bakkers, L.P. Kouwenhoven, and S. De Franceschi, Science **309**, 272 (2005).

[18] J.A. van Dam, Yu.V. Nazarov, E.P.A.M. Bakkers, S. De Franceschi, and L.P. Kouwenhoven, Nature **442**, 667 (2006).

[19] T. Sand-Jespersen, J. Paaske, B.M. Andersen, K. Grove-Rasmussen, H.I. Jørgensen, M. Aagesen, C.B. Sørensen, P.E. Lindelof, K. Flensberg, and J. Nygård, Phys. Rev. Lett. **99**, 126603 (2007).

[20] R.S. Deacon, Y. Tanaka, A. Oiwa, R. Sakano, K. Yoshida, K. Shibata, K. Hirakawa, and S. Tarucha, Phys. Rev. Lett. **104**, 076805 (2010).

[21] Y. Kanai, R.S. Deacon, A. Oiwa, K. Yoshida, K. Shibata, K. Hirakawa, and S. Tarucha, Phys. Rev. B **82**, 054512 (2010); Y. Kanai, R.S. Deacon, S. Takahashi, A. Oiwa, K. Yoshida, K. Shibata, K. Hirakawa, Y. Tokura, and S. Tarucha, Nature Nanotech. **6**, 511 (2011).

[22] E.J.H. Lee, X. Jiang, R. Aguado, G. Katsaros, C.M. Lieber, and S. De Franceschi, Phys. Rev. Lett. **109**, 186802 (2012).

[23] W. Chang, V.E. Manucharyan, T.S. Jespersen, J. Nygård, and C.M. Marcus, preprint arXiv:1211.3954.

[24] E.J.H. Lee, X. Jiang, M. Houzet, R. Aguado, C.M. Lieber, and S. De Franceschi, preprint arXiv:1302.2611.

[25] H.A. Nilsson, P. Samuelsson, P. Caroff, and H.Q. Xu, Nano Lett. **12**, 228 (2012).

[26] G. Katsaros, P. Spathis, M. Stoffel, F. Fournel, M. Mongillo, V. Bouchiat, F. Lefloch, A. Rastelli, O.G. Schmidt, and S. De Franceschi, Nature Nanotech. **5**, 458 (2010).

[27] E. Majorana, Nuovo Cimento **14**, 171(1937).

[28] L. Fu and C. L. Kane, Phys. Rev. Lett. **100**, 096407 (2008).

[29] M.Z. Hasan and C.L. Kane, Rev. Mod. Phys. **82**, 3045 (2010).

[30] X.L. Qi and S.C. Zhang, Rev. Mod. Phys. **83**, 1057 (2011).

[31] C.W.J. Beenakker, Annu. Rev. Con. Mat. Phys. **4**, 113 (2013).

[32] J. Alicea, Rep. Prog. Phys. **75**, 076501 (2012).

[33] M. Leijnse and K. Flensberg, Semicond. Sci. Techn. **27**, 124003 (2012).

[34] Y. Oreg, G. Refael, and F. von Oppen, Phys. Rev. Lett. **105**, 177002 (2010).

[35] R.M. Lutchyn, J.D. Sau, and S. Das Sarma, Phys. Rev. Lett. **105**, 077001 (2010).

[36] V. Mourik, K. Zuo, S.M. Frolov, S.R. Plissard, E.P.A.M. Bakkers, and L.P. Kouwenhoven, Science **336**, 1003 (2012).

[37] L. Rokhinson, X. Liu, and J. Furdyna, Nature Phys. **8**, 795 (2012).

[38] A. Das, Y. Ronen, Y. Most, Y. Oreg, M. Heiblum, and H. Shtrikman, Nature Phys. **8**, 887 (2012).

[39] M.T. Deng, C.L. Yu, G.Y. Huang, M. Larsson, P. Caroff, and H.Q. Xu, Nano Lett. **12**, 6414 (2012).

[40] E.V. Bezuglyi, A.S. Rozhavsky, I.D. Vagner, and P. Wyder, Phys. Rev. B **66**, 052508 (2002).

[41] I.V. Krive, L.Y. Gorelik, R.I. Shekhter, and M. Jonson, Fiz. Nizk. Temp. **30**, 535 (2004) [Low Temp. Phys. **30**, 398 (2004)].

[42] I.V. Krive, A.M. Kadigrobov, R.I. Shekhter, and M. Jonson, Phys. Rev. B **71**, 214516 (2005).

[43] O.V. Dimitrova and M.V. Feigel'man, JETP **102**, 652 (2006).

[44] L. Dell'Anna, A. Zazunov, R. Egger, and T. Martin, Phys. Rev. B **75**, 085305 (2007).

[45] T. Lottermoser, T. Lonkai, U. Amann, D. Hohlwein, J. Ihringer and M. Fiebig, Nature **430**, 541 (2004)

[46] Q. Sun, J. Wang and H. Guo, Phys. Rev. B **71**, 165310 (2005).

[47] B. Béri, J.H. Bardarson, and C.W.J. Beenakker, Phys. Rev. B **77**, 045311 (2008).

[48] A.A. Reynoso, G. Usaj, C.A. Balseiro, D. Feinberg, and M. Avignon, Phys. Rev. Lett. **101**, 107001 (2008).

[49] A. Buzdin, Phys. Rev. Lett. **101**, 107005 (2008).

[50] A. Zazunov, R. Egger, T. Jonckheere, and T. Martin, Phys. Rev. Lett. **103**, 147004 (2009).

[51] J.F. Liu and K.S. Chan, Phys. Rev. B **82**, 125305 (2010).

[52] A.A. Reynoso, G. Usaj, C.A. Balseiro, D. Feinberg, and M. Avignon, Phys. Rev. B **86**, 214519 (2012).

[53] T. Yokoyama, M. Eto, and Yu.V. Nazarov, J. Phys. Soc. Jpn. **82**, 054703 (2013).

[54] E. Goldobin, D. Koelle, R. Kleiner, and R.G. Mints, Phys. Rev. Lett. **107**, 227001 (2011).

[55] H. Sickinger, A. Lipman, M. Weides, R.G. Mints, H. Kohlstedt, D. Koelle, R. Kleiner, and E. Goldobin, Phys. Rev. Lett. **109**, 107002 (2012).

[56] V.B. Geshkenbein and A.I. Larkin, Pis'ma Zh. Eksp. Teor. Fiz. **43**, 306 (1986) [JETP Lett. **43**, 395 (1986)].

[57] S. Yip, Phys. Rev. B **52**, 3087 (1995).

[58] Y. Tanaka and S. Kashiwaya, Phys. Rev. B **56**, 892 (1997).

[59] Y. Asano, Y. Tanaka, M. Sigrist, and S. Kashiwaya, Phys. Rev. B **71**, 214501 (2005).

[60] Y. Avishai and T.K. Ng, Phys. Rev. B **81**, 104501 (2010).

[61] T. Novotný, A. Rossini, and K. Flensberg, Phys. Rev. B **72**, 224502 (2005).

[62] A. Schulz, A. Zazunov, and R. Egger, Phys. Rev. B **79**, 184517 (2009).

[63] M.S. Choi, C. Bruder, and D. Loss, Phys. Rev. B **62**, 13569 (2000).

[64] R. Zitko, M. Lee, R. López, R. Aguado, and M.S. Choi, Phys. Rev. Lett. **105**, 116803 (2010).

[65] C. Karrasch, S. Andergassen, and V. Meden, Phys. Rev. B **84**, 134512 (2011).

[66] S. Droste, S. Andergassen, and J. Splettstoesser, J. Phys.: Cond. Matt. **24**, 415301 (2012).

[67] M. Leijnse and K. Flensberg, Phys. Rev. B **86**, 134528 (2012).

[68] A.R. Wright and M. Veldhorst, preprint arXiv:1303.1570.

[69] Yu.V. Nazarov and Ya.M. Blanter, *Quantum Transport: Introduction to Nanoscience* (Cambridge University Press, 2009).

[70] A.A. Abrikosov, L.P. Gorkov, and I.E. Dzyaloshinksi, *Methods of Quantum Field Theory in Statistical Physics* (Prentice-Hall, Inc., Englewood Cliffs, New Jersey, 1963).

[71] A. Zazunov, A. Brunetti, A. Levy Yeyati and R. Egger, Phys. Rev. B **90**, 104508 (2014)

[72] M.H. Devoret and R.J. Schoelkopf, Science **339**, 1169 (2013).

[73] J.M. Martinis, M. Ansmann, and J. Aumentado, Phys. Rev. Lett. **103**, 097002 (2009).

[74] M. Lenander, Phys. Rev. B **84**, 024501 (2011).

[75] G. Catelani, R.J. Schoelkopf, M.H. Devoret, and L.I. Glazman, Phys. Rev. B **84**, 064517 (2011).

[76] J. Wenner *et al.*, Phys. Rev. Lett. **110**, 150502 (2013).

[77] D. Ristè, C.C. Bultnik, M.J. Tiggelman, R.N. Schouten, K.W. Lehnert, and L. DiCarlo, Nat. Comm. **4**, 1913 (2013).

[78] E.M. Levenson-Falk, F. Kos, R. Vijay, L. Glazman, and I. Siddiqi, Phys. Rev. Lett. **112**, 047002 (2014).

[79] J. Aumentado *et al.*, Phys. Rev. Lett. 92, 066802 (2004).

[80] M. Zgirski, L. Bretheau, Q. Le Masne, H. Pothier, D. Esteve, and C. Urbina, Phys. Rev. Lett. **106**, 257003 (2011).

[81] L. Bretheau, Ç.Ö. Girit, H. Pothier, D. Esteve, and C. Urbina, Nature **499**, 312 (2013).

[82] L. Bretheau, Ç.Ö. Girit, C. Urbina, D. Esteve, and H. Pothier, **3**, 041034 (2013).

[83] N. Agrait, A. Levy Yeyati, and J.M. van Ruitenbeek, Phys. Rep. **377**, 81 (2003).

[84] N.M Chtchelkatchev and Yu.V. Nazarov, Phys. Rev. Lett. **90**, 226806 (2003).

[85] C. Padurariu and Yu.V. Nazarov, EPL **100**, 57006 (2012).

[86] A. Zazunov, V.S. Shumeiko, E.N. Bratus, J. Lantz, and G. Wendin, Phys. Rev. Lett. **90**, 087003 (2003).

[87] A. Zazunov, V.S. Shumeiko, G. Wendin, and E.N. Bratus, Phys. Rev. B **71**, 214505 (2005).

[88] M.A. Despósito and A. Levy Yeyati, Phys. Rev. B **64**, 140511 (2013).

[89] B. van Heck, F. Hassler, A.R. Akhmerov, and C.W.J. Beenakker, Phys. Rev. B **84**, 180502 (2011).

[90] D. Rainis and D. Loss, Phys. Rev. B **85**, 174533 (2012).

[91] F. Kos, S.E. Nigg, and L.I. Glazman, Phys. Rev. B **87**, 174521 (2013).

[92] L. Bretheau, Ç.Ö. Girit, M. Houzet, H. Pothier, D. Esteve, and C. Urbina, preprint arXiv:1406.6301.

[93] D.G. Olivares, A. Levy Yeyati, L. Bretheau, Ç.Ö. Girit, H. Pothier, and C. Urbina, Phys. Rev. B **89**, 104504 (2014).

[94] M. Tinkham and J. Clarke, Phys. Rev. Lett. **28**, 1366 (1972).

[95] M. Tinkham, Phys. Rev. B **6**, 1747 (1972).

[96] F. Hübler, J. Camirand Lemyre, D. Beckmann, and H.v. Löhneysen, Phys. Rev. B **81**, 184524 (2010).

[97] T.E. Golikova, M.J. Wolf, D. Beckmann, I.E. Batov, I.V. Bobkova, A.M. Bobkov, and V.V. Ryazanov, Phys. Rev. B **89**, 104507 (2014).

[98] A. Martín-Rodero, A. Levy Yeyati, and F.J. García-Vidal, Phys. Rev. B **53**, R8891 (1996).

[99] R. Avriller and F. Pistolesi, preprint arXiv:1407.5561.

[100] R.-P. Riwar, M. Houzet, J.S. Meyer, and Yu.V. Nazarov, preprint arXiv:1407.0534.

Acknowledgments

I would like to acknowledge the role that some people played in the last years. I refer to people in the Institut für Theoretische Physik IV whom I worked with and, in some cases, from whom I learnt a lot. Among them I would like to mention Prof. Dr. Reinhold Egger, head of the institute to whom I am particularly grateful for having given me the chance to start a PhD under his supervision and for having given me the chance to visit a lot of interesting conferences and workshops, seeing new places and new cultures and enlarging my scientific knowledge. Special mention deserves Dr. Alex Zazunov, to whom I am thankful for the fruitful discussions during the past years and for all the physics technique I had the chance to learn. I acknowledge also two collaborators present in the published papers presented in this thesis: Prof. Dr. Alfredo Levy Yeyati form the Universidad Autonoma de Madrid, for having been his guest in the occasion of our joined project, and Dr. Arijit Kundu of the University of Bloomington. I also would like to thank my colleagues of the Institut für Theoretische Physik IV with whom I shared the free moments and breaks in front of a coffee.
During the PhD period, as it happens, one has moments with variable mood. All the times I had a bad-mood period, I always could count on my few, precious and irreplaceable friends, to whom I really owe more than a 'Thank You'. I am sure they will understand that I refer to them even if I do not write down their names fully.
Last but not least, I would like to thank the support of my family. The more I grow old, the better I understand how important it is to have strong ties. They make you feel free to go anywhere, knowing that you unquestionably belong to somewhere. That 'somewhere' that one can call Home. I dedicate this work especially to them.

Ringraziamenti

Quanto segue è la resa in italiano dei ringraziamenti riguardanti gli amici e la famiglia.
Durante il periodo del dottorato, come spesso accade, si hanno momenti di umore variabile. Tutte le volte in cui la variazione è stata negativa, ho sempre potuto contare sui miei pochi,

preziosi ed insostituibili amici, ai quali devo ben più di un semplice "Grazie ". Sono sicuro che, quando leggeranno, capiranno che mi riferisco a loro anche senza scrivere tutti i loro nomi.
Ultimo ma non ultimo viene il ringraziamento alla mia famiglia. Con l'andare del tempo, crescendo, capisco sempre di più quanto sia importante avere legami solidi e punti di riferimento. Ti fanno sentire libero di andare ovunque nel mondo, sapendo però di appartenere indiscutibilmente ad un "qualcosa". Quel "qualcosa" che posso chiamare Casa. Dedico specialmente a loro questo lavoro di tesi.

Erklärung

Die hier vorgelegte Dissertation habe ich eingeständig und ohne unerlaubte Hilfe angefertigt. Die Dissertation wurde in der vorgelegten oder ähnlichen Form noch bei keiner anderen Institution eingereicht. Ich habe bisher keine erfolglosen Promotionsversuche unternommen.

Düsseldorf, den . .2014

(Aldo Brunetti)